709978

WSRC-TR-95-0070

SIMULATION AND ANALYSIS OF THE PLUTONIUM OXIDE/METAL STORAGE CONTAINERS SUBJECT TO VARIOUS LOADING CONDITIONS (U)

By

CHUNG GONG and ROBERT F. MILLER

MAY 1995

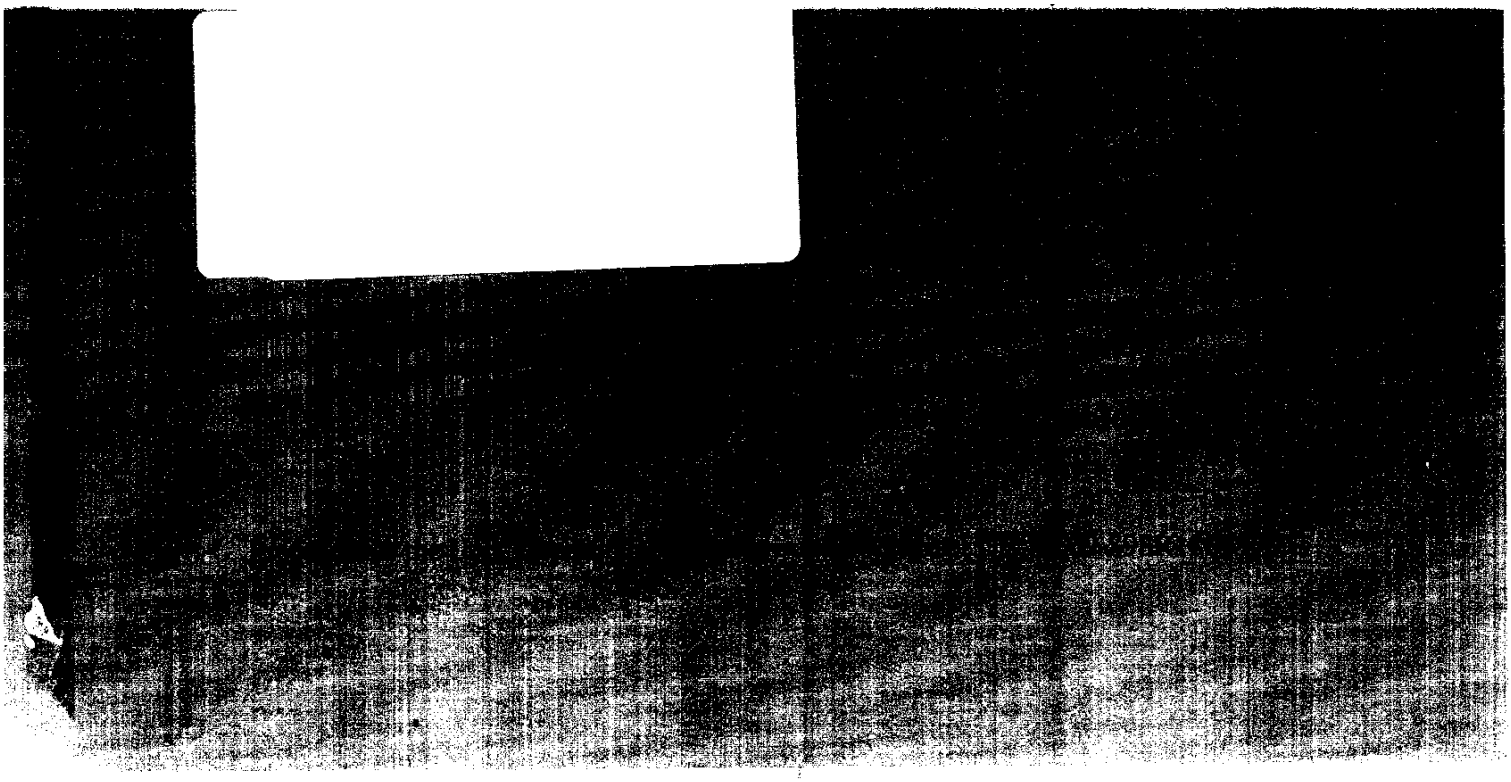

DISCLAIMER

DOCUMENT: WSRC-TR-95-0070

TITLE:

SIMULATION AND ANALYSIS OF THE PLUTONIUM OXIDE/METAL STORAGE CONTAINERS SUBJECT TO VARIOUS LOADING CONDITIONS (U)

TABLE OF CONTENTS

0.0 EXECUTIVE SUMMARY 1

1.0 INTRODUCTION 2

1.1 GENERAL REQUIREMENTS OF PRIMARY CONTAINMENT VESSELS 3

1.2 STRUCTURAL DESIGN REQUIREMENTS 4

1.3 CONTAINER INTEGRITY EVALUATION 4

1.4 OXIDE/METAL STORAGE CONTAINER REFERENCE CONTAINER DESCRIPTION 4

2.0 PURPOSE AND SCOPE OF THE STUDY 6

2.1 DESCRIPTION OF THE PROBLEMS 6

2.1.1 Geometric Configuration 7

2.1.2 Materials 7

2.1.3 Type of Problems Considered 7

3.0 METHOD OF ANALYSIS 8

3.1 Pre- and Post-processor 8

3.2 Main Processor 8

4.0 FINITE ELEMENT MODELS 8

4.1 Vertical upright drop of the whole plutonium storage containment vessel from 30-foot height 9

4.2 Inclined upside-down drop of the whole plutonium storage containment vessel from 30-foot height 10

4.3 Pressure load in the bagless transfer can with springs between the can top lid and the primary containment vessel 11

4.4 Pressure load in the primary containment vessel 11

4.5 Stresses in the primary containment vessel with the laser sampler in locked position 12

5.0 RESULTS 13

5.1 Vertical upright drop of the whole plutonium storage containment vessel from 30-foot height 13

5.2 *Inclined upside-down drop of the whole plutonium storage containment vessel from 30-foot height*....16

5.3 *Pressure load in the bagless transfer can with springs between the can top lid and the primary containment vessel*....18

5.4 *Pressure load in the primary containment vessel*....19

5.5 *Stresses in the primary containment vessel with the laser sampler in locked position*....21

6.0 CONCLUSION....24

7.0 REFERENCES....25

8.0 ACKNOWLEDGMENT....26

FIGURES....27

TABLES....55

APPENDIX I....69

A.1 Incremental plasticity theory....69

A.2 von Mises Equivalent Stress....69

APPENDIX II....71

Initial Plutonium Storage Container Impact Analysis Results (U)....72

1. Summary....72

2. Introduction....72

2.1 The Modeling Approach....72

3. Finite Element Models....73

3.1. Model Descriptions....74

3.1.1. 2D Axisymmetric Models....74

3.1.2. 3D Models....74

3.2. Modeling Techniques....74

3.2.1. Dynamic Analysis....74

3.2.2. Quasi-Static Impact Analysis....75

3.2.3. Other Modeling Assumptions....75

3.3. Material Properties.....76

4. Results.....76

4.1. Dynamic vs. Quasi-Static Analysis.....76

4.2. Shell vs. Solid Elements.....76

4.3. Best Estimate Test Predictions.....78

4.3.1. The Metal Oxide Container.....78

4.3.2. The Pit Container.....79

5. Conclusions.....83

Attachment I - *Detailed Tensile Property Data for Container Materials* 84

LIST OF FIGURES

Figure 1-1. *The Reference Oxide/Metal Primary Containment Vessel Concept.*

Figure 2-1. *The Present Design of the Primary Containment Vessel.*

Figure 2-2. *Stress strain curves for 304 and 304L Stainless Steel.*

Figure 2-3. *Stress strain curves for 304 and 304L Stainless Steel (in Engineering Scale)*

Figure 4-1. *Two Dimensional Finite Element Analysis Mesh of the Primary Container and the Bagless Can for the Upright Drop Case.*

Figure 4-2. *Three Dimensional Finite Element Analysis Mesh of the Primary Container for the Upside-Down Drop Case.*

Figure 4-3. *The Laser Sampler Assembly.*

Figure 4-4. *The Contact Areas between the Flange and the Arms (Section A-A). The Contact Areas between the Laser Sampler and the PU Container (Section B-B).*

Figure 4-5. *Three Dimensional Finite Element Analysis Mesh of the upper portion of the Primary Container for the Laser Sampling Case.*

Figure 5-1. *Maximum von Mises Stress in the Primary Container and the Bagless Can.*

Figure 5-2. *von Mises Equivalent Stress in the Bagless Can in the First Millisecond.*

Figure 5-3. *Maximum von Mises Equivalent Stress in the Primary Container and Bagless Can.*

Figure 5-4. *Energy Transfer and Dissipation in the Container System (15 milliseconds).*

Figure 5-5. *Energy Transfer and Dissipation in the Container System (4 milliseconds).*

Figure 5-6 . *Deformation of the Primary Container and the Bagless Transfer Can at Four Stages during the Impact.*

Figure 5-7. *The Modified Design of the Primary Containment Vessel.*

Figure 5-8. *The Deformed Primary Container at the End of the Upside Down Dropping.*

Figure 5-9. *The Detail of the Deformation in the Fitting Region.*

Figure 5-10. The Deformed Sampling Tube , in 3-D Beam Model.

Figure 5-11. The Deformed Sampling Tube , in 3-D Shell Model.

Figure 5-12.. The Deformed Fitting System under 2.10 psi Pressure on the Cap. (The deformation Magnification Factor = 600)

Figure 5-13. The Deformed Fitting System under 1162.50 psi Pressure on the Cap. (The deformation Magnification Factor = 600)

Figure 5-14. Maximum von Mises Stresses in the Flange, Cap and the Vertical Plates (INTER4 elements).

Figure 5-15. Maximum von Mises Stresses in the Flange, Cap and the Vertical Plates (Bézier surfaces).

Figure 5-16. Comparison of the Maximum von Mises Stresses in the Flange, Cap and the Vertical Plates (with two types of interfaces).

Figure 5-17. The Maximum von Mises Stresses in the Flange, Cap and the Vertical Plates (with relaxed interface constraints).

Figure 5-18. The Deformed Fitting System under 1162.50 psi Pressure on the Cap. (with relaxed interface constraints) (The deformation Magnification Factor = 600).

LIST OF TABLES

Table 2-1. *Digitized Stress Strain data for Type 304L Stainless Steel at 77°F. (in True measurement)*

Table 2-2. *Digitized Stress Strain data for Type 304L Stainless Steel at 77°F (in Engineering measurement)*

Table 2-3. *Digitized Stress Strain data for Type 304L Stainless Steel at 257°F. (in True measurement)*

Table 2-4 *Digitized Stress Strain data for Type 304L Stainless Steel at 257°F. (in Engineering measurement)*

Table 5-1. *Maximum von Mises Equivalent Stress in the Primary Container and the Bagless Transfer Can.*

Table 5-1. *Maximum von Mises Equivalent Stress in the Primary Container and the Bagless Transfer Can (Continued).*

Table 5-2. *Transfer of Kinetic Energy, Strain Energy and Plastic Dissipation in the Container System.*

Table 5-3. *Spring Constants for the Springs on the Top of the Lid.*

Table 5-4. *Plutonium Oxide/Metal Storage Container Internal Pressure in the Bagless Can without Spring.*

Table 5-5. *Plutonium Oxide/Metal Storage Container Internal Pressure in the Bagless Can with Springs on the Lid Top.*

Table 5-6. *Plutonium Oxide/Metal Storage Container Internal Pressure in the Bagless Can with Pre-stress in Springs.*

Table 5-7. *Plutonium Oxide/Metal Storage Container Internal Pressure in the Primary Container without Internal Components..*

Table 5-8. *Plutonium Oxide/Metal Storage Container Internal Pressure in the Primary Container with Internal Components.*

Table 5-9. *Plutonium Oxide/Metal Storage Container Laser Sampler Assembly Maximum von Mises Stresses in the Flange, Cap and the Vertical Plates- the Supporting Surfaces are modeled with 3-D Interface Elements.*

Table 5-9. *Plutonium Oxide/Metal Storage Container Laser Sampler Assembly Maximum von Mises Stresses in the Flange, Cap and the Vertical Plates- the Supporting Surfaces are modeled with 3-D Interface Elements (continued).*

Table 5-10. *Plutonium Oxide/Metal Storage Container Laser Sampler Assembly Maximum von Mises Stresses in the Flange, Cap and the Vertical Plates- the Supporting Surfaces are modeled with BÉZIER Rigid Surface.*

SIMULATION AND ANALYSIS OF THE PLUTONIUM OXIDE/METAL STORAGE CONTAINERS SUBJECT TO VARIOUS LOADING CONDITIONS

Chung Gong and Robert F. Miller

0.0 EXECUTIVE SUMMARY

The structural and functional requirements of the Plutonium Oxide/Metal Storage Containers are specified in the Report "Complex 21 Plutonium Storage Facility Material Containment Team Technical Data Report" [Complex 21, 1993]. There are no existing storage containers designed for long term storage of plutonium and current codes, standards or regulations do not adequately cover this case.

As there is no extensive experience with the long term (50+ years) storage of plutonium, the design of high integrity storage containers must address many technical considerations. This analysis discusses a few potential natural phenomena that could theoretically adversely affect the container integrity over time.

The plutonium oxide/metal storage container consists of a primary containment vessel (the outer container), a bagless transfer can (the inner container), two vertical plates on top of the primary containment vessel, a circular plate (the flange) supported by the two plates, a tube for gas sampling operations mounted at the center of the primary containment vessel top and a spring system being inserted in the cavity between the primary containment vessel and the cap of the bagless transfer can. The dimensions of the plutonium oxide/metal storage container assembly can be found in Figure 2-1. The primary container, the bagless transfer can, and all the attached components are made of Type 304L stainless steel.

The problems considered in this report are as follows: To perform the dynamic impact analysis for the 30-foot drop of the containers that will crash upon the rigid ground surface. The containers can be either in vertical upright position or in 10° tilt upside down position when the containers touch the ground. To carry out stress strain analysis for the internal pressure build-up in either the bagless transfer can or in the primary container. To clarify the stress distribution in the fitting system that is attached on top of the primary container during the laser sampling process.

The dynamic analysis of the vertical 30-foot upright drop includes both the internal bagless transfer can and the primary container. The drop inflicts the bottom of the primary container that is in direct impact against the rigid ground surface, with large strain. However, the boundary conditions around the bagless can enhances the wave propagation in the medium and consequently it intensifies the impact effect. The plastic stress and strain in the bagless transfer can are much higher than those in the primary container. The maximum plastic strain in the primary container is 24.33%, whereas in the bagless transfer can the maximum plastic strain is 35.40%. The allowable plastic strain in the 304L stainless steel is 40% [Sindelar, 1993].

The dynamic analysis provides capacious guidance for the quasi-static analysis of the inclined upside down drop of the containers. The inclined upside down drop of the containers exposes the container top fitting structure to the most vulnerable position. The internal bagless transfer can which is supported by soft springs will be shielded from severe impact. The drop impact will inflict elastic and plastic deformation upon the container. It is extremely conservative, if the total kinetic energy is absorbed in the fitting members alone in plastic dissipation. The maximum plastic strain at the intersection of the flange and one of the vertical plates reaches 37.75%. The sampler tube at the top of the container is bent with a maximum plastic strain of 21%. The fitting system survives the conservative impact loading.

The 30-foot free fall impact in both upright and upside-down drops is considerably severe. However, the analysis confirms that the design of the containers is structurally adequate to resist dynamic impact.

The primary container and the bagless transfer can are quite durable for internal pressure loading. The specified pressure for the primary container is 1,000 psig (it is reduced to 750 psig according to the DOE Standard [DOE Standard, 1994]) at 400°F, whereas the specified pressure for the bagless transfer can is only 500 psig at room temperature. The analysis shows that the maximum plastic strain in the primary container is only 2.15% for applied pressure at 1,500 psig with the bagless transfer can in contact at the bottom of the container. However, in the primary container without the interference of the bagless transfer can, the container stress state remains elastic for applied pressure at 1,500 psig The bagless transfer can attains 3.3% of plastic strain at 1,000 psig that is twice the prescribed magnitude. With the specified pressure of 500 psig the plastic strain in the bagless transfer can reaches only 1.76%.

The contact boundary conditions and the intricate loading paths in the laser sampling process connote nonlinearity in this analysis. The suggested total load on the top of the primary container is 650 pounds or 1,110 psi in pressure. The whole fitting remains within elastic limit when the applied pressure reaches 2,200 psi that is almost twice the specified load.

This analysis considered five hypothetical mechanical problems of the plutonium storage containment vessels. From different point of views, under specific loading conditions the plutonium storage containment vessels are proved to be structurally intact in each case. The loading and boundary conditions are mechanically conservative according to the principles of applied mechanics.

1.0 INTRODUCTION

The structural and functional requirements of the Plutonium Oxide/Metal Storage Containers are specified in the Report "Complex 21 Plutonium Storage Facility Material Containment Team Technical Data Report" [Complex 21, 1993].

There are no existing storage containers designed for long term storage of plutonium and current codes, standards or regulations do not adequately cover this case.

As there is no extensive experience with the long term (50+ years) storage of plutonium, the design of high integrity storage containers must address many technical

considerations. Potential natural phenomena that could theoretically adversely affect the container integrity over time are noted below.

Pressure Build-Up
Container Inner Surface Corrosion
Intermetallic Interface Phenomena
Intermetallic Transformations
Thermal Stresses and Other Effects
Diffusion of Gases
Electrical Phenomena

1.1 GENERAL REQUIREMENTS OF PRIMARY CONTAINMENT VESSELS

- The storage container will be designed for dual use as a primary containment vessel for shipping and for long term storage.
- The storage container will be welded closed at the shipper site and will not be opened at the Plutonium Storage facility.
- Maximum mass of fissile plutonium for Pu oxide/metal storage container will be 4.5 Kg.
- Oxide and metal will be packaged in an inner bagless transfer can.

The primary containment vessel performs a dual role of providing the primary containment for shipping as well as providing the primary containment barrier for storage. Because of this dual role, the primary containment vessel must meet all the requirements for both shipping and storage. There are eleven regulations, codes and standards applicable to the primary containment vessel [Complex 21, 1993, Table 3.2.1.1-1].

The qualification of the primary containment vessels can be divided into two categories of operation: (1) Shipping and (2) Storage. Each of these categories can be further sub-divided into two different phases:

(1) ***Design*** - The initial efforts to develop and test prototypes to certify a container for shipping or to qualify a container for long term storage.

(2) ***In-Process*** - The efforts to continually monitor, test or otherwise evaluate the container for continued service.

The Primary Containment Vessel will be a robust, high integrity vessel fabricated of materials that are corrosion resistant. The vessel will be designed to survive a 30-foot drop and any credible accident scenario expected in a seismically qualified structure with minimum combustible material loading. Combustible packaging materials are required by DOE Order 6430.1A to be placed in metal containers or structures outside the Plutonium Storage Facility in a location that will not endanger the storage facility or the stored material if a fire occurs in the packaging material.

Requirements for design basis accident resistance of the primary containment system, i.e., the primary containment vessel, are specified for DOE-owned Pu storage facilities in section 1305 of DOE Order 6430.1A. Subsection 1305-5.2 requires that storage

containers shall provide primary confinement during normal operations, anticipated operational occurrences and for all design base accidents.

1.2 STRUCTURAL DESIGN REQUIREMENTS

Following are the structural design requirements for the primary containment vessels [Complex 21, 1993, pp 25-26]:

(1) Vessel meets the requirements of the ASME Boiler and Pressure Vessel Code.

(2) Vessel meets storage requirements after the following normal occurrences:

- 4-foot drop
- 2-foot crush with primary container vessels interacting
- vehicle vibration
- handling shock
- compression weight of 5 primary containment vessels

Items listed are postulated events that are possible during routine handling within the Plutonium Storage Facility. This requirement states that the vessel will be designed to withstand these normal occurrences and still meet the storage requirements. Actual occurrences will require careful procedural evaluation prior to allowing a vessel into long term storage. This is a design objective.

(3) Vessel remains leaktight as defined by ANSI N14.5 after any one of the following abnormal occurrences:

- 30-foot drop (maximum vault ceiling height)
- 30-foot crush with primary containment vessels interacting
- vehicle crush as defined in the Facility SAR
- puncture as described in the Facility SAR

Items listed above are postulated design basis accident events that are judged credible but not likely within the Plutonium Storage Facility. This requirement states that the vessel must remain leaktight after these events, however, damage to the vessel or contents is likely which will require repackaging, such that the container can be placed on storage rack.

1.3 CONTAINER INTEGRITY EVALUATION

Evaluations of the container integrity will be required during the life (50+ years) of the container. Evaluations of container will be required prior to shipment and periodically for statistical evaluations. Several methods are proposed that may be used for evaluating the integrity of the assembled storage containers. These methods include

(1) leak checking
(2) digital radiography
(3) laser holographic interferometry, and
(4) acoustic resonance spectroscopy.

1.4 OXIDE/METAL STORAGE CONTAINER

REFERENCE CONTAINER DESCRIPTION

The reference oxide/metal primary containment vessel concept is shown in Figure 1-1. The vessel is designed to the requirements of Section III of the ASME Boiler and Pressure Vessel Code. The vessel is of all welded design providing a hermetically sealed containment for the oxide/metal. The reference concept provides a simple, robust, high integrity pressure vessel, fabricated from commercial components with all welded closures and ports, that requires no routine maintenance over the 50-year life cycle.

The plutonium oxide or metal will be placed in a bagless transfer can. The can will in turn be placed in the primary containment vessel and the vessel sealed. No credit for containment is taken for the transfer can which is regarded only as a clean method of transferring and handling the plutonium outside a glovebox.

Attached to the top of the vessel is a fixture that is used for multiple functions. These functions are:

(1) Remote handling by the Automated Guided Vehicle inside the vault area.
(2) Remote handling by a robot during calorimetry and assay processes.
(3) Suspension device when stored in the vault.
(4) Aid during gas sampling and leak testing processes.
(5) Protection for the gas sampling/leak testing tube.

The maximum internal pressure for the oxide/metal primary containment vessel is derived from several sources. The sources are:

(1) Radiolysis of water absorbed in material at time of storage
(2) Helium generation due to alpha decay of plutonium
(3) Helium present at the time of packaging
(4) Pressure increase due to temperature rise

The storage of oxide results in the worst case of pressure increases because the oxide produces more free helium and will contain absorbed moisture whereas the metal will produce less helium and will not contain absorbed moisture.

The hypothetical case that will result in the greatest pressure increase is described below:

- Oxide container in storage for fifty years
- Helium generation for fifty years
- Complete radiolysis of absorbed water into hydrogen and oxygen
- Pressure increase due to temperature rise from bare container in storage
- Pressure increase due to temperature rise from shipping package exposed to fire

This case assumes that the inner bagless transfer can has ruptured allowing the pressure to be retained by the full volume of the primary containment vessel.

Each long term container being designed for the new plutonium storage facility will require leak testing before and after shipping in addition to approximately three random leak or containment tests during its intended 50 years of use. A method of sampling for contamination and subsequently leak testing the containers that will allow the container design to stay as simple as possible is needed to minimize the cost of the thousands of new containers to be built. In addition, the method of sampling should be highly automated to reduce personal exposure at the plutonium storage facility and shipping sites. The laser penetration and sealing method is a very cost effective method of opening

and closing the containers for the required tests because the complexity is engineered out of the many containers, and into the one laser end effector.

The design temperature and pressure for the reference oxide/metal container are as follows:

Design Temperature	400°F
Design Pressure	1000 psig (750 psig now [DOE Standard, 1994])

Austenitic stainless steel, Type 304L, is regarded as the best choice for construction of long term storage containers for plutonium metal and oxide. Stainless steel will provide a container that is resistant to corrosion from the contents as well as provide a good surface for external decontamination if required. Type 304L stainless steel is an approved material for use by the ASME Boiler and Pressure Vessel Code.

2.0 PURPOSE AND SCOPE OF THE STUDY

The mathematical modeling and simulation of a physical system can serve many purposes, for instance:

- To search for optimized geometric configuration of the containment vessel subjected to various physical conditions.
- To demonstrate and clarify some possible structurally weak mechanism in the containment vessel subjected to various physical situations.
- To provide detail stress analysis for the components of the containment vessel during the design process.

It is essential to understand the mechanical effects of the modification of a component in the containment vessel with respect to a certain applied loading. This preliminary study provides the stress distribution and deformation configuration of the containment vessel for each design modification and loading condition. The structural design of the vessel is based upon the reference oxide/metal primary containment vessel concept as shown in Figure 1-1. The present design of the primary containment vessel is shown in Figure 2-1. This structural analysis program is a part of the project in improving and perfecting the design of an oxide/metal primary containment vessel through the processes of testing, analysis, redesign and improvement.

On the basis of the requirement specified in "Complex 21 Plutonium Storage Facility Material Containment Team Technical Data Report" [Complex 21, 1993] and design modifications, the scope of work in this analysis involves:

- Geometrically linear and non-linear deformations
- Materially elastic and inelastic behaviors
- Static and dynamic loading conditions
- Kinematically continuous and discontinuous

2.1 DESCRIPTION OF THE PROBLEMS

2.1.1 Geometric Configuration

The plutonium oxide/metal storage container consists of a primary containment vessel (the outer container), a bagless transfer can (the inner container), two vertical plates on top of the primary containment vessel, a circular plate (the flange) supported by the two plates, a tube for gas sampling operations mounted at the center of the primary containment vessel top and a spring system being inserted in the cavity between the primary containment vessel and the cap of the bagless transfer can. The dimensions of the plutonium oxide/metal storage container assembly can be found in Figure 2-1. The primary containment vessel is made of cylinder with 5.563 inches outer diameter and 0.258 inches in thickness. The cylinder is 7.24 inches long with a 5-inch schedule 40 pipe cap on each end and the total height of the primary containment vessel becomes 13.19 inches. The bagless transfer can is formed with 0.06-inch metal and is 4.914 inches in diameter, the bottom of the can is a quarter inch thick hemispherical shell and the top is sealed with 0.125-inch thick plate. The vertical plates and the circular flange were made of 0.1875-inch plates, then were changed to 0.25-inch plates. The tube is 0.25-inch in diameter and 0.035-inch in thickness.

2.1.2 Materials

The primary containment vessel, the bagless transfer can, and all the attached components are made of Type 304L stainless steel. The mechanical properties of the Type 304L stainless steel are provided by Sindelar [Sindelar, 1993]. The digitized true stress natural strain data from tensile testing at 77°F and 257°F are shown in Figure 2-2 and listed in Tables 2-1 and 2-3. The corresponding engineering stress and strain data are plotted in Figure 2-3 and list in Tables 2-2 and 2-4 for reference. The data at 257°F can be applied as material properties in the structural analyses for temperatures up to 400°F and for strain rates up to 100 in/in/sec. The modulus of elasticity, Poisson's ratio and mass density for the Type 304L stainless steel are 28,300,000 psi, 0.30 and 0.0007324 pound-sec^2/inch^4, respectively.

Degradation of the container material due to irradiation was considered and shown to be negligible. The bulk radiation field required to cause surface erosion of the stainless steel is not present for the conditions considered for this analysis [Imrich, Sindelar, 1994].

2.1.3 Type of Problems Considered

In this preliminary study, only a few loading conditions listed below have been considered. The process of solving these problems is directly associated with the design and testing program in Equipment Engineering Section (EES). Each of the analyses is in support of the EES program at different phases of design and testing of the plutonium storage containment vessels.

(1) Vertical upright (bottom) drop of the whole plutonium storage containment vessel from 30-foot height
(2) Inclined upside-down drop of the whole plutonium storage containment vessel from 30-foot height
(3) Pressure load in the bagless transfer can with springs between the can top lid and the primary containment vessel
(4) Pressure load in the primary containment vessel

(5) Stresses in the primary containment vessel with the laser sampler in locked position

3.0 METHOD OF ANALYSIS

3.1 Pre- and Post-processor

P3/PATRAN® [P3/PATRAN®, 1993] is a geometric and graphic modeling code developed by PDA Engineering. The P3/PATRAN system's ability to interface with a large array of applications is provided by the PATRAN Neutral File, PATRAN Results File, and Application Interface. Post-processing of the results was accomplished using ABAQUS® POST.

3.2 Main Processor

ABAQUS® [ABAQUS®, 1993, Hibbitt et al, 1993] is a general purpose finite element analysis program with special emphasis on advanced linear and nonlinear structural engineering and heat transfer applications. Hibbitt, Karlsson & Sorensen, Inc. (HKS) developed and support this computer code. The ABAQUS® version presently in use at SRS (5.3-1N) is marketed by HKS as a "Nuclear QA Grade" code that complies with the NQA-1 quality assurance standard. Details of the Quality Assurance controls for the ABAQUS code may be found in the Technical and QA Plan for ABAQUS [Technical, 1993].

ABAQUS has extensive material, element and procedure libraries. Material models include plasticity for metals, soils, plastics, foam, composites, and concrete as well as rubber elasticity. Element formulations include beams, shells and continuum elements allowing finite rotation and finite strain calculations. Analysis procedures include capabilities for statics, dynamics, eigenvalue extraction, soil consolidation, acoustics, coupled temperature-displacement, and heat transfer. A super-element/substructuring capability is also available.

A key aspect of the way ABAQUS provides simulations is that a clear distinction is made between steps involving nonlinear analysis and linear perturbation steps. Nonlinear analysis steps define a sequence of events that follow one another, in the sense that the state of the model at the end of the step provides the initial conditions for the start of the next step. A linear perturbation analysis step provides the linear response of the system at the base state: the state at the end of the last nonlinear analysis step prior to the linear perturbation analysis.

4.0 FINITE ELEMENT MODELS

The geometric configuration of the primary containment vessel and the bagless transfer can is essentially axially symmetric, however, the attached components, such as the vertical plates and the top flange are not axially symmetric. Except in the case of internal pressure loading, the applied loading and boundary conditions are asymmetric in most cases. Ideally, the whole plutonium storage containment vessel system can be modeled in three dimensional finite element mesh with various combinations of initial conditions and boundary conditions. The dynamic impact loading during the postulated drop tests will

inflict traumatic deformation to the plutonium storage containment vessel system. The impact loading generates elastic and plastic waves in the plutonium storage containment vessel system. In order that the finite element analysis can sufficiently simulate the stress waves at high frequencies in the plutonium storage containment vessel system, the finite element mesh must be sufficiently fine such that the distortion of the wave forms in the system will be within the tolerance [Gong, 1977]. If all the mathematical and mechanical precision conditions as discussed were satisfied, the finite element analysis model would consist of at least 10,000 elements (Each simple quadrilateral element has four corner nodes; usually each node may join with four adjacent elements. The number of nodal points in a mesh may be in the same order of the number of the elements. For a structural member, the degrees of freedom are six. Therefore, in a model with 10,000 shell elements, the degrees of freedom may be in the order of 60,000). In the current computation environment, for a numerical model of more than 50,000 degrees of freedom it may be very time consuming to obtain dynamic solution implicitly, if not impossible.

Based upon preliminary analytical study, instead of constructing one universal model, a specific finite element model is created for each problem. Miller (in Appendix II) discussed the bases for modeling and analysis techniques in an internal memorandum. A brief discussion of the modeling and analysis approaches for each of the problems is as follows:

4.1 Vertical upright drop of the whole plutonium storage containment vessel from 30-foot height

As discussed previously, the main body of the containers is essentially axially symmetric except the vertical plates and the holed top flange attached to the top cap of the primary containment vessel (the group of the plates and flange is also called a fitting). Since the vertical upright drop of the whole plutonium storage containment vessel will cause significant deformation only at the bottom of the vessel, the kinematic effect of the top fixture will be negligible. Instead of parallel plates, the top fitting is modeled in cylindrical shells with equivalent mass. Then the whole vessel is modeled with shell elements (SAX1, in ABAQUS element library). Figure 4-1, shows the half revolution view of the finite element analysis mesh of the vertical upright drop of the whole plutonium storage containment vessel.

In a dynamic analysis, the mass distribution in the body at each instance during the impact process will influence the behavior of the dynamic system. In this analysis, the plutonium oxide powder in the bagless transfer can (also referred as inner container) will be drastically disturbed during the impact. A preliminary study indicated that the powder in the bagless transfer can circulates as a fluid in the vessel with heat at the bottom of the vessel. The motion of the powder particles is similar to the convection motion of a fluid. The center portion that is directly above the impact area moves upward, while the neighboring particles outside the central column move downward.

The finite element analysis formulation is based on the theory of continuum mechanics. The method cannot simulate the separation of elements that were connected initially. Also the elements cannot be distorted too much such that the volume of an element becomes numerically negligible. In solid mechanics, Lagrangian formulation is applied so that the motion of the particles can be traced continuously. Thus no matter how small an element, the movement of a node in this element could distort and stretch the element to a hundred times its original size. In this problem the large relative movement between powder particles cannot be modeled with continuum elements.

Physically, the movement of the powder particles will dissipate kinetic energy and alleviate the damage to the vessel during the drop impact. If the equivalent mass of the powder is attached to the wall of the bagless transfer can, the impact deformation at the area in contact will be slightly aggravated.

The spring between the inner surface of the cap of the primary containment vessel and the top lid of the bagless transfer can is modeled with linear springs (type=SPRINGA in ABAQUS).

The drop of the whole plutonium storage containment vessel onto an unyielding surface will cause the bottom of the vessel to contact a rigid surface and consequently the impact between the bagless transfer can and the primary containment vessel. Interface elements are provided between all the surfaces that will likely be in contact during the drop.

In this model, there are:

165 SAX1 shell elements
66 MASS elements
105 interface elements
4 SPRING elements
176 Nodal points

In this case the room temperature mechanical property of the stainless steel 304L is used.

The calculation begins at the moment the bottom of the vessel touches the ground. After traveling 30 feet under gravity, the vessel gained a vertical velocity of 527.45 inches per second. The initial velocity used in the ABAQUS input file is 527.5 in/sec. The ground surface is a rigid surface. In addition to initial velocity, the vessel system is also in the influence of the gravity field with gravity acceleration equal to 386.04 in/sec^2.

4.2 Inclined upside-down drop of the whole plutonium storage containment vessel from 30-foot height

In this upside-down drop the impact load will be directly applied to the fitting. The weakest deformation mode for the vertical plates in this inclined drop will be bending out-of the plate planes. The upside-down vessel will hit the ground at an angle 10 degrees from the vertical axis. The deformed configuration of the vessel, especially in the fitting and top cap region, during the impact will be asymmetrical. The whole vessel system must be modeled in three dimensional geometry. Figure 4-2 shows the 3-D finite element analysis mesh of the upside-down drop of the plutonium storage containment vessel.

The primary containment vessel and the fitting are meshed with 4,628 shell and interface elements and 3,948 nodal points. This model generates 26,160 variables for solution. If a full dynamic analysis of the vessel system would be carried out, the bagless transfer can, the masses of the plutonium powder and the springs should also be modeled in three dimensional geometry. Then the total number of elements would be twice as many as that of the primary containment vessel. With the present computation device, it is difficult to perform a full dynamic analysis for such a big problem.

The prime interest in this analysis is to obtain the deformation and stress distribution in the vessel due to the impact from a 30-foot drop. A quasi-static analysis will accomplish

the task with slight conservatism. The conservative assumptions in this analysis can be elucidated as follows:

The total mass (Mg=34 pounds in weight) of the whole vessel system at h=30 feet above the ground, possesses a potential energy of Mgh=34*30*12=12,240 in-lbs. When the vessel starts falling and eventually hits the ground the potential energy in the vessel will partially transfer into kinetic energy (Theoretically a mass particle drops from an elevated position will convert all the potential energy into kinetic energy when it hits the ground. However, in this analysis, when the bottom or the top of the container touches the ground the center of the mass is still above the ground. Consequently, the maximum velocity from the free fall is not attained). In this analysis, the quasi-static calculation, with progressive increase of displacement, will carry up to the point when the total energy, potential plus kinetic energy, has been dissipated through plastic deformation of the vessel. In reality, the energy in the system is dispersed in several different ways, e.g., the vessel deforms both elastically and plastically. The elastic strain energy is stored in the vessel and causes the vessel rebounding from the ground as the elastic strain energy is released. Also a large amount of the energy is dissipated in the motion of the plutonium oxide particles.

In a quasi-static analysis the stresses in the vessel induced by its own weight statically are negligible. To move the upside-down vessel vertically toward an inclined rigid surface is equivalent to dropping the vessel at an inclined angle onto a horizontal surface. In this analysis, the first approach is adopted.

Interface elements are attached on the top of the circular flange surface and between the vertical plates and the central tube.

The vessel is at room temperature.

In a first attempt, the analysis indicated that the 3/16-inch thick plates in the fitting were insufficient to protect the tube from excessive bending during the drop. After separate detailed modeling of the tube, it was suggested that the thickness of the fitting plates should be increased to 0.25-inch. This thickness is slightly less than the thickness of the wall of the primary containment vessel, such that the fitting system absorbs most of the energy, and the top cap of the vessel remains at low stress and less deformation.

4.3 Pressure load in the bagless transfer can with springs between the can top lid and the primary containment vessel

Essentially, the model of the vessel in this case is identical to that in the vertical bottom drop problem. Internal pressure in the bagless transfer can is loaded up to 500 psig as required by the design group. The springs on the top of the lid are rather soft as compared with the stiffness of the bagless transfer can itself. In order to eliminate the influence of the springs, a separated model of the bagless transfer can is considered. The pressure in the isolated bagless transfer can is gradually increased up to 1,000 psig.

4.4 Pressure load in the primary containment vessel

The finite element model for the vertical bottom drop problem may also be used in this case. However, another model consisting of only the primary containment vessel with the fitting removed is also considered.

In both models the internal pressure applied is 1,000 psig and the mechanical property of the 304L stainless steel is at 400°F.

4.5 Stresses in the primary containment vessel with the laser sampler in locked position

The laser penetration and sealing leak testing system for long term plutonium storage containers is designed for high reliability and automation in operation. The laser sampler assembly is a well-conceived sturdy system. The purpose of this analysis is to expound the mechanical effects upon the primary containment vessel in the leak testing process.

The procedure in the laser sampling process may be described as follows:

A specific container is placed on a pedestal where the laser penetration and sealing leak testing system is installed. The pedestal, then raises the container into the position such that the leak testing system and the fitting on top of the container will couple together with the arms in the unlocked position (see Figure 4-3). A nut-runner moves down to the top of the ACME screw. The nut-runner turns the nut at the top of the screw and moves the arms into the locked position. A predetermined number of turns of the nut will compress the spring washers in the leak testing system about half of an inch such that the o-ring in the engaged system will have sufficient pressure to seal the testing chamber during the laser penetration. Depending on the strength of the spring washer, the force in the spring, as well as at the interface of the laser sampler subassembly and the top surface of the container, ranges from 260 to 650 pounds. This coupled system is essentially in stable self equilibrium state. The same amount of force is at the interface of the fitting flange and the flat tips of the locked arms. As far as the container fitting system is concerned, the mechanical function among the components can be interpreted as follows:

The top flange of the containment vessel is supported by a rigid surface. The flange and the rigid surface are in contact over two patches that are the size of the flat tip of the sampler arms. At the top of the container cap, pressure is applied over a circular area around the testing tube. The circular area is coincident with the contact area of the laser sampler subassembly and the top surface of the container. Mechanically the pressure distribution over the contact area may not be uniform. Also the pressure over the o-ring cannot be determined. The flat tips of the sampler arms will certainly remain flat in the stressing process, nevertheless, the flange will deform and warp as the laser sampler subassembly pushes the top surface of the container down. The warping of the flange will alter the area of contact. In light of this perception, a sensible mathematical model can be constructed.

The force and deformation are considerably small and are concentrated in the container top and fitting region. The finite element model will consist of the top cap and the fitting of the container and the rigid surface of the flat tips of the sampler arms. The area in contact is in the form of two rings on the top-cap of the container. The inner ring is sided with two circles of radii 0.375 and 0.455 inches. The outer ring is between circles 0.55 and 0.65 inches in radii (see Figure 4-4). The area between the inner and outer rings is the location of the o-ring. No pressure is assigned in the o-ring area. If the pressure distribution over the contact area is uniform, the corresponding pressure to the 650-pound force will be 650/0.5856=1,110 psi. Since the uniformity of pressure is not confirmed, the applied pressure will be higher. Figure 4-5, shows the finite element analysis mesh of the top of the primary containment vessel. At the center of the topcap where the testing tube connects to the container, a hole is left in the model for possible stress concentration.

At the interface of the sampler arms and the fitting flange, interface elements are inserted. ABAQUS introduces a family of elements that allow for the modeling of contact between a deforming body and an arbitrarily shaped rigid body that may move during the history being modeled. At each integration point these elements construct a measure of overclosure (penetration of the point on the surface of the deforming body into the rigid surface) and measures of relative shear sliding. These kinematic measures are then used, together with appropriate Lagrange multiplier techniques, to introduce surface interaction theories. ABAQUS provides several different approaches to the modeling of the surfaces of rigid bodies. General surfaces can be defined by meshing the surface with Bézier surface patches. In this analysis two distinct types of interface elements are considered. The Bézier rigid surfaces are meshed to the flat tip of the sampler arms and the stress-displacement interface elements INTER4 are introduced between the rigid surface and the fitting flange.

5.0 RESULTS

5.1 Vertical upright drop of the whole plutonium storage containment vessel from 30-foot height

The finite element analysis of this problem begins right at the moment when the bottom of the primary containment vessel touches the rigid ground surface. At this moment all the container masses fall down at the speed of 527.5 in/sec, except the point of contact. The motion of the container is also under the influence of the gravitational field. The deceleration in the area around the point of contact generates high stresses and deformation. In the region of contact the deformation modifies the extent of interfacial contact. Mathematically the adjustment of contact geometry at the container-rigid ground and the inner-outer container interfaces requires many iterations to reach mechanical equilibrium. With reasonably small tolerance, the initial time increment reduces to 2.402E-08 seconds. Several different tolerances are considered, the stable solution has been obtained.

The extent and degree of severity of deformation dictate the size of time increments in the process of computation. Mechanically the deforming process involves closing and opening of the gaps and changing of material states from elastic to plastic behaviors. In the container system, mechanical waves propagate during the impact. Since the wave speed in the container will be influenced by the geometric configuration, states of the material as well as the large deformation of the container, theoretically the wave speeds vary as the impact is in progress.

In the 304L stainless steel, within the elastic limit, a dilatational wave will propagate at speed c_1 = 228,069 inches/sec (or 19,006 feet/sec), and a shear wave will propagate at speed c_2 = 121,908 inches/sec (or 10,159 feet/sec). In the plastic region, the speed of shear waves is approximately equal to 11,621 inches/sec (or 968.4 feet/sec).

The container system is made of steel shells, the dominant wave modes generated in the impact will be flexural modes. The wave speed of the flexural modes is different from the wave speeds in an infinite medium. In a structure, like the container system that consists of members of various sizes and shapes, the wave speed also varies with wave length. This phenomenon is well expounded by Mindlin [Mindlin, 1960].

At the moment when the bottom of the dropping container touches the rigid surface, elastic waves propagate upward from the surface in contact through the primary container as well as the bagless transfer can. It takes 0.07269 milliseconds for the first signal of the elastic wave reaching the edge of the bagless transfer can lid. The corresponding wave velocity is 146,169 inches/sec (or 12,181 feet/sec). With a slightly higher velocity (164,050 inches/sec or 13,671 feet/sec) the first elastic wave travels from the bottom of the primary containment vessel to the top of the fitting flange. The traveling time is 0.09696 milliseconds. The impact generates high frequency vibration, 116,280 Hertz, initially, then the vibration is gradually slowing down as the impact area increases. In the cylindrical walls, the elastic waves that are generated from impact and reflection from the cylindrical ends are soon overtaken by plastic waves.

At the moment of initial impact the bottom elements of the bagless can and the primary container are both in collision with the rigid surface. The impact forces at the contact areas of both inner and outer vessels are comparable at this moment. However, the boundary conditions at the top ends are different. The top end of the primary container (including the fitting) is traction free, whereas, between the lid of the bagless can and top cap of the primary container there are elastic springs. Waves reflected from a traction free surface will annihilate the incoming waves. The waves reflected from a fixed boundary surface will intensify the wave effects in the medium. The springs at the top of the bagless can may not provide a condition of fixity, the high frequency contents in the spring-supported lid, nevertheless, indicates forceful reflection (see Figure 5-3).

In an inelastic analysis the von Mises equivalent stress (see Appendix I for the explanation of the von Mises equivalent stress) is one of the useful tools for examining the stress state of a structural element. Figure 5-1 shows the entire time history of the maximum von Mises stresses in the primary container and the bagless can during the 15 milliseconds' simulation. Table 5-1 lists the maximum von Mises stresses in the primary container and the bagless can during the 15 milliseconds' history.

During the history of the impact, at certain moments the von Mises equivalent stress in the bagless can lid is higher than that in the impact area of the can. Figure 5-2 shows the von Mises stress in the lid and the bottom of the bagless can during the first millisecond of impact. For instance, at 0.8135 millisecond after the container touching the ground, the maximum von Mises equivalent stress in the center of the lid is 43,549 psi, which is in the plastic region, the yield limit is 37,840 psi. In the meantime the corresponding stress in the bottom of the can is only 29,734 psi that has been unloaded to the elastic region. The bottom of the bagless can deforms much more than the primary container, such that the bottom of the bagless can separates from the primary container. At 0.9061 millisecond the stress in the bottom of the bagless can increases to 60,095 psi and the stress state in the can lid recovers to the elastic region with a maximum stress of 30,842 psi. In this short duration the bottom of the bagless can is suspended in the air and it has no contact at all. The stress variation in the can is the consequence of propagation of both elastic and plastic waves. The propagation of elastic and plastic waves are extensively discussed in [Love, 1944; Achenbach, 1973; Cristescu, 1967, Goldsmith, 1960].

The traction free boundary condition on the top of the primary container provides a force equilibrium condition such that the reflecting waves will neutralize the incoming waves. The waves in the primary container do not intensify through multiple reflections. The bottom part of the container deforms plastically while the fitting and the top of the container remain elastic.

The maximum plastic strain in the bagless can is 35.40 % at the bottom center. The maximum strain first occurred at 0.6179 millisecond when the von Mises equivalent

stress in the can reached maximum value of 120,590 psi. In the primary container the maximum plastic strain of 24.33 % occurred at a later time, 1.105 millisecond with a maximum von Mises equivalent stress of 99,337 psi that attained at 1.064 millisecond.

The von Mises equivalent stress reaches maximum in the primary container immediately after the containers rebound from the rigid surface. The rebounding of the primary container starts at 1.046 millisecond. The rebounding (or separation) of the bagless can from the bottom of the primary container begins, apparently at an earlier time. The von Mises equivalent stress in the bagless can reaches its maximum long before the rebounding of the primary container. Figure 5-3 plots the maximum von Mises equivalent stresses in the primary container and the bagless can. In the first 1.1 milliseconds the stresses in both containers reach the maximums. At the bottom of the primary container the initial stress is comparatively high (that is 34.46 ksi at 0.0003859 millisecond, whereas in the bagless can the initial stress is only 9.864 ksi). Within 0.6 millisecond the maximum stress in the primary container fluctuates rapidly about 90 ksi level. The average frequency of the fluctuation is about 80,000 Hertz. The maximum stress in the bagless can increases monotonically to the extreme when the can starts rebounding from the bottom of the primary container. The rebounding of the bagless can momentarily reduces the magnitude of maximum stress in the primary container and also slows the fluctuation of the stress. The maximum stress in the primary container, after the brief dip, stays at the plateau of 99 ksi, until the primary container rebounds from the rigid surface.

The over all motion of the container system can be interpreted by the energy transfer in the system. At the moment the container bottom touches the rigid surface, the total kinetic energy in the system is 10,640 inch-pounds. The impact at the contact area stresses the bottom of the container to the plastic state. The plastic deformation dissipates most of the energy. A small portion is stored as recoverable strain energy. Figure 5-4 shows the energy transfer and dissipation during the 15 milliseconds of simulation. Table 5-2 lists the kinetic energy, recoverable strain energy and plastic dissipation in the whole container system in the 15 milliseconds. During the first millisecond, more than 90% of the kinetic energy is dissipated through plastic deformation and only 5% is stored as recoverable strain energy. At 1.046 millisecond the kinetic energy in the system reduces to the minimum, 396 inch-pounds. In the meantime, the plastic dissipation reaches the maximum, 9,889 inch-pounds. It indicates that the container system stops descending and begins to rebound from the ground surface. The recoverable strain energy also diminishes. Even though waves still propagate in the system, the whole system is relaxed. The peak recoverable strain energy of 622 inch-pounds at 0.6179 millisecond, implies, in most part, the bagless transfer can starts rebounding from the bottom of the primary container and releases a part of its strain energy. Figure 5-5 shows the energy transfer and dissipation in the first 4 milliseconds and provides details for the variation of the recoverable strain energy that indicates the rebounding of the bagless can and the whole system. The plastic dissipation, i.e., the energy spent, remains virtually constant after the rebounding. The regaining of kinetic energy in the system is from the releasing of the elastic strain energy.

Figure 5-6 shows the primary container and the bagless can at four deformation stages during the dynamic impact. Figure 5-6-1 shows the containers touching the rigid ground surface at 0.3859 microsecond. At 0.6344 millisecond the bagless transfer can begins to rebound from the bottom of the primary container as shown in Figure 5-6-2. The whole system starts rebounding from the rigid ground surface at 1.046 milliseconds when both the stress and deformation in the primary container are approaching the maximum. The moment of maximum deformation is depicted in Figure 5-6-3. After the containers rebound from the rigid ground surface, the separation of the bagless transfer can from the

primary container becomes obvious. Figure 5-6-4 catches one of the rebounding motion of the containers at 20.77 milliseconds.

In this analysis, the plutonium oxide powder mass is redistributed over the walls of the bagless transfer can. The turbulent motion of the powder particles during the impact is eliminated from the analysis. This turbulent motion of the powder particles will certainly consume a lot of kinetic energy. Consequently both the recoverable strain energy and the plastic dissipation will be reduced. The reduction of recoverable strain energy will decrease the possibility of rebounding. Also the powder is not an effective medium in transmitting impact. The downward momentum of the particles beyond the region of impact will not be much reduced by the upward thrust. This is another factor for the reduction of rebounding. The turbulent motion of the powder particles will also mitigate the damage from plastic deformation.

The maximum plastic strain in the bagless can is 35.40%, while in primary vessel it is only 24.33%. The maximum allowable strain is 40% [Sindelar, 1993].

This dynamic analysis provides comprehensive understanding of the mechanical behavior of the container system during an impact. A few important findings are as follows:

- For a dynamic analysis all the movable members should be included in the numerical model, because, the motion of any individual member in the system will influence the mechanical behavior of the whole system.

- Depending on the constraints in the system, the internal members may have more severe damage than that inflicted upon the external vessel which is in direct impact.

- The motion of unconfined particles in a container during impact will dissipate kinetic energy and reduce the damage to the container.

- The dynamic analysis provides guidance for performing quasi-static analysis.

- The results obtained from this analysis are conservative for engineering design, since the calculated stresses and strains in the containers are higher than that in the system with the real mechanical conditions. In the real situation, more energy will be dissipated through the motion of the plutonium oxide powder.

The ABAQUS calculation files are saved in the Common File System (CFS), under the Data Tree: /y6749/can-drop. The input file is: canlowtol.inp. The animation files are in /y6749@orion, with titles as tt.rst, candrop.flc.

5.2 *Inclined upside-down drop of the whole Plutonium storage containment vessel from 30-foot height*

In a dynamic analysis, the size of the finite element mesh is a function of the possible wave lengths in the system [Gong, 1977]. The impact of a 30-foot drop on the fitting of the primary container will generate short mechanical waves through direct contact and multiple reflections. To construct a model that can accommodate all the possible wave lengths in the problem is practically prohibitive.

Except at a few joint interfaces, the waves in the thickness of the container and fitting walls are of high order phenomena [Mindlin, 1960]. By ignoring the thickness modes, the whole container is modeled with shell elements. The size of the elements is on the

order of the thickness of the shells. In order that the accuracy of the responses will be maintained during the wave reflections, refractions and deflections in the containers, the element size must be uniform in the medium.

The purpose of this analysis is a rigorous, conservative solution. The study of the vertical upright drop case provides a guidance for this calculation. Instead of direct dynamic analysis, a proper quasi-static analysis of the inclined upside-down drop case will be sufficient for a conservative solution. In a quasi-static analysis, as long as the element sizes are compatible with the anticipated deformation, the uniformity of element size distribution in the system is not an essential factor. In the direct impact area, fine element meshes are implemented. The sizes of elements away from the center of drastic deformation are gradually increased to a proper extent.

The drop motion is driven by giving displacement at the bottom of the container. The impact is concentrated in the fitting members. The rate of increment of movement in the calculation is determined by a set of parameters that control the convergence and accuracy of the solution. After the flange of the fitting touches the rigid ground surface, the energy dissipation through plastic deformation increases monotonically. The solution of the problem is picked at the moment when the plastic dissipation is equal to or greater than the total kinetic energy (which equals the total potential energy of the system at 30 feet elevation). The kinetic energy calculated in the previous case is slightly less than the amount 12,240 inch-pounds computed directly. The reason for this discrepancy is that the finite element code numerically integrates the kinetic energy through all the nodal points; each node may have different mass and velocity at the moment. The velocities of the nodal points do not reach the maximum value simultaneously at the time of impact. The reduction in total kinetic energy is realistic. For conservatism, in this quasi-static analysis, the maximum value, 12,240 inch-pounds, will be considered.

The shell and plate members of the fitting are 3/16 inches in thickness according to the original design. The fitting system absorbs most of the energy during the impact. With the maximum kinetic energy equal to 12,240 inch-pounds, the fitting is crushed in the calculation. The sampling tube at the top of the primary container breaks during the crush.

One of the functions of the fitting system is to protect the sampling tube from breaking. The fitting system must be sufficiently strong to shield the sampling tube and adequately flexible such that the fitting system will absorb most of the impact and ward off damage to the primary container. A satisfactory choice for the thickness of the fitting members is a quarter of an inch. Figure 5-7 shows the modified design of the primary containment vessel.

The calculation will be carried out for the modified primary containment vessel.

Comparing with the in-plane deformation, the bending in the fitting system will absorb much more energy. In actual drop, the inclination of the container axis with respect to the vertical normal to the ground will inflict bending deformation upon the fitting members (i.e., the flange, two vertical plates and the tube). The inclination angle for maximum impact damage to the container is a function of the geometry and mass distribution (both integrated and disintegrated) of the container. For the quasi-static analysis, the drop angle will be 10° that is a little less than the angle between the center axis and the line connecting the mass centroid of the container and the edge of the top flange. The edge of the top flange will contact the rigid surface first during impact.

This is a displacement driven quasi-static analysis. There are no waves propagating in the media. The work done by the driving movement is partially stored as elastic strain energy and most of the energy is dissipated in plastic deformation. The conservative assumption for this analysis is that the amount of energy dissipated in plastic deformation equals the total potential energy of the system at the height of 30 feet. The potential energy is being converted into kinetic energy as the vessel descends from the original position in free fall. The total amount of potential energy will be converted into kinetic energy at the moment when the container touches the ground. In this finite element analysis, the total plastic dissipation is 12,290 in-lbs which is slightly higher than 12,240 in-lbs, the total kinetic energy.

The deformation of the system is concentrated in the fitting that is in direct contact with the rigid surface. The conspicuous pattern of the crash is the bending of the two vertical plates and the warping of the flange as shown in Figure 5-8. The primary container is virtually intact in this displacement driven impact. Figure 5-9 shows the detail of the deformation. The tube is pressed aside by one of the bent vertical plates. The maximum bending deformation is at the junction of the plate and the container cap. The plates and the flange are in plastic deformation. The maximum von Mises equivalent stress at the junction of one of the plates and the container cap is 124.65 ksi. This high stress is in the plate. The maximum von Mises equivalent stress in the container cap is only 40.42 ksi, which is close to the elastic limit, 37.84 ksi. The plastic strain induced in the cap is 0.41659%. The maximum plastic strain in the plate is 37.75% that is considerably high, even though it is still below the rupture strain limit 40% [Sindelar, 1993].

The tube attached on the top of the container cap is modeled with 20 3-D beam elements (B31 in ABAQUS element library). The maximum von Mises equivalent stress at the bottom of the tube is 6.31 ksi that is insignificant. Apparently, the beam stress is misleading. In order to compute the true stresses and strains in the tube, a 3-D shell model is constructed with 3,840 shell elements (S4R).

A set of boundary conditions and loading formulation is created, such that it will produce a similar deformation configuration in the shell model as that in the beam model. The maximum lateral deflection of the beam model is 0.7032 inches. Whereas the maximum lateral deflection of the shell model is 0.7121 inches. The bulging of the shell surface on the compressing side of the tube adjacent to the fixed end is missing in the beam model. The maximum von Mises equivalent stress in the shell elements is 92.55 ksi and the maximum plastic strain is 21% which is about half of the rupture strain. Figure 5-10 shows the deformed tube modeled with beam elements. Figure 5-11 delineates the deformed tube modeled with 3-D shell elements. The bulging of the tube is discernible in the vicinity of the fixed end.

The ABAQUS calculation files are saved in the Common File System (CFS), under the Data Tree: /y6749/can-top-drop. The input files are: can3ds24.inp, canrest25.inp.

5.3 *Pressure load in the bagless transfer can with Springs between the can top lid and the primary containment vessel*

The boundary conditions around the bagless transfer can, especially the springs on the top of the lid, will affect the stresses and strains in the pressurized can.

The given spring constant is 45.40 pounds per inch of displacement. The over all model is axisymmetric and accordingly, the spring elements adopted in this model will also be axisymmetric. Therefore, except along the central axis, the springs are in the form of

concentric cylinders. With the same spring constant the cylindrical springs with larger radii will have less force per displacement per circumferential length. In order to assure uniform distribution of the spring force, four springs are attached on the top of the lid. The other ends of the springs are connected to the inner surface of the primary container. The spring element for this model is SPRINGA (in ABAQUS). The spring constants for the four springs are listed in Table 5-3.

The springs will exert equal force per unit length on the lid surface for equal displacement. With internal pressure in the bagless can the actual deformation of the lid is not uniform. The displacements in the four springs are thus not equal.

To keep the springs affixed at the location and hold the lid tightly closed, a load of 30-pound prestress is applied to the springs.

In a nonlinear analysis, the stress and strain distribution in the pressurized bagless can will vary with different loading and boundary conditions. The bagless transfer can may be subject to three boundary conditions, namely,

- traction free over the exterior surface;
- four initially unstressed springs on the top of the lid, otherwise traction free;
- same as the previous boundary condition, except that the springs are preloaded with 30 pounds.

In all the three cases the large deformation and stresses are concentrated in the lid and the top rim area of the bagless can. In Tables 5-4 to 5-6, the maximum values of vertical displacement, von Mises equivalent stress and plastic strain are enumerated at the increment of every 100 psig pressure in the bagless can.

Due to the boundary conditions at the top of the lid, the stress distribution in the bagless can shows variation from case to case. However, the maximum values (irrespective of the locations in the bagless can) of the stress, strain and displacement are comparable in all the three cases. The results indicate that the effects of the springs initially reduce the stresses in the bagless can. As the pressure increases in the can, the extra constraints will heighten the stresses and deformation at certain locations. For the traction free case the calculation carries up to 1,000 psig pressure in the can. The maximum plastic strain is only 3.3%.

The ABAQUS calculation files are saved in the Common File System (CFS), under the Data Tree: /y6749/can-pressure. The input files are: canpress.inp, baglessonly.inp, canrest.inp.

5.4 Pressure load in the primary containment vessel

The pressure inside a closed thin-walled vessel has a tendency to deform the container into a sphere. This deformation process will minimize the total strain energy in the system and consequently the process reduces the stress gradient in the vessel.

The bagless transfer can has a flat top lid. The pressure over the lid will cause bending at the intersection of the lid edge and the top rim of the can as well as in the lid. Therefore during the pressurization stresses are concentrated in the lid and around the bagless can rim. The primary container has both ends covered with pseudo hemispherical caps. The stresses in the pressurized primary container are the dominantly membrane stress. The

stress gradient in the primary container is much less than that in the bagless transfer can under comparable pressure conditions.

The geometric configuration of the primary container is evidently appropriate for the pressure containment vessel. Nevertheless, the internal structures inside the primary container alter the stress homogeneity in the wall of the container. The pre-stressed springs on the top of the bagless can lid force the bottom of the bagless can to contact the bottom of the primary container. The size of the contact area is theoretically infinitesimal. Therefore, no matter how small the contact force is, the contact stress will be high. In the finite element analysis, the contacted elements increase the stiffness in the region. In a statically indeterminate structure, as this container system, the region of higher stiffness will store more strain energy. At the interface of two structural members, the weaker member will have more distortion.

When the primary container is pressurized internally, the bagless transfer can is supposedly subject to external pressure. In this analysis the pressure over the bagless can is ignored, such that the interference of the bagless can to the stress distribution in the primary container will be protrudent. Two distinct cases are considered, the material for both cases is the 304L stainless steel at 400°F temperature:

- A decorticated primary container without any structural components attached to it, is subject to internal pressure.

- The full container system which includes the primary container, the fitting, the springs and the bagless transfer can is pressurized over the inner wall of the primary container only.

The results of these two calculations are listed in Tables 5-7 and 5-8. The first problem is simply a cylinder with both ends capped with pseudo hemispherical shells. Pressure in the container is gradually increased up to 1,500 psig. The container remains elastic throughout the pressurizing process. The maximum von Mises equivalent stresses are in the caps on both ends of the cylinder. The actual location of the maximum stress in each of the caps is at the apex of the cap. The von Mises equivalent stresses in the cylinder are about three fourths of those in the caps. The deformation of the container is barely discernible.

The responses of the primary container that includes all the accessories to internal pressurization are shown in Table 5-8. The container is yielded under merely 100 psig pressure. The von Mises equivalent stress reached 34,394 psi that is higher than the elastic limit, 24,580 psi. The high stress is concentrated at the central bottom element where the bottom of the bagless can and the primary container are in contact. As the internal pressure in the primary container increases, the von Mises equivalent stress and plastic strain increase slowly in the container. The maximum stress and strain are still in the central bottom element. When the internal pressure increases up to 1,500 psig the maximum von Mises equivalent stress in that central bottom element reaches 36,727 psi. The plastic strain in that element is only 2.15% that is far from the 40% limit.

The hole at the apex of the top cap for the installation of the sampling tube may cause stress concentration in the cap. During the pressurization of the primary container the stress state in the cap is dominantly membrane stresses. The maximum radial (as well as circumferential) stress in the apex area is 13,852 psi for the internal pressure of 1,000 psig. With the stress concentration factor of two [Young, 1989], the maximum stress at the rim of the hole is 27,704 psi which is about 12.71% above the elastic limit, 24,580 psi. However, as the new DOE Standard [DOE Standard, 1994] recommended, that

primary containment vessels shall be designed to withstand 750 psig internal pressure at 400 °F. In this calculation the maximum radial stress at the apex with 800 psig internal pressure is 11,093 psi. Consequently the maximum stress at the rim of the hole is 22,186 psi which is within the elastic limit.

The primary containment vessel is durable under 1,500 psig internal pressure at 400°F temperature. This analysis connotes that in a boundary value problem a slight modification of the boundary conditions and/or the geometry of the original problem may drastically change the stress state in the system.

The ABAQUS calculation files are saved in the Common File System (CFS), under the Data Tree: /y6749/can-pressure. The input files are: canmike.inp, canoutpr.inp

5.5 *Stresses in the primary containment vessel with the laser sampler in locked position*

Kinematically this problem is symmetric about the plane that is normal to the flange surface (consequently parallel to the vertical plates) and passing the line connecting the centers of the two holes. The contact areas between the tips of the locking arms and the flange bottom surface are not physically symmetric. On one side the contact area is a 2-inch by 0.69-inch rectangular, while on the other side the contact area is depleted by a half of the small hole (Figure 4-4). This asymmetric contact condition will introduce high stress concentration in the region between the two holes. The pressure from the laser sampler is applied over the double-ring area on the top of the container cap (as described in Section 4.5 and depicted in Figure 4-4). A hole at the center of the cap is left open for expected stress concentration. The maximum pressure specified is 1,110 psi.

At the interface of the sampler arm tip and the fitting flange, the sampler arm tip is very stiff as compared with the flange. Initially the interface is flat and the two surfaces are in perfect contact. The contact characteristics will be modified at the moment the laser sampler touches the top of the container cap. The kinematic symmetry of the problem suggests that the deformed flange may contact the sampler arm tips along the center line connecting the centers of the two holes in the flange. In reality, the contact at each tip is reduced to point contact. The contact point is close to the edge of the small hole on one side. On the other side the contact point is near the edge of the large hole.

When the applied pressure is less than 300 psi, the initially flat flange surface is deformed into a surface with concave upward. The von Mises stresses are concentrated in the areas of contact. The maximum von Mises stress is in the interstitial region between the two circular holes. The magnitude of the maximum von Mises stress decreases with increase in applied pressure. The region of stress concentration gradually spreads as the applied pressure on the container cap increases.

In the vertical plates, the region of stress concentration also shifts as the applied pressure increases. The high stress region is adjacent to the lines of intersection of the flange and the vertical plates. The maximum von Mises stress zone in each plate moves from the area near middle of the line to the ends of the line as load increases from 0.6 psi to 155 psi. During this initial loading spell, the magnitude of maximum von Mises stress decreases from 1,604 psi to its minimum, 1,241 psi. As the applied pressure (on the top of the container) aggrandizes further, the maximum von Mises stress in the vertical plates grows linearly.

The stress distribution in the container top cap is heavily influenced by the structural discontinuities over the cap surface. With applied pressure around the double ring in the neighborhood, the small center hole absorbs most of the strain energy. At the intersection of the cap and each of the vertical plates, the structural discontinuity also causes stress concentration. The maximum von Mises stress in the cap is at the rim of the small center hole. The maximum von Mises stress grows linearly with the applied pressure.

The characteristics of deformation of the fitting members vary reconditely as the applied pressure increases. In the range from 0.6 psi to 350 psi, the flange deforms into a shallow bowl with two dimples at bottom where the flange touches the rigid surface. At the intersection of the flange and vertical plates, the orthogonality between the flange and the vertical plate is maintained during the loading process. Since the flange bends upward, the orthogonality condition forces the vertical plates bend outward. The upward bending of the flange and the outward arching of the vertical plates lift the container up slightly.

The over all loading in this structural system is considerably small. The stress and strain state is within the elastic limit of the material through the whole loading history. Consequently the deformation of the structural members is diminutive. In order to demonstrate the characteristics of the deformation, the deformed configuration of the fitting system is magnified 600 times for clarity. Figure 5-12 shows the deformed fitting system with only 2.10 psi load on top of the cap. In this figure the bending and warping of the flange and the outward arching of the vertical plates are distinguishable.

Gradually, as the applied pressure increases, the two vertical plates pull the flange down. Along the axis of rigid support, the flange still bends upward, whereas on both sides the pulling of the vertical plates drives the wings of the flange down. The orthogonality of the connection pushes the vertical plates arching inward to each other. In Figure 5-13 it shows that at 1,162.5 psi cap pressure, the deformed flange turns into a saddle surface and the vertical plates bend toward the center. The cap is slightly depressed in the central area. The saddle surface can be described by the surface of a hyperbolic paraboloid.

The peculiar characteristics of stress distribution and deformation during the loading history prompt a close examination of the fitting system. All the members are of the same material, 304L stainless steel. The thickness of the flange and vertical plates is 0.25 inches. The container cap is 0.258 inches in thickness that is only slightly thicker than other members. The dome-shaped configuration of the container cap is structurally stronger. Shell members in a structure are vulnerable to bending stresses. In most cases, shell structures constructed with consistent smaller radii of curvature will be less affected by bending under uniform pressure. The flange and vertical plates are susceptible to bending stress from the out-of-plane loading. Primarily the cap is under top pressure, the vertical plates transmit the loading through membrane stress to the flange. The flange with rigid supports and out-of-plane pulling (from the vertical plates) will bend accordingly. The bending of the flange rotates the vertical plates at the intersections, thus the plates bend correspondingly. The complexity in this deformation leads to the unique characteristics of stress distribution in the fitting system. Initially the maximum von Mises stress in the flange is concentrated in the interstitial region between the two circular holes. As the cap top pressure increases the region of maximum stresses spreads to both sides of the center line along the rim. The magnitude of the maximum von Mises stress decreases as the applied pressure steadily increases until it reaches 1534.20 psi. At this level of pressure the maximum value of the von Mises stress in the flange attains its minimum, 7,461 psi. Further increase in applied pressure will raise the stress level in the flange.

Through the specified loading history, the stress-strain state in the fitting system remains within elastic limit. The system is linear in material behavior. Nevertheless, the variation of contact conditions with respect to loading turns this system into a nonlinear boundary value problem.

ABAQUS provides two formulations for modeling the interaction between a deformable body and an arbitrarily shaped rigid body that may move during the history being modeled. The first is a small-sliding formulation in which the contacting surfaces can only undergo relatively small sliding relative to each other, but arbitrary rotation of the surfaces is permitted. The second is a finite-sliding formulation where separation and sliding of finite amplitude, and arbitrary rotation of the surfaces, may arise.

The elements with small-sliding capability can be used to model the interaction between two deformable bodies or between a deformable body and a rigid body in two and three dimensions. The stress-displacement interface element for use with 3-D 4-node shell elements is INTER4. For arbitrary rigid surfaces involved in finite-sliding contact, ABAQUS uses Bézier surfaces to smooth the faceted rigid element mesh.

If the sliding at the interface between the flange and the tips of the sampler arms is small as compared with other components of displacements, theoretically either the interface element INTER4, or the Bézier surfaces should be applicable to the present problem. In general the two approaches accommodate different mathematical formulations and constraints [ABAQUS, 1993]. For a problem involving loading dependent boundary conditions, the variation of contact attribute at the boundary will influence the solution profoundly. Therefore, both small-sliding interface elements INTER4 and finite-sliding Bézier surfaces are considered in this analysis.

The interface element INTER4 is actually an 8-node, two-piece element with each piece attached to one side of the bodies in contact. As discussed previously, the von Mises stress in the flange varies inversely with respect to the applied pressure on the cap top. Figure 5-14 plots the von Mises in the flange, container top cap and vertical plates. In this calculation the applied pressure advances to 2,200 psi that is well beyond the specified loading of 1,110 psi. Except in the pressure range from 0.6 psi to 154.80 psi, the stresses in the vertical plates increase linearly with respect to the applied pressure. The container top cap is comparatively much stiffer. The maximum von Mises stress in the cap (actually at the rim of the central hole) varies linearly with the applied pressure. Table 5-9 lists the maximum von Mises stresses in all the members at every stage of the pressure history.

Depending on the direction, magnitude, and location of the applied loads as well as the configuration of the structure, the interaction between a deformable body and a rigid surface may cause multiple separation, contact and sliding of finite amplitude during the history of loading. Bézier surfaces are used to smooth the faceted rigid element mesh. The deformed configuration of the fitting system using Bézier surfaces is closely matching with that using INTER4 interface elements. The maximum von Mises stresses in the system are also comparable for the two calculations using small-sliding and finite-sliding contact interfaces. The results are shown in Figure 5-15 and listed in Table 5-10 for applied pressure up to 1,118.70 psi that is little over the specified load (1,110 psi). The maximum von Mises stresses in both calculations are cross plotted in Figure 5-16 for comparison. The close matching of the two sets of solutions from different conceptual approaches indicates that the results obtained in this analysis are at least mathematically correct.

The maximum von Mises stress in the fitting system for the entire loading process is 12,408 psi. The maximum von Mises stress is at the interstitial region between the two circular holes of the flange, while the applied pressure on the container top is at the minimum, 0.6 psi. As the applied pressure steadily increases, the stress in the vertical plates reaches the same value, 7,480 psi, as that in the flange when the applied pressure at 1,590 psi (Figure 5-16). At the end of the applied pressure of 2,200 psi that is almost double the value of the specified pressure, the maximum von Mises stress in the vertical plates is only 10,089 psi that is less than the maximum stress in the flange at the beginning of loading. The maximum von Mises stress of 12,408 psi is well below the initial yield stress, 37,840 psi. The whole system with nonlinear boundary conditions behaves elastically during the loading process. The system is structurally sound under this type of loading considered in this analysis. In realistic situations the applied pressure may not be axially symmetric and over the surface of contact the friction may be insufficient to prevent the flange from slipping. Different loading and interface contact conditions in the problem may yield results different from those discussed above.

The mechanical constraints at the contact interface of the flange and the sampler arms give rise to nonlinear stress concentration in the flange. The interface elements INTER4 permit more freedom at the interfaces. In further relaxing the constraints at the interfaces, the initial stress concentration in the flange is removed. The stresses in all parts of the fitting system vary linearly with respect to the increase of pressure on top of the cap. The maximum von Mises stresses in the flange, cap and the vertical plates are shown in Figure 5-17. As the pressure reaches 2,200 psi the maximum von Mises stresses in the flange, cap and the vertical plates are 8,361 psi, 5,663 psi, and 7,651 psi respectively. Except the initial stress concentration in the flange, the maximum stresses are comparable in all the three calculations. The maximum von Mises stress in the flange is always in the interstitial region between the two circular holes of the flange. Figure 5-18 shows the deformed configuration of the fitting system with the displacement magnified 600 times.

The ABAQUS calculation files are saved in the Common File System (CFS), under the Data Tree: /y6749/can-sampler. The input files are bbb.inp, interf.inp and interfnosf.inp.

6.0 CONCLUSION

In the mathematical modeling of a physical system, there are many uncertainty factors in material properties, geometric configurations, boundary conditions as well as loading conditions. Through mechanical testing and modeling experience, the results from the analysis can be fully interpreted in terms of physics.

The dynamic analysis of the vertical 30-foot upright drop includes both the internal bagless transfer can and the primary container. The drop inflicts the bottom of the primary container that is in direct impact against the rigid ground surface, with large strain. However, the boundary conditions around the bagless can enhances the wave propagation in the medium and consequently it intensifies the impact effect. The plastic stress and strain in the bagless transfer can are much higher than those in the primary container. The maximum plastic strain in the primary container is 24.33 %, whereas in the bagless transfer can the maximum plastic strain is 35.40 %. The allowable plastic strain in the 304L stainless steel is 40 %.

The dynamic analysis provides capacious guidance for the quasi-static analysis of the inclined upside down drop of the containers. The inclined upside down drop of the containers exposes the container top fitting structure to the most vulnerable position. The

internal bagless transfer can which is supported by soft springs will be shielded from severe impact. The drop impact will inflict elastic and plastic deformation upon the container. It is conservative, if the total kinetic energy is imposed upon the fitting members alone in plastic dissipation. The maximum plastic strain at the intersection of the flange and one of the vertical plates reaches 37.75%. The sampler tube at the top of the container is bent with a maximum plastic strain of 21%. The fitting system survives the conservative impact loading.

The 30-foot free fall impact in both upright and upside-down drops is considerably severe. However, the analysis confirms that the design of the containers is mechanically adequate to resist dynamic impact.

The primary container and the bagless transfer can are quite durable for internal pressure loading. The specified pressure for the primary container is 1,000 psig (it is reduced to 750 psig according to the DOE Standard [DOE Standard, 1994]) at 400°F, whereas the specified pressure for the bagless transfer can is only 500 psig at room temperature. The analysis shows that the maximum plastic strain in the primary container is only 2.15% for applied pressure at 1,500 psig with the bagless transfer can in contact at the bottom of the container. However, in the primary container without the interference of the bagless transfer can, the container stress state remains elastic for applied pressure at 1,500 psig. The bagless transfer can attains 3.3% of plastic strain at 1,000 psig that is twice the prescribed magnitude. With the specified pressure of 500 psig the plastic strain in the bagless transfer can reaches only 1.76%.

The contact boundary conditions and the intricate loading paths in the laser sampling process connote nonlinearity in this analysis. The suggested total load on the top of the primary container is 650 pounds or 1,110 psi in pressure. The whole fitting remains within elastic limit when the applied pressure reaches 2,200 psi that is almost twice the specified load.

This analysis considered five hypothetical mechanical problems of the plutonium storage containment vessels. From different point of view, under specific loading conditions the plutonium storage containment vessels are proved to be structurally intact in each case. The loading and boundary conditions are mechanically conservative according to the principles of applied mechanics.

7.0 REFERENCES

ABAQUS® (version 5.3-1N), 1993, is a registered trademark of a finite element analysis computer code developed by Hibbitt, Karlsson & Sorensen, Inc., 1080 Main Street, Pawtucket, Rhode Island 02860.

Achenbach, J. D., 1973, *"Wave Propagation in Elastic Solids"*, North-Holland Publishing Company, Amsterdam.

Complex 21 Plutonium Storage Facility Material Containment Team Technical Data Report, 1993.

Cristescu, N., 1967, *"Dynamic Plasticity"*, North-Holland Publishing Company, Amsterdam.

DOE Standard, 1994, "Criteria for Safe Storage of Plutonium Metals and Oxides", Draft, DOE Standard, November 15, 1994 4:00 PM Draft, DOE-STD-3013-94, October 1994.

Fung, Y. C., 1965, *"Foundations of Solid Mechanics"*, Prentice-Hall, Inc., Englewood Cliffs, New Jersey.

Goldsmith, W., 1960, ***"Impact, The Theory and Physical Behaviour of Colliding Solids"***, Edward Arnold (Publishers) Ltd., London.

Gong, C., 1977, "Dispersion and Anisotropy Induced in Finite Element Analysis," a paper presented at *Fourth International Conference on Structural Mechanics in Reactor Technology*, San Francisco, CA, U.S.A. August 15-19, 1977.

Hibbitt, Karlsson & Sorensen, Inc., 1993, "*ABAQUS Theory Manual*," version 5.3.

Hill, R., 1950, "*The Mathematical Theory of Plasticity*," chapter II, section 2, pp. 14-23, Oxford at the Clarendon Press.

Imrich, K. J., Sindelar, R. L., 1994, "Corrosion Evaluation of F-Area Tank 17.1 (U)", WSRC-TR-93-619, Rev. 1. A technical report to A. P. Gouge.

Love, A. E. H., 1944, "*A Treatise on The Mathematical Theory of Elasticity*," Cambridge: University Press, fourth edition 1927. Reprinted New York: Dover Publication.

Malvern, L. E., 1969, "*Introduction to the Mechanics of a Continuous Medium*," Chapter 6, Constitutive Equations, Prentice-Hall, Inc, Englewood Cliffs, New Jersey.

Mindlin, R. D., 1960, "Waves and Vibrations in Isotropic, Elastic Plates", in J. N. Goodier and N. J. Hoff (eds.), *Structural Mechanics*, Pergamon Press, Oxford, 199-232.

P3/PATRAN® (version 1.2), 1993, is a registered trademark of PDA Engineering, Software Production Division, 2975 Redhill Avenue, Costa Mesa, California 92626.

Sindelar, R. L., 1993, "Tensile Properties of Type 304/304L Stainless Steel for Impact Deformation Analysis of Nuclear Materials Containers (U)", SRI-MTS-93-3113, Inter Office Memorandum to R. F. Miller, November 10, 1993.
Note: This Memorandum is attached to this Report on pages 84 ~ 90.

Technical and QA Plan, 1993, "Certification of the ABAQUS Finite Element Code," Task No. 91-055-1, by E. P. Hope, Revision 1, March 3, 1993.

Young, W. C., 1989, *"Roark's Formulas for Stress & Strain"*, Sixth Edition, (Table 37, page 732), McGraw-Hill, Inc., New York, New York.

8.0 ACKNOWLEDGMENT

The authors would like to thank Ms. Harriet Bunch Haynes of Remote Engineering & Complex Support, Equipment Engineering, for her continuous unfailing supports to our needs in engineering drawings and rationalization of the laser sampling operations.

FIGURES

Figure 1-1. The Reference Oxide/Metal Primary Containment Vessel Concept.

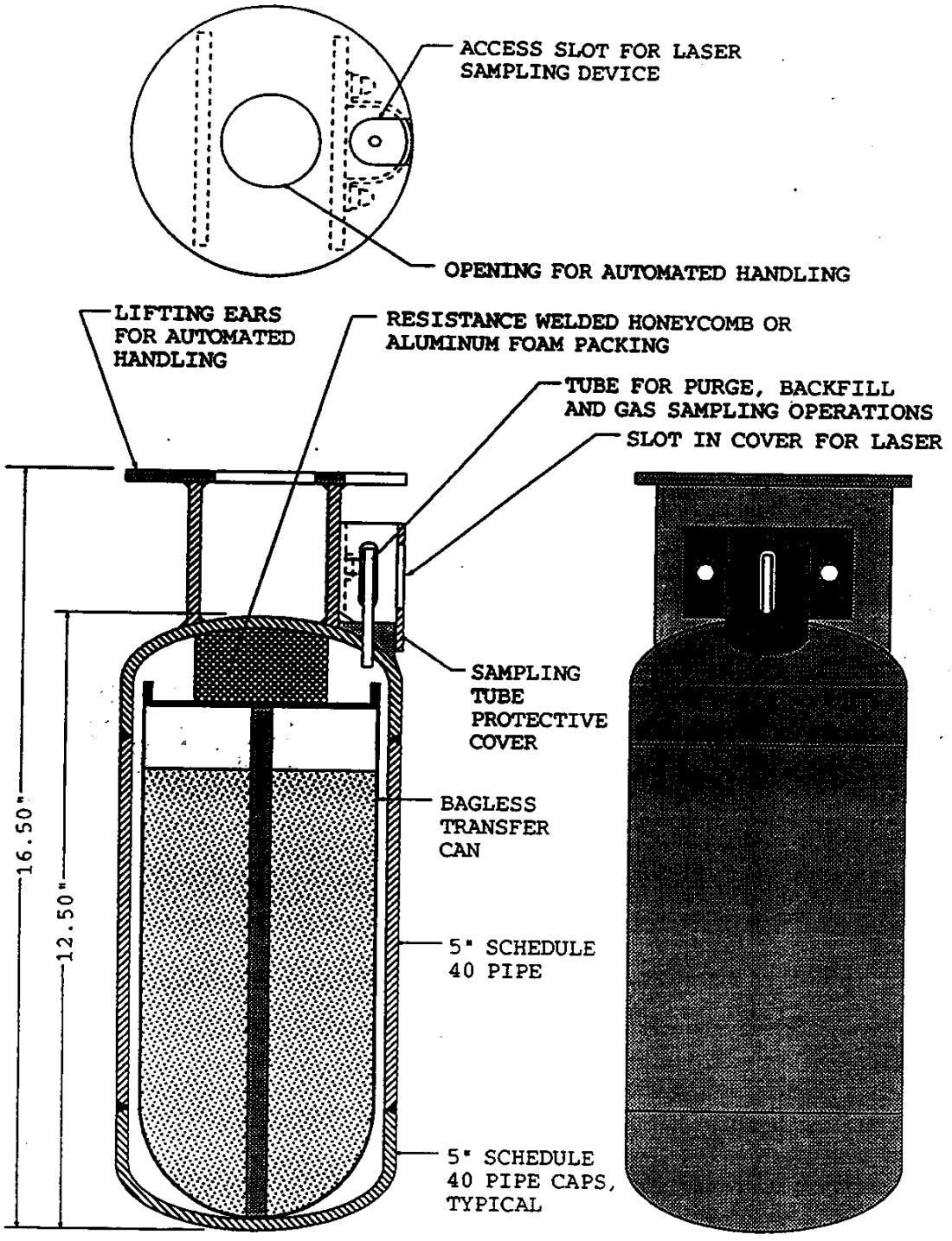

Figure 1-1. The Reference Oxide/Metal Primary Containment Vessel Concept.

Figure 2-1. The Present Design of the Primary Containment Vessel.

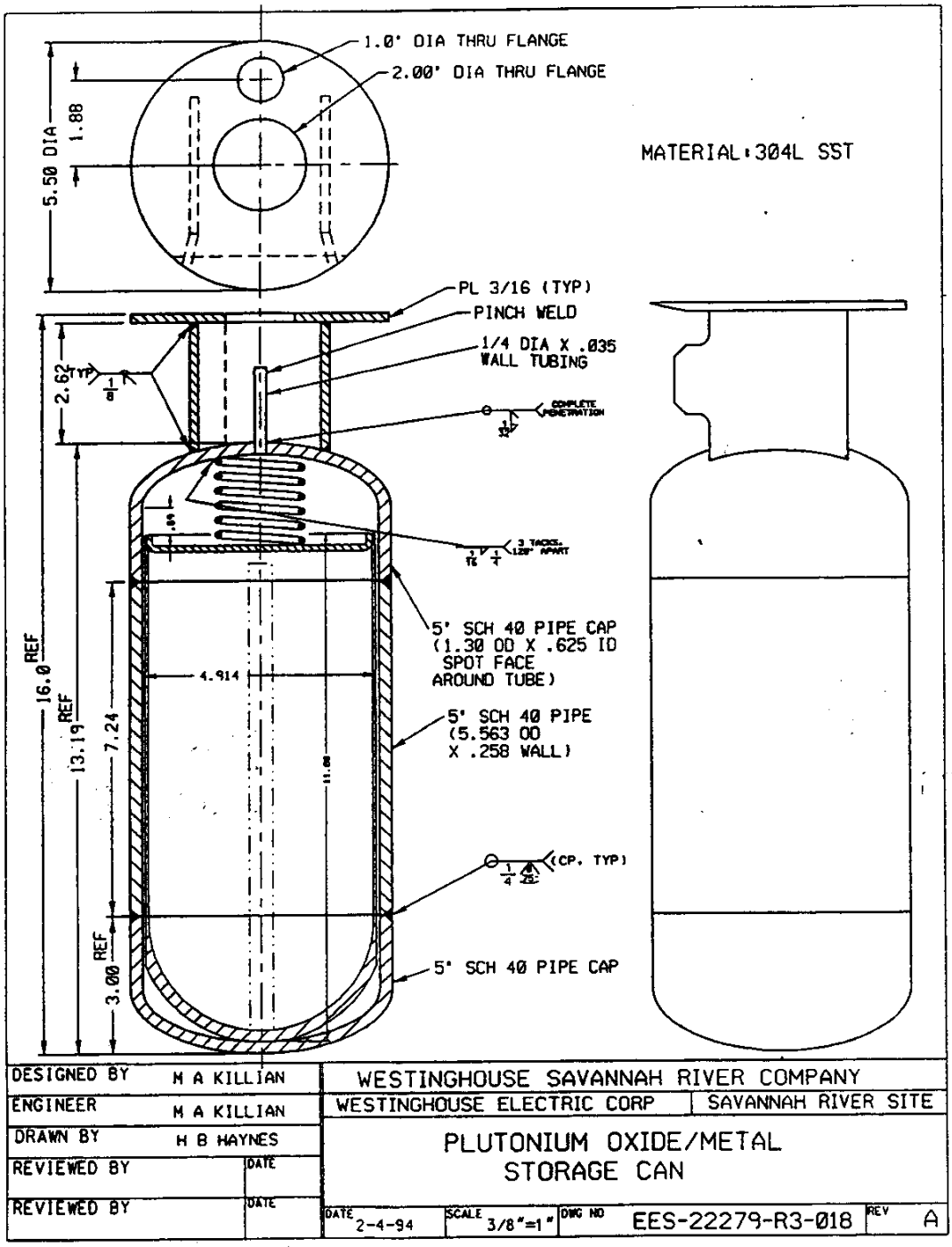

Figure 2-1. The Present Design of the Primary Containment Vessel.

Figure 2-2. Stress strain curves for 304 and 304L Stainless Steel (in True Scale)

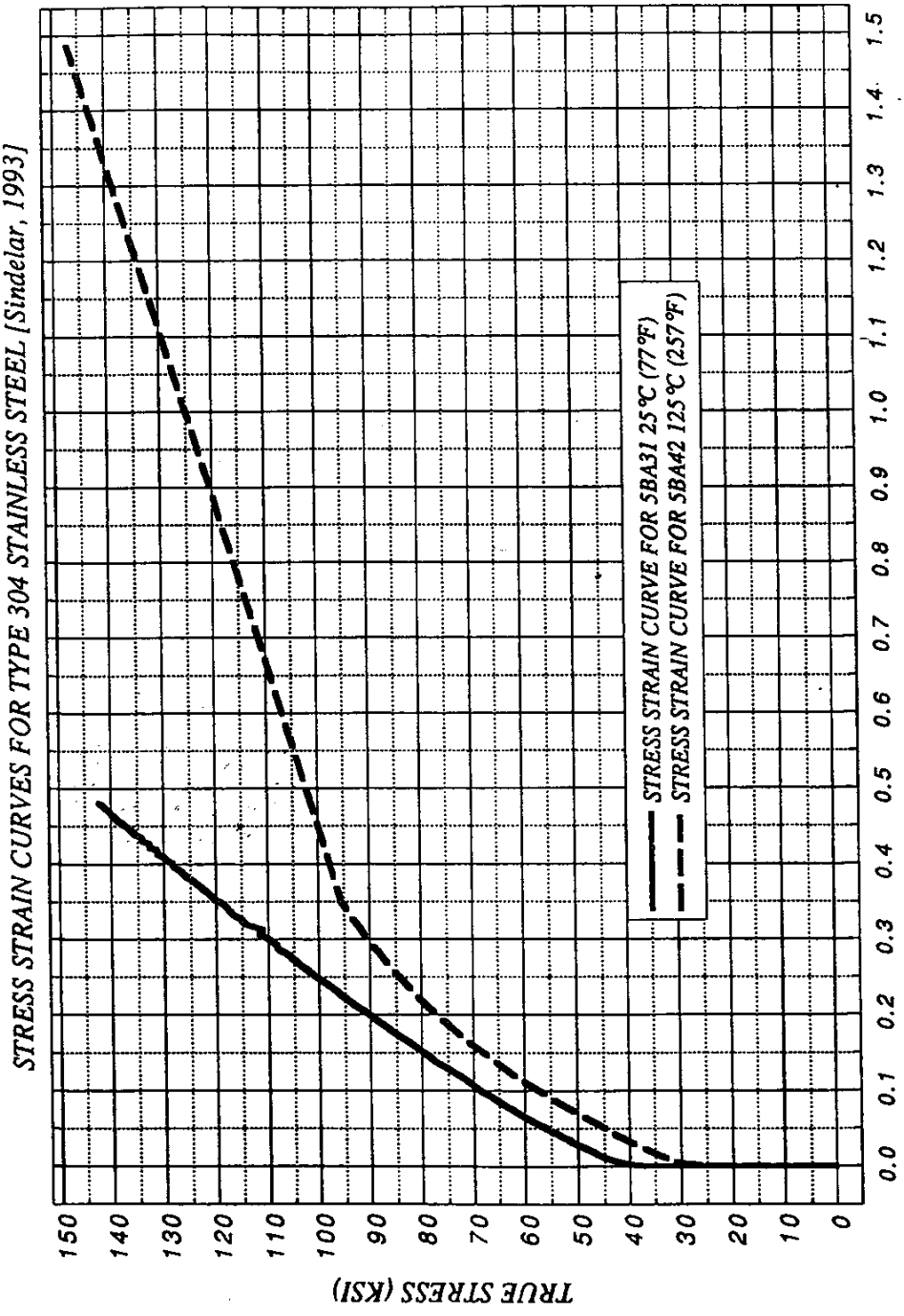

Figure 2-2. Stress Strain Curves for 304 and 304L Stainless Steel (in True Scale).

Figure 2-3. Stress strain curves for 304 and 304L Stainless Steel (in Engineering Scale)

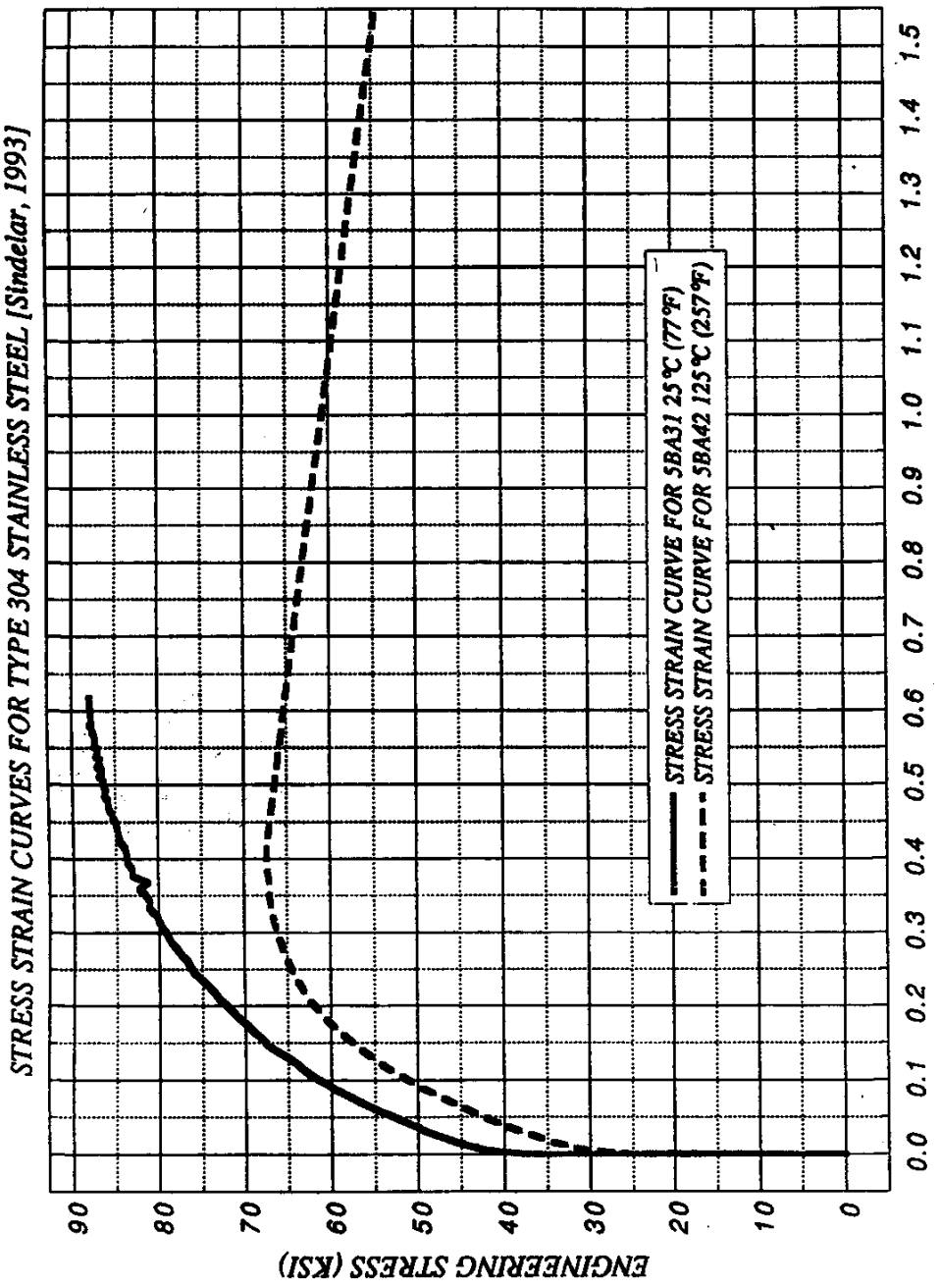

Figure 2-3. Stress Strain Curves for 304 and 304L Stainless Steel (in Engineering Scale).

Figure 4-1. Two Dimensional Finite Element Analysis Mesh of the Primary Container and the Bagless Can for the Upright Drop Case.

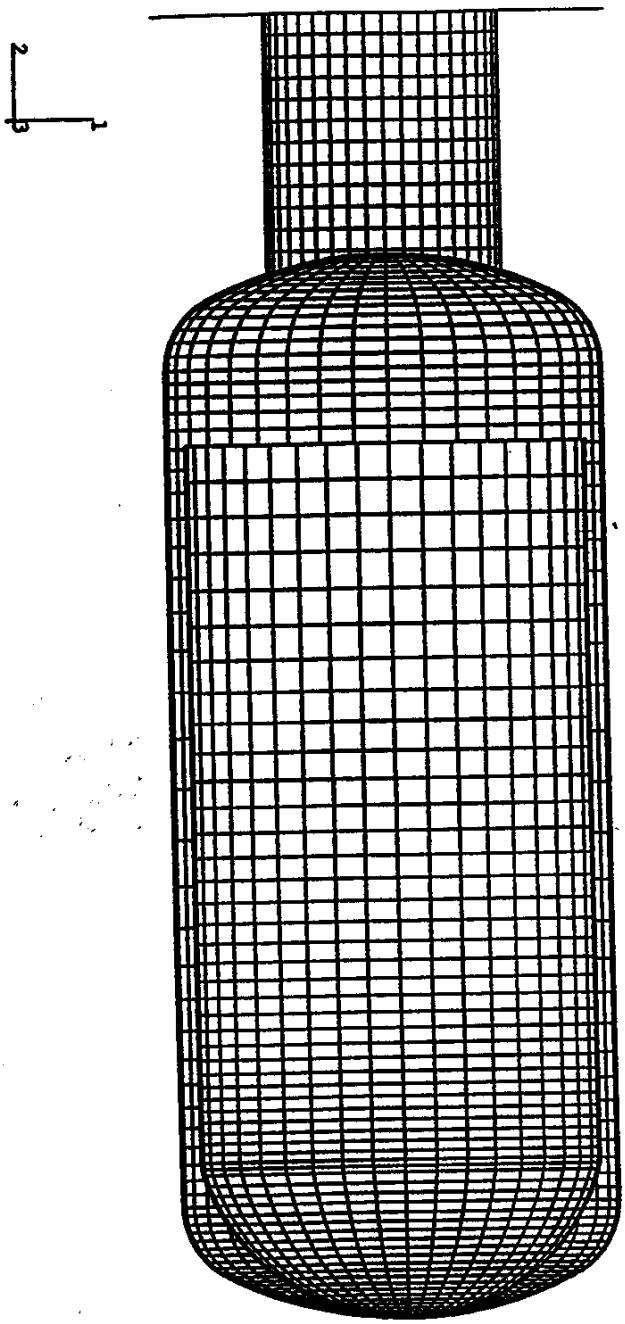

Figure 4-1. Two Dimensional Finite Element Analysis Mesh of the Primary Container and the Bagless Can for the Upright Drop Case.

Figure 4-2. ***Three Dimensional Finite Element Analysis Mesh of the Primary Container for the Upside-Down Drop Case.***

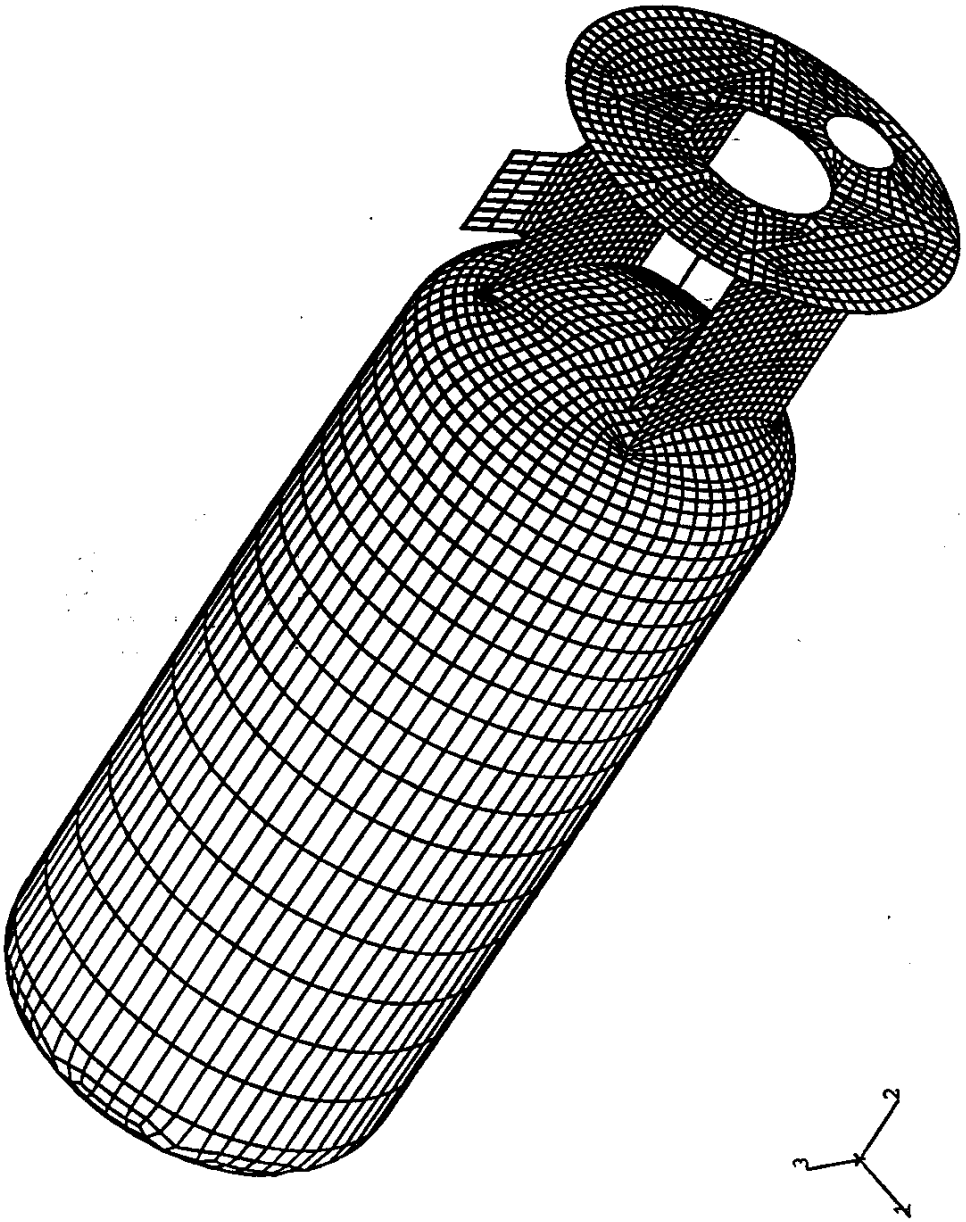

Figure 4-2. Three Dimensional Finite Element Analysis Mesh of the Primary Container for the Upside-Down Drop Case.

Figure 4-3. ***The Laser Sampler Assembly.***

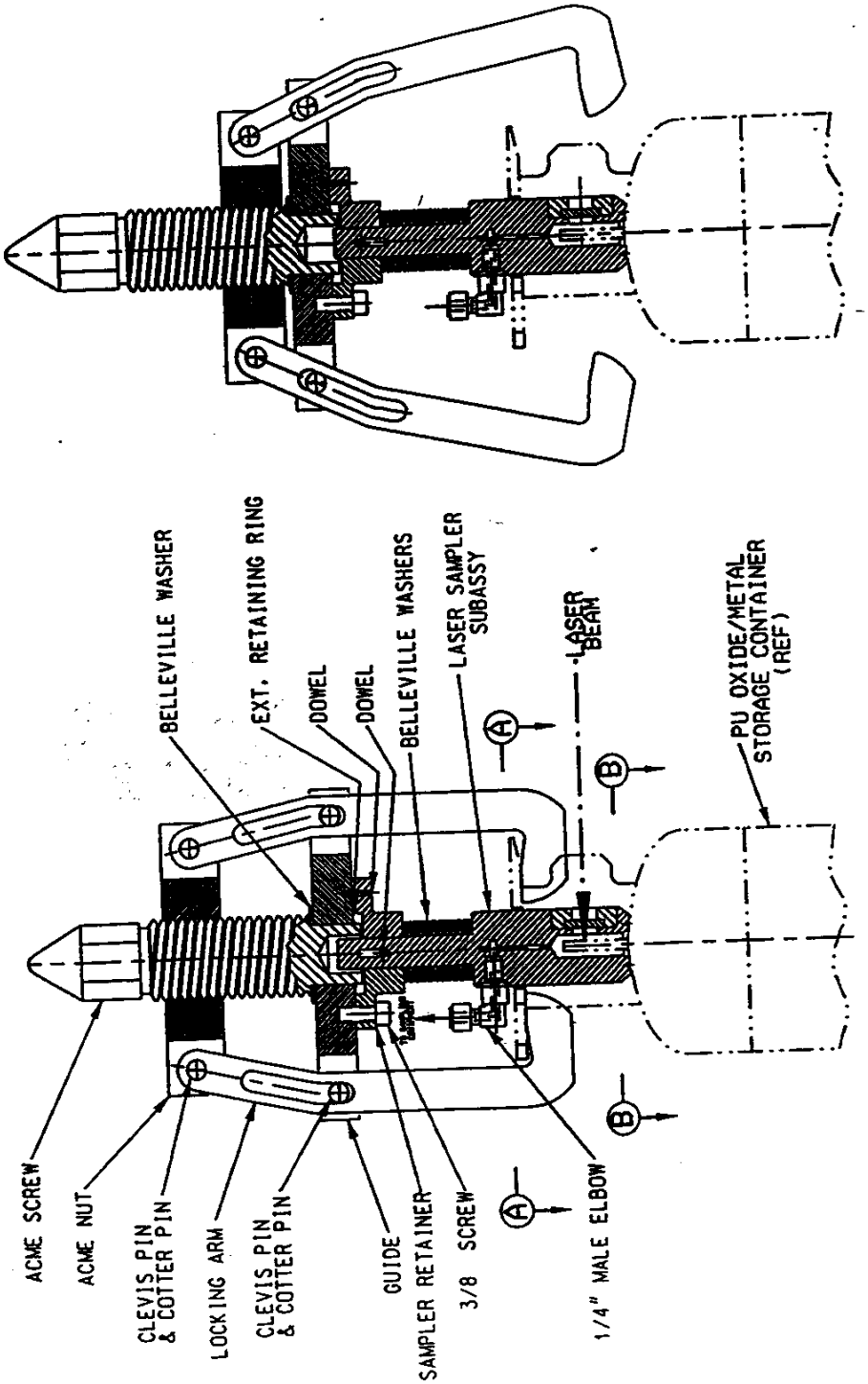

Figure 4-3. The Laser Sampler Assembly.

Figure 4-4. The Contact Areas between the Flange and the Arms (Section A-A). The Contact Areas between the Laser Sampler and the PU Container (Section B-B).

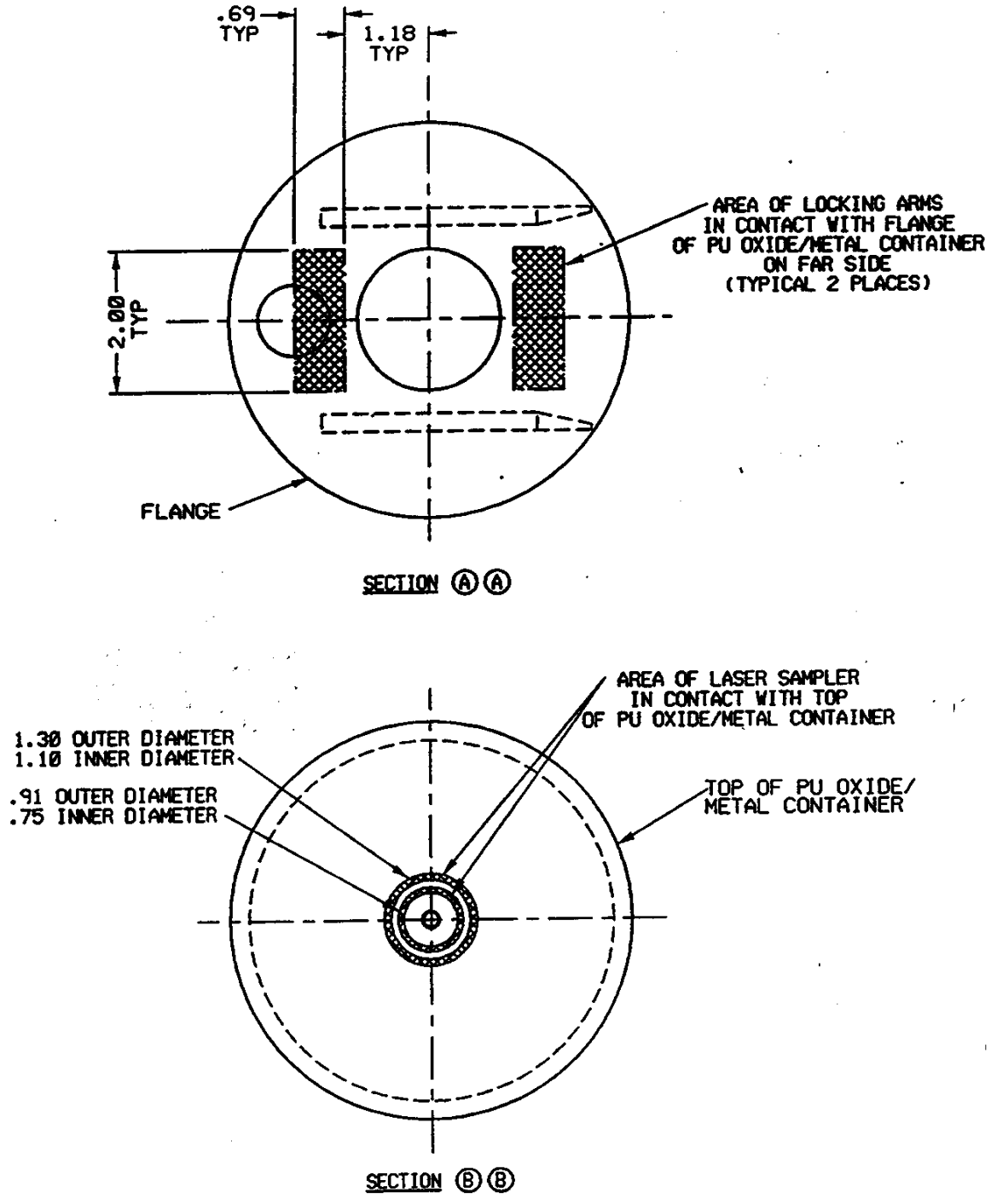

Figure 4-4. The Contact Areas between the Flange and the Arms (Section A-A). The Contact Areas between the Laser Sampler and the PU Container (Section B-B).

Figure 4-5. ***Three Dimensional Finite Element Analysis Mesh of the upper portion of the Primary Container for the Laser Sampling Case.***

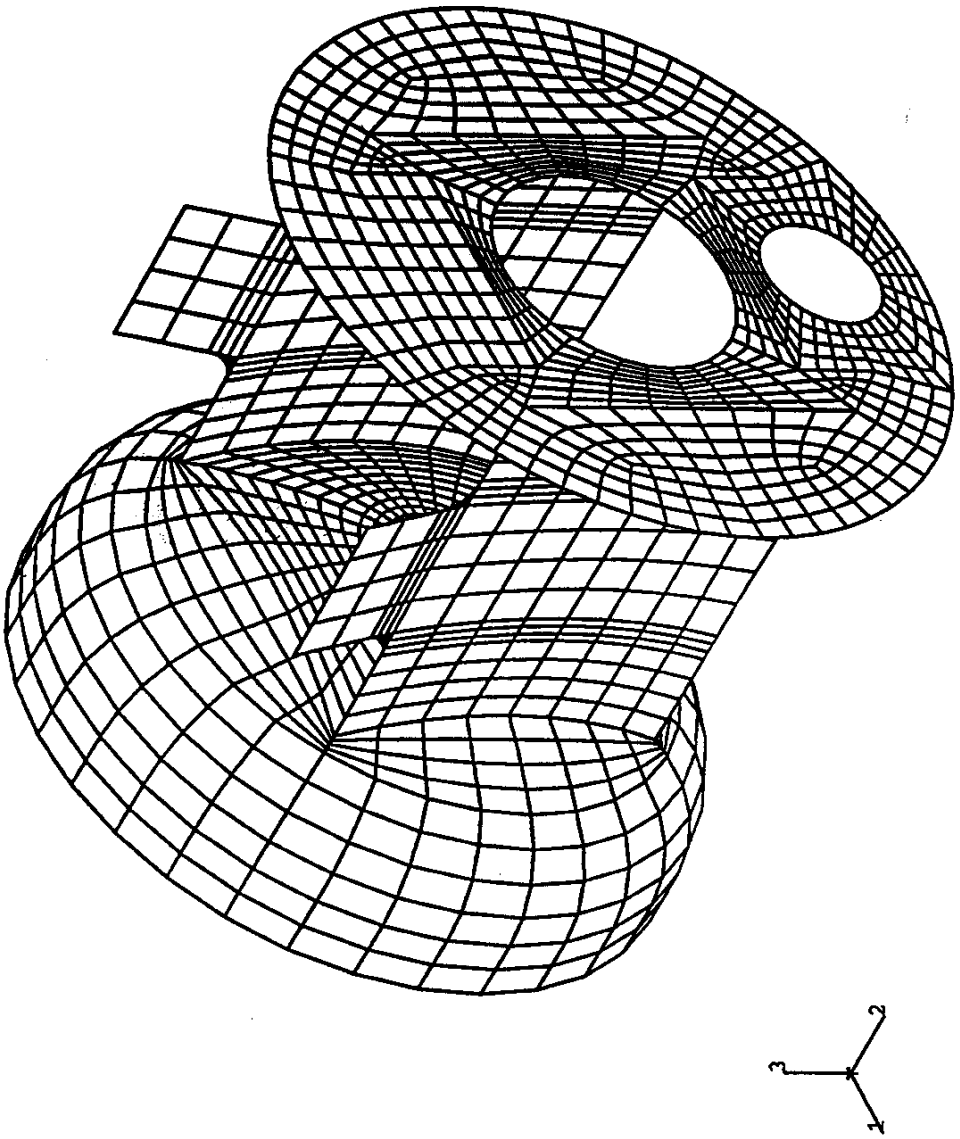

Figure 4-5. Three Dimensional Finite Element Analysis Mesh of the upper portion of the Primary Container for the Laser Sampling Case.

Figure 5-1. ***Maximum von Mises Stress in the Primary Container and the Bagless Can.***

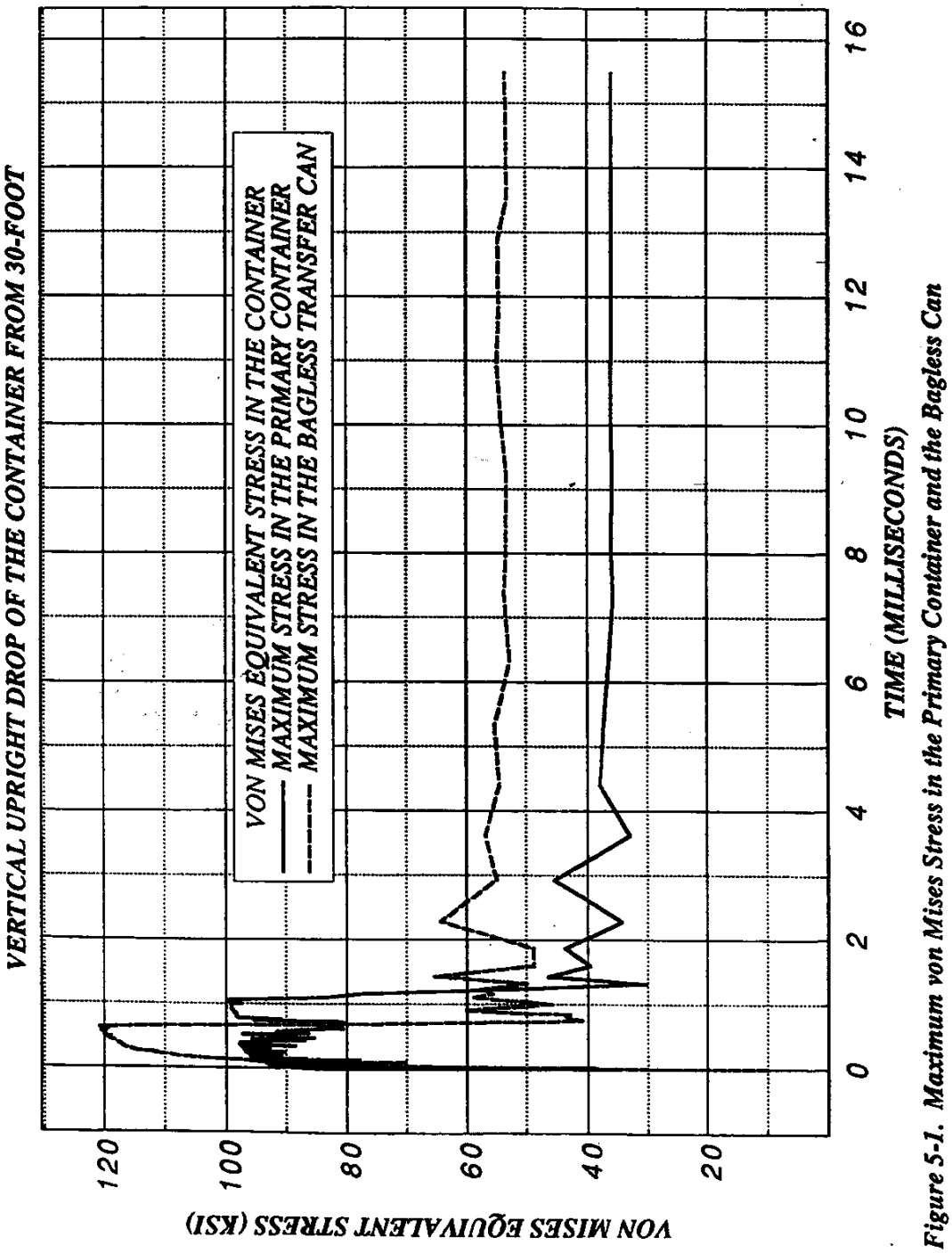

Figure 5-1. Maximum von Mises Stress in the Primary Container and the Bagless Can

Figure 5-2. von Mises Equivalent Stress in the Bagless Can in the First Millisecond.

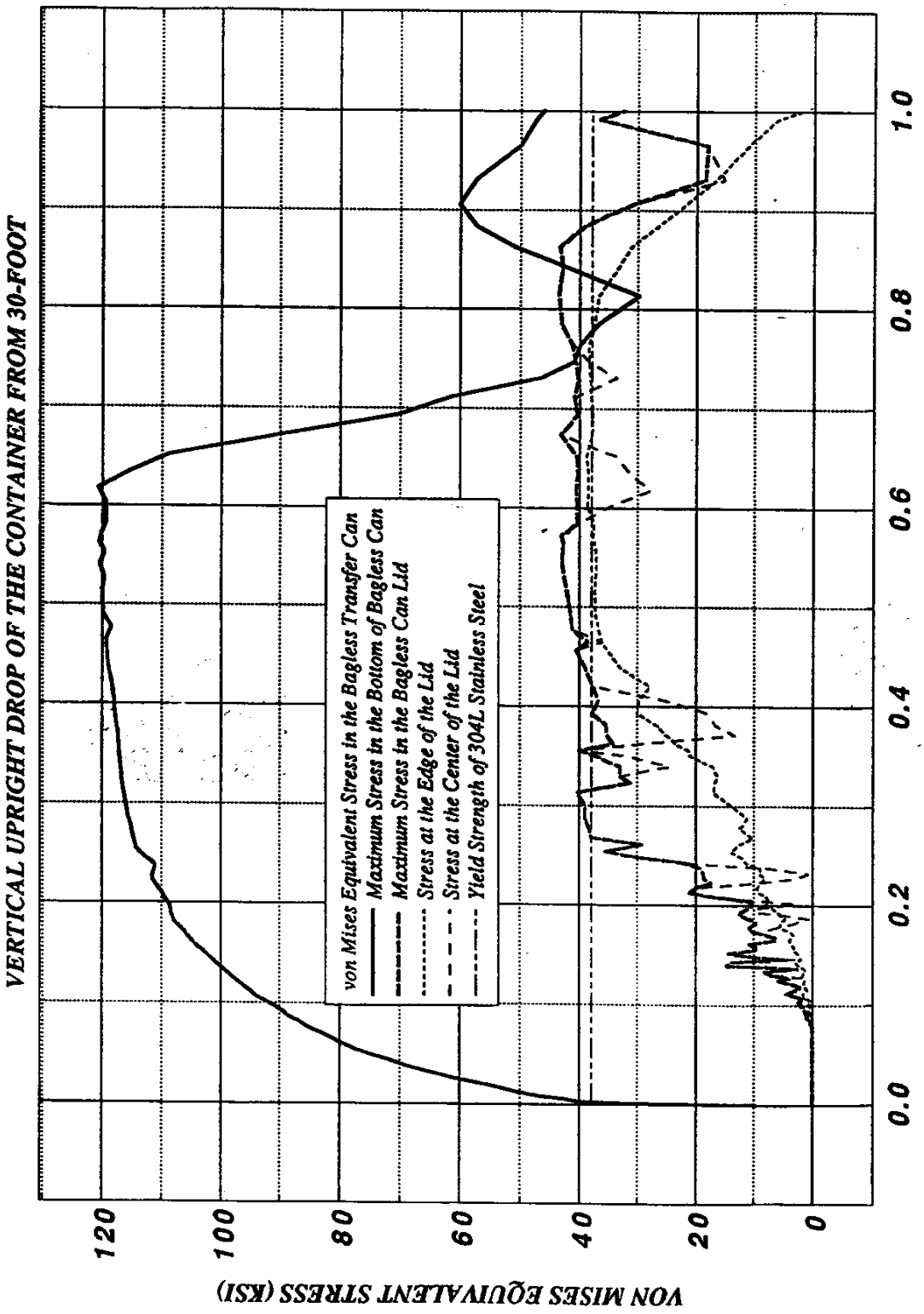

Figure 5-2. von Mises Equivalent Stress in the Bagless Can in the First Millisecond

Figure 5-3. Maximum von Mises Equivalent Stress in the Primary Container and Bagless Can.

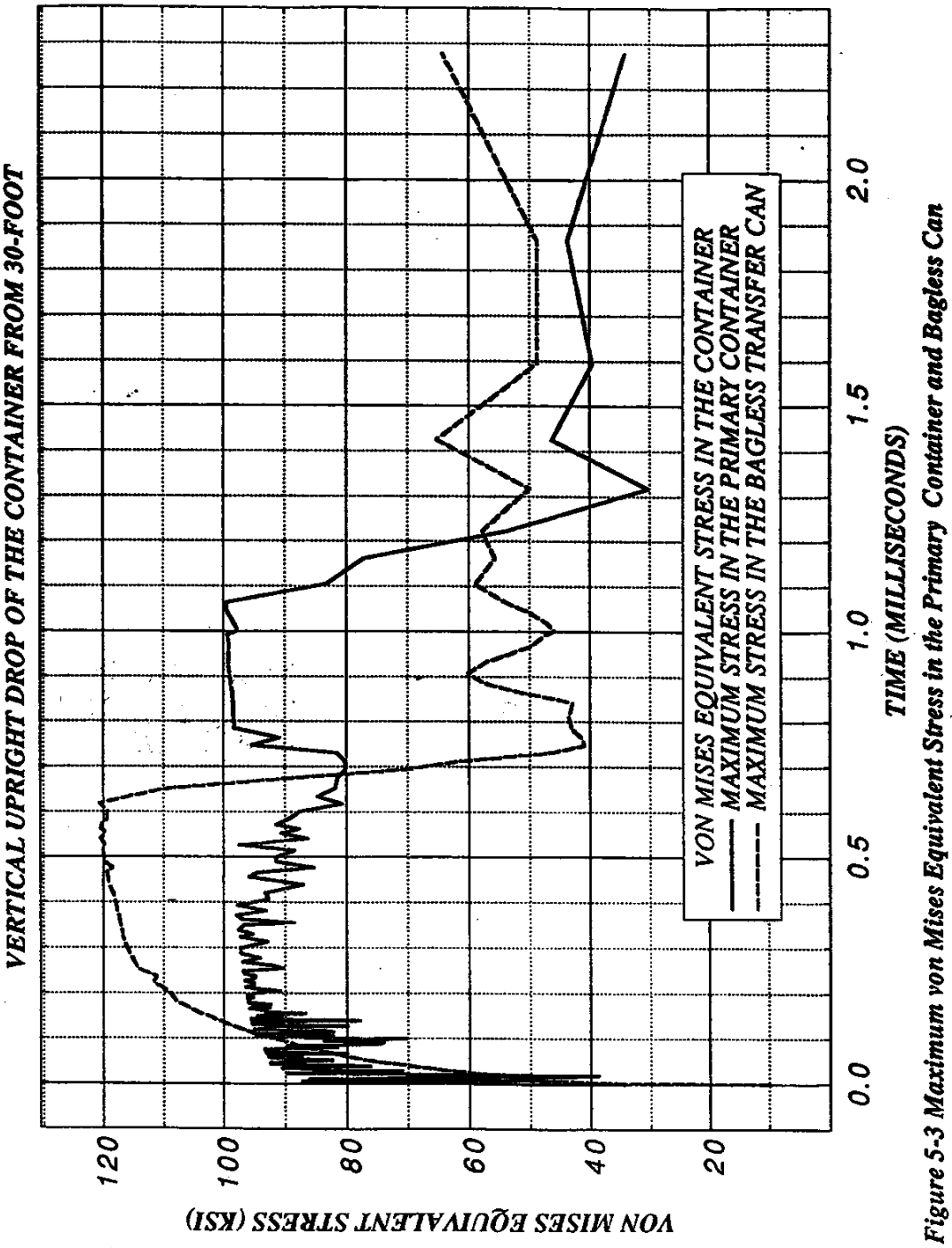

Figure 5-3 Maximum von Mises Equivalent Stress in the Primary Container and Bagless Can

Figure 5-4. ***Energy Transfer and Dissipation in the Container System (15 milliseconds).***

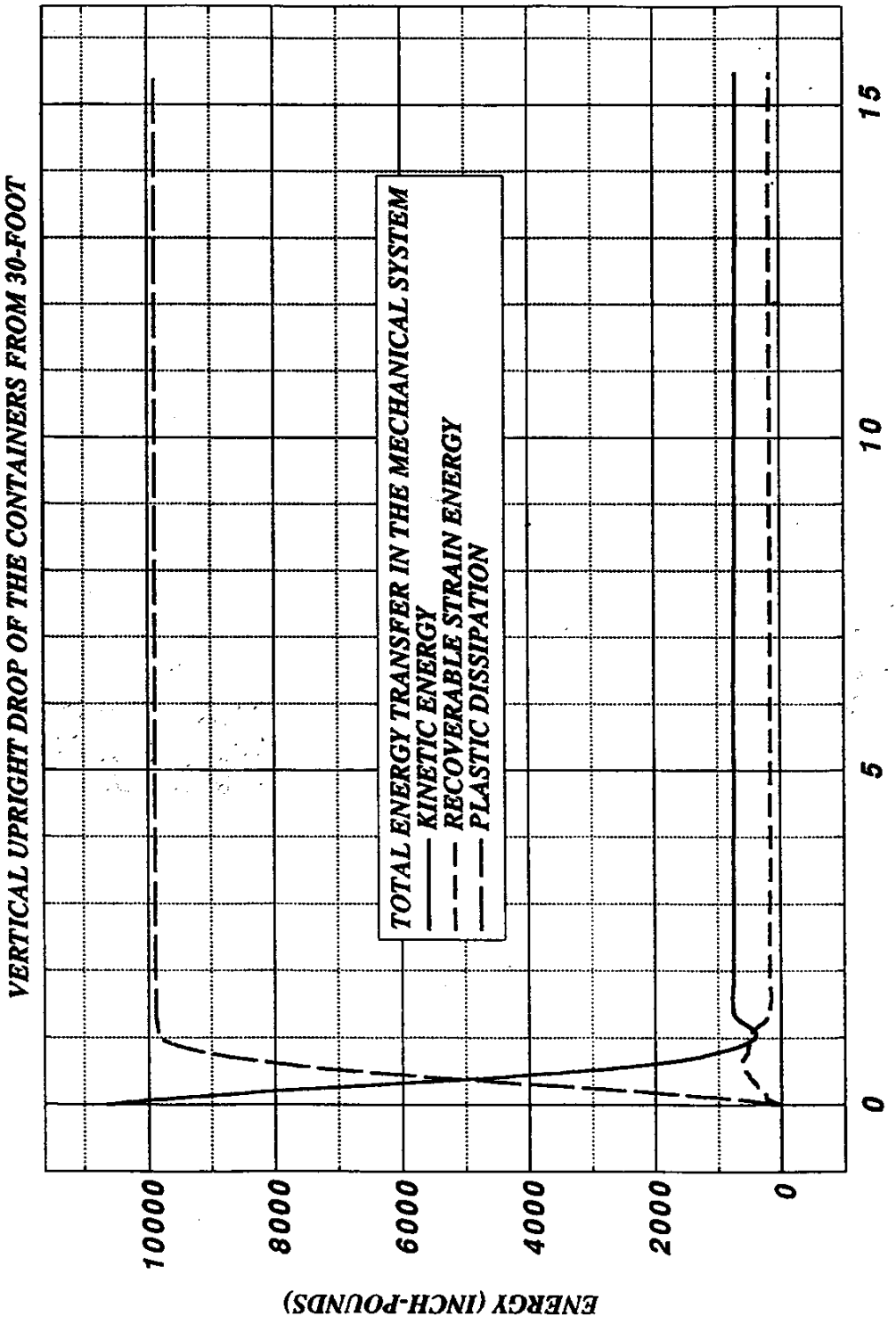

Figure 5-4. Energy Transfer and Dissipation in the Container System (15 milliseconds)

Figure 5-5. ***Energy Transfer and Dissipation in the Container System (4 milliseconds).***

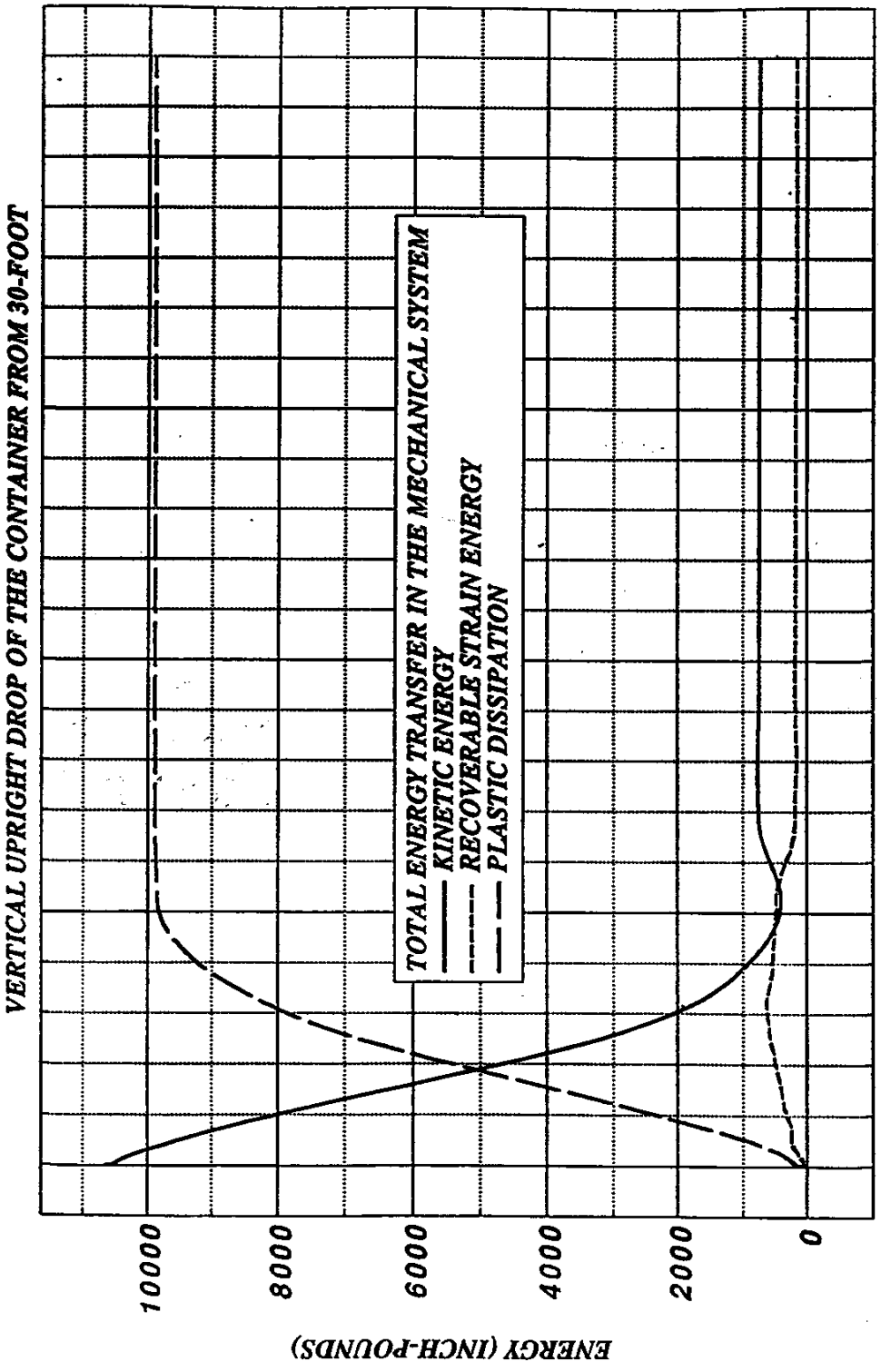

Figure 5-5. Energy Transfer and Dissipation in the Container System (4 milliseconds)

Figure 5-6. ***Deformation of the Primary Container and the Bagless Transfer Can at Four Stages during the Impact.***

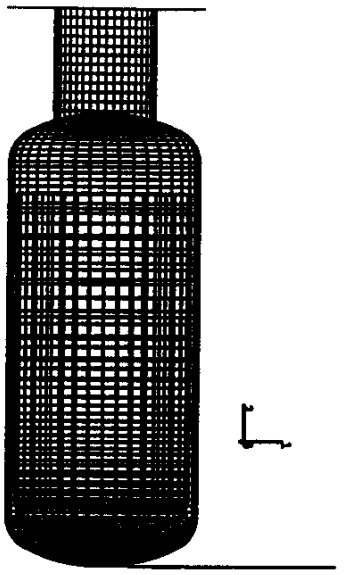

Figure 5-6-1

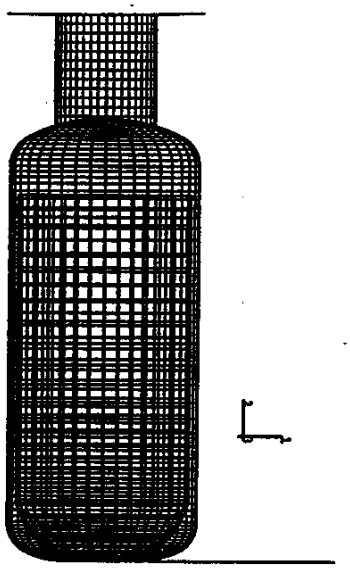

Figure 5-6-2

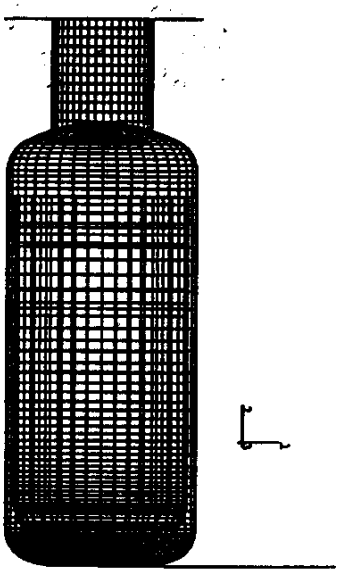

Figure 5-6-3

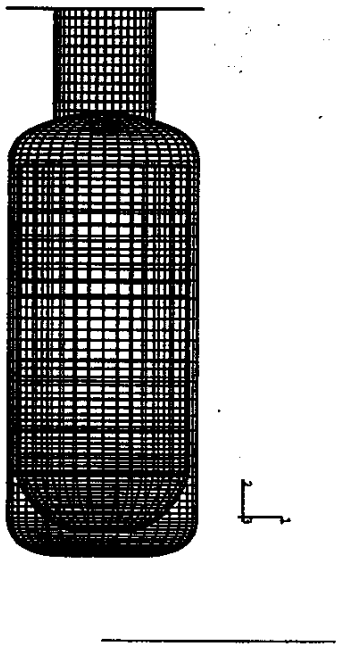

Figure 5-6-4

Figure 5-6 . Deformation of the Primary Container and the Bagless Transfer Can at Four Stages during the Impact.

Figure 5-7. The Modified Design of the Primary Containment Vessel.

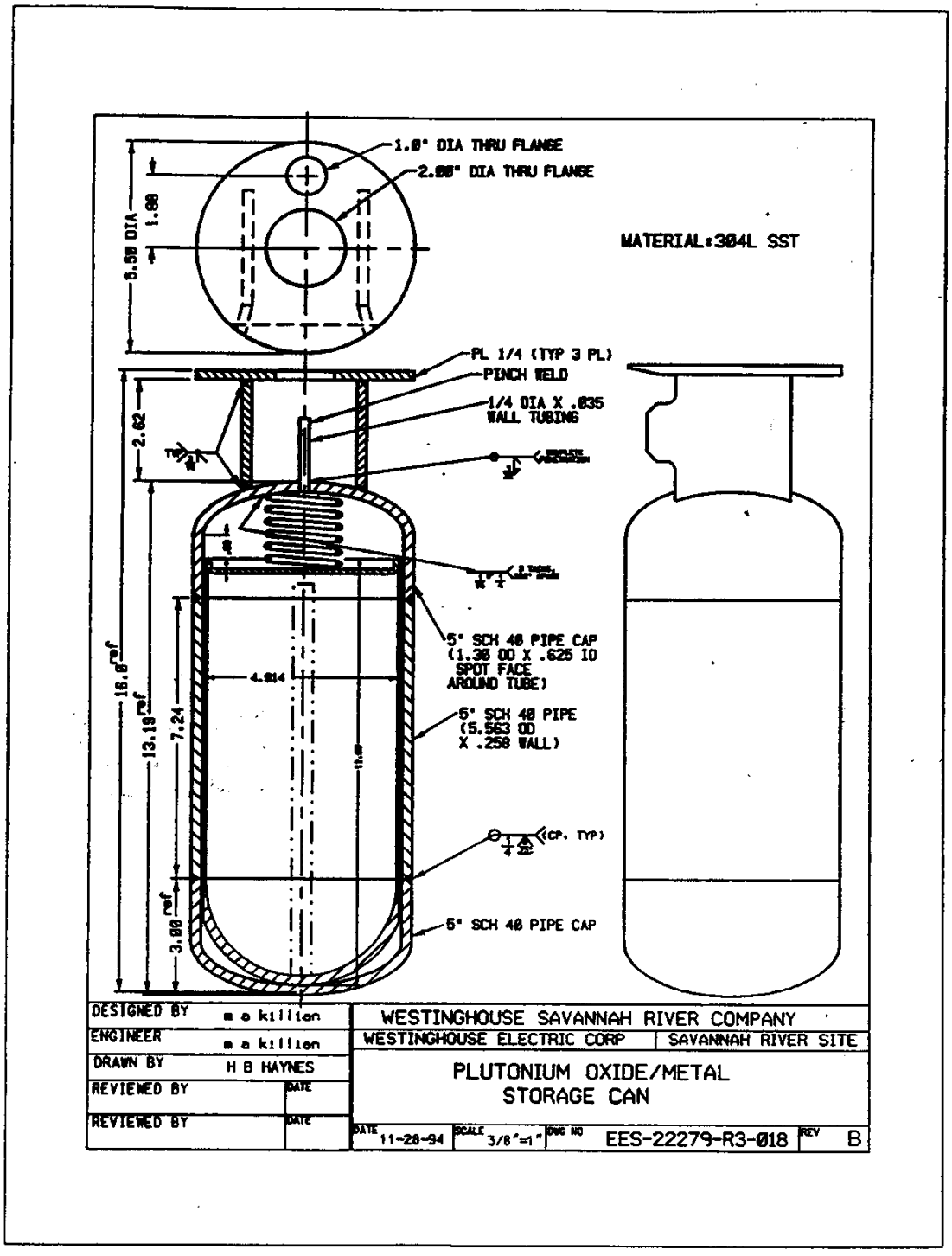

Figure 5-7. The Modified Design of the Primary Containment Vessel.

Figure 5-8. *The Deformed Primary Container at the End of the Upside Down Dropping.*

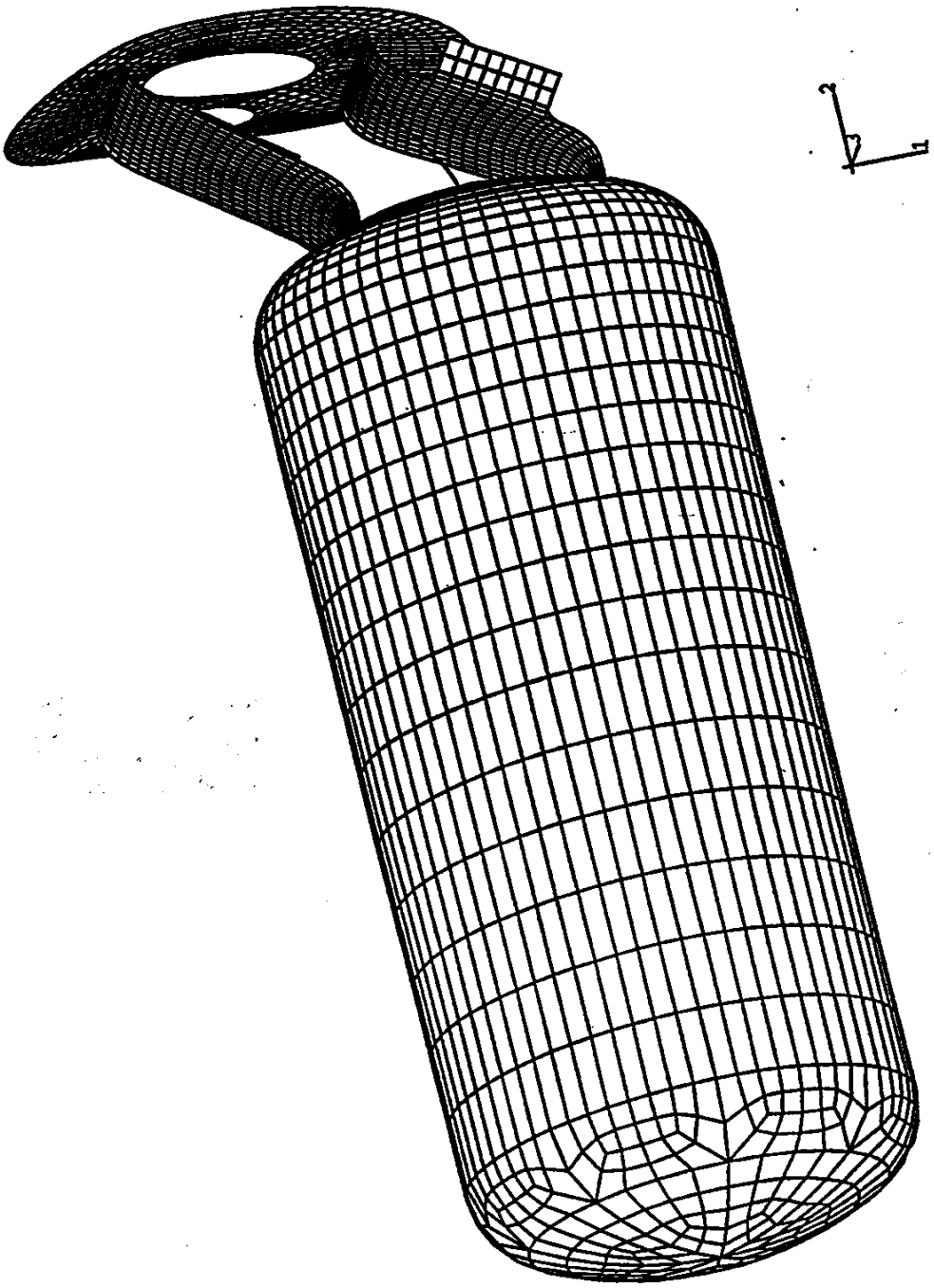

Figure 5-8. The Deformed Primary Container at the End of the Upside Down Dropping.

Figure 5-9. The Detail of the Deformation in the Fitting Region.

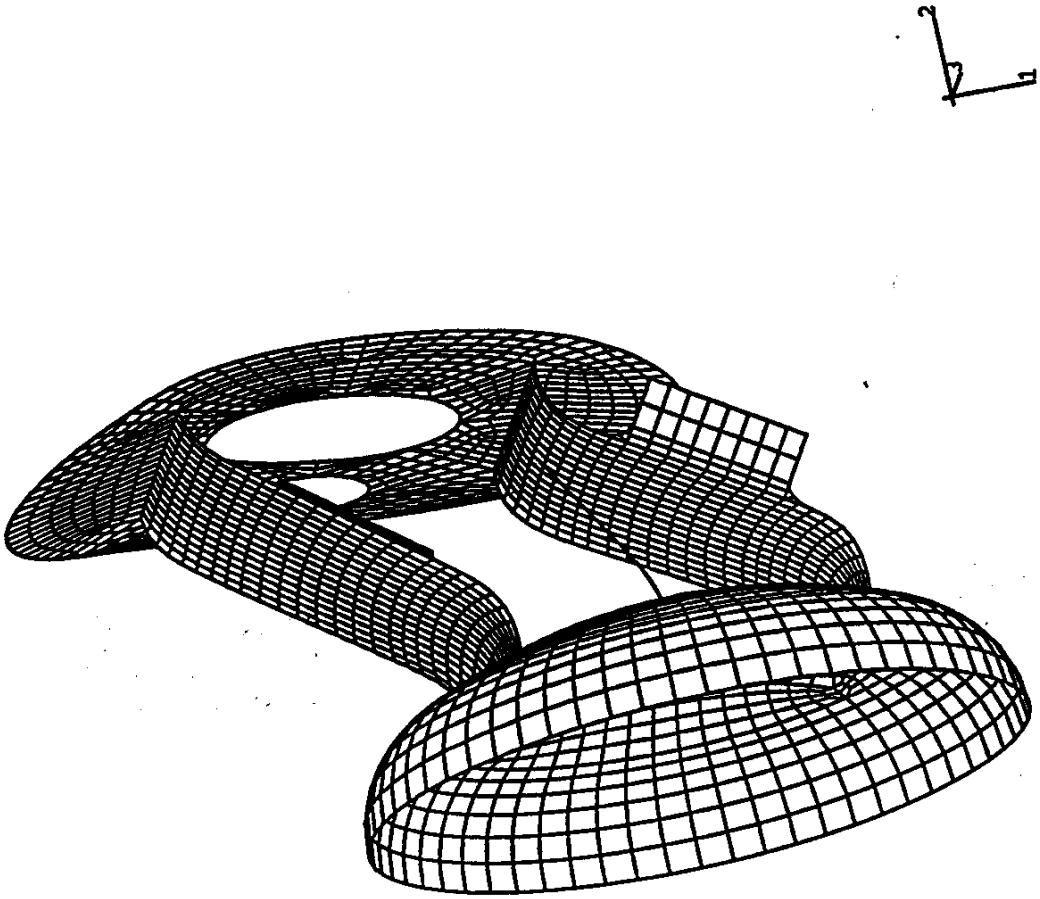

Figure 5-9. The Detail of the Deformation in the Fitting Region.

Figure 5-10. The Deformed Sampling Tube , in 3-D Beam Model.

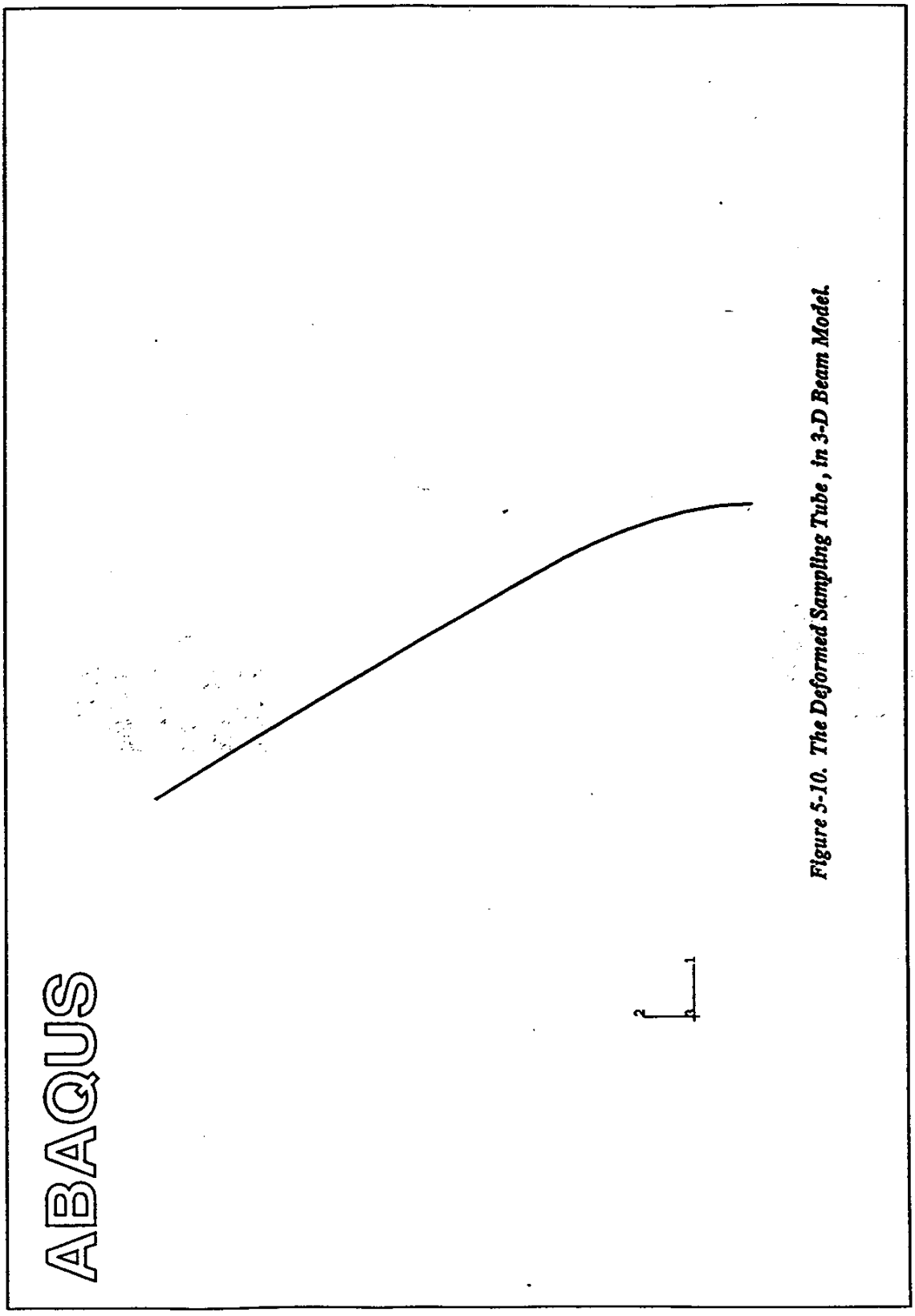

Figure 5-10. The Deformed Sampling Tube , in 3-D Beam Model.

Figure 5-11. The Deformed Sampling Tube , in 3-D Shell Model.

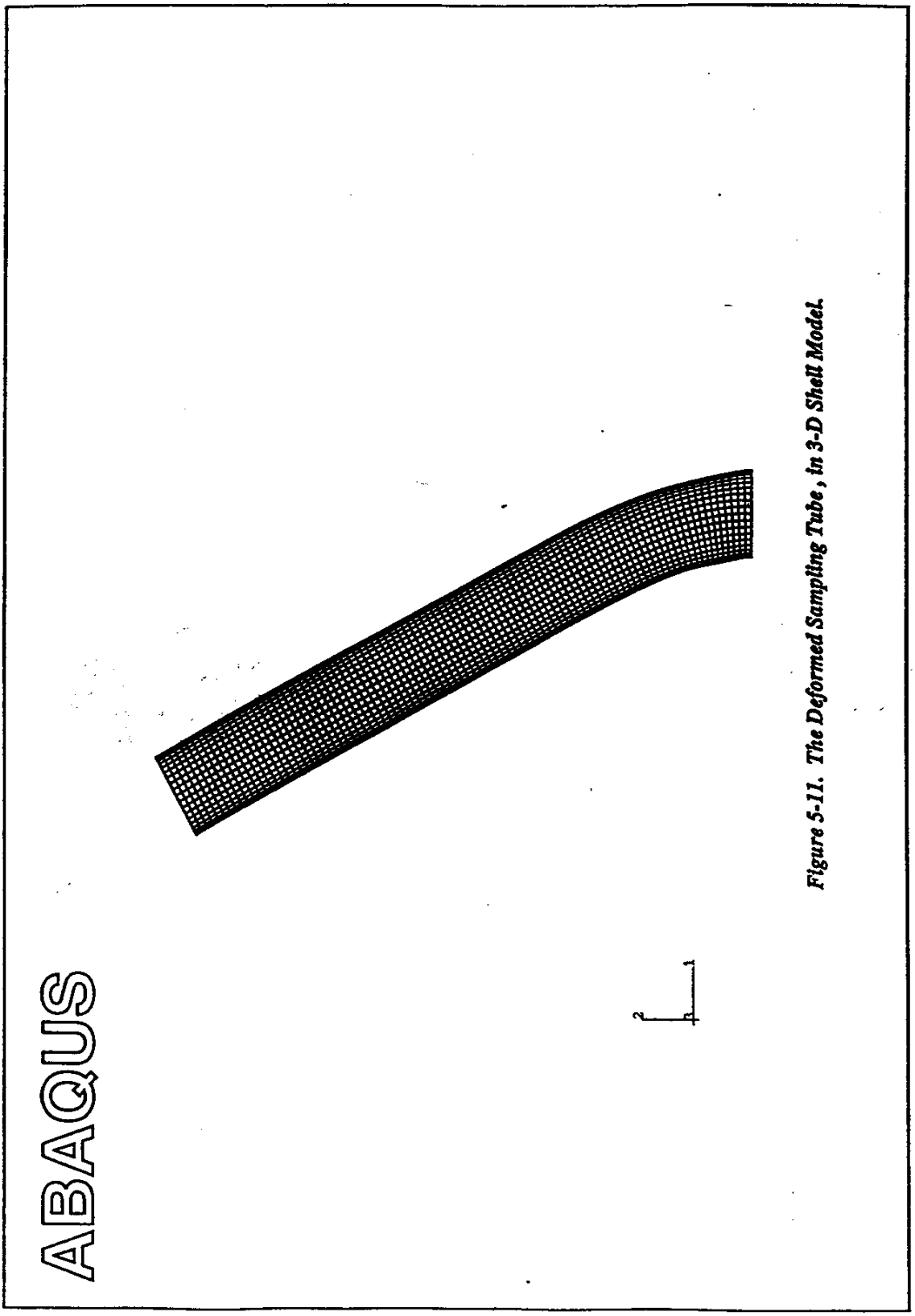

Figure 5-12.. The Deformed Fitting System under 2.10 psi Pressure on the Cap. (The deformation Magnification Factor = 600)

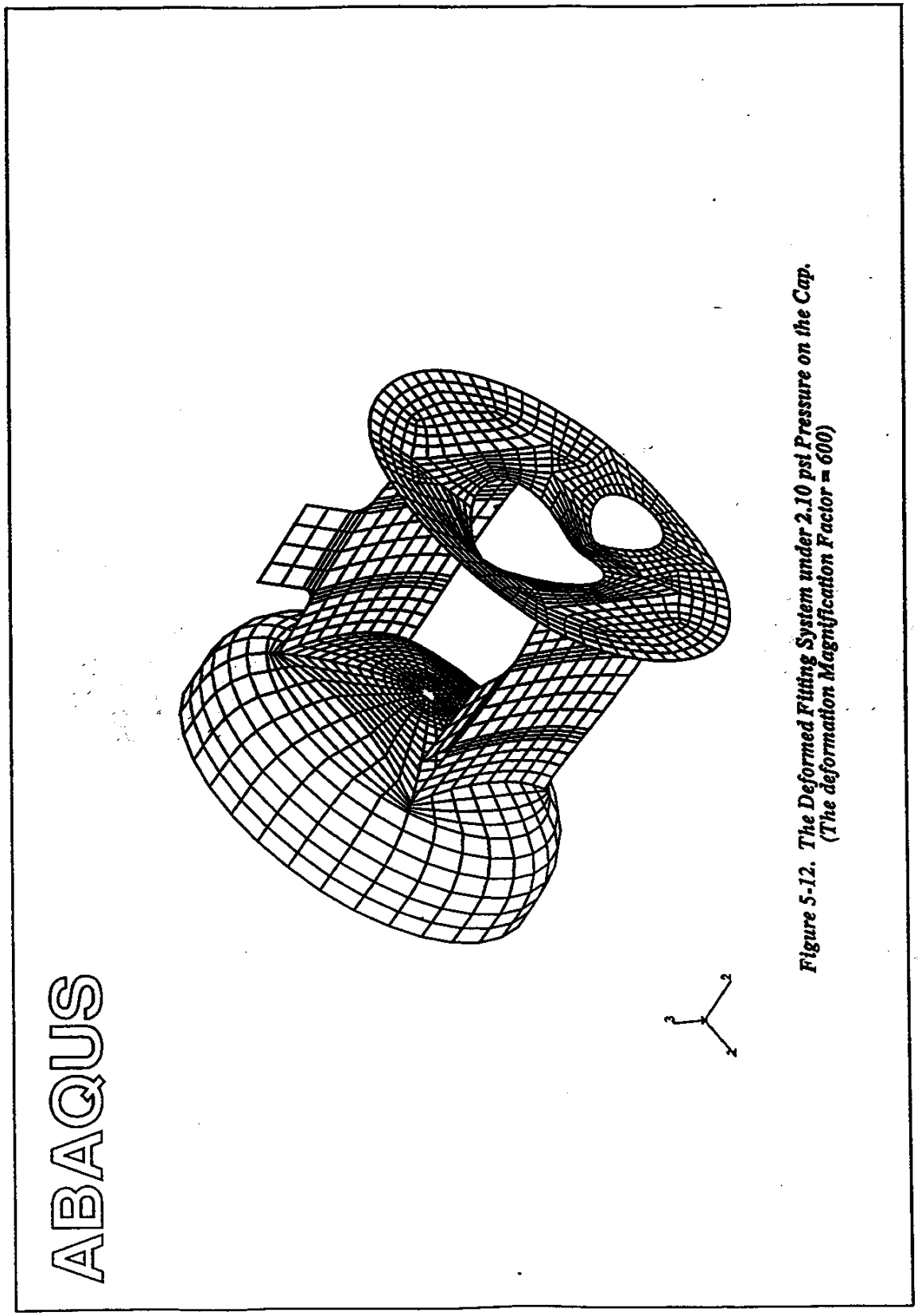

Figure 5-12. The Deformed Fitting System under 2.10 psi Pressure on the Cap. (The deformation Magnification Factor = 600)

Figure 5-13. The Deformed Fitting System under 1162.50 psi Pressure on the Cap. (The deformation Magnification Factor = 600)

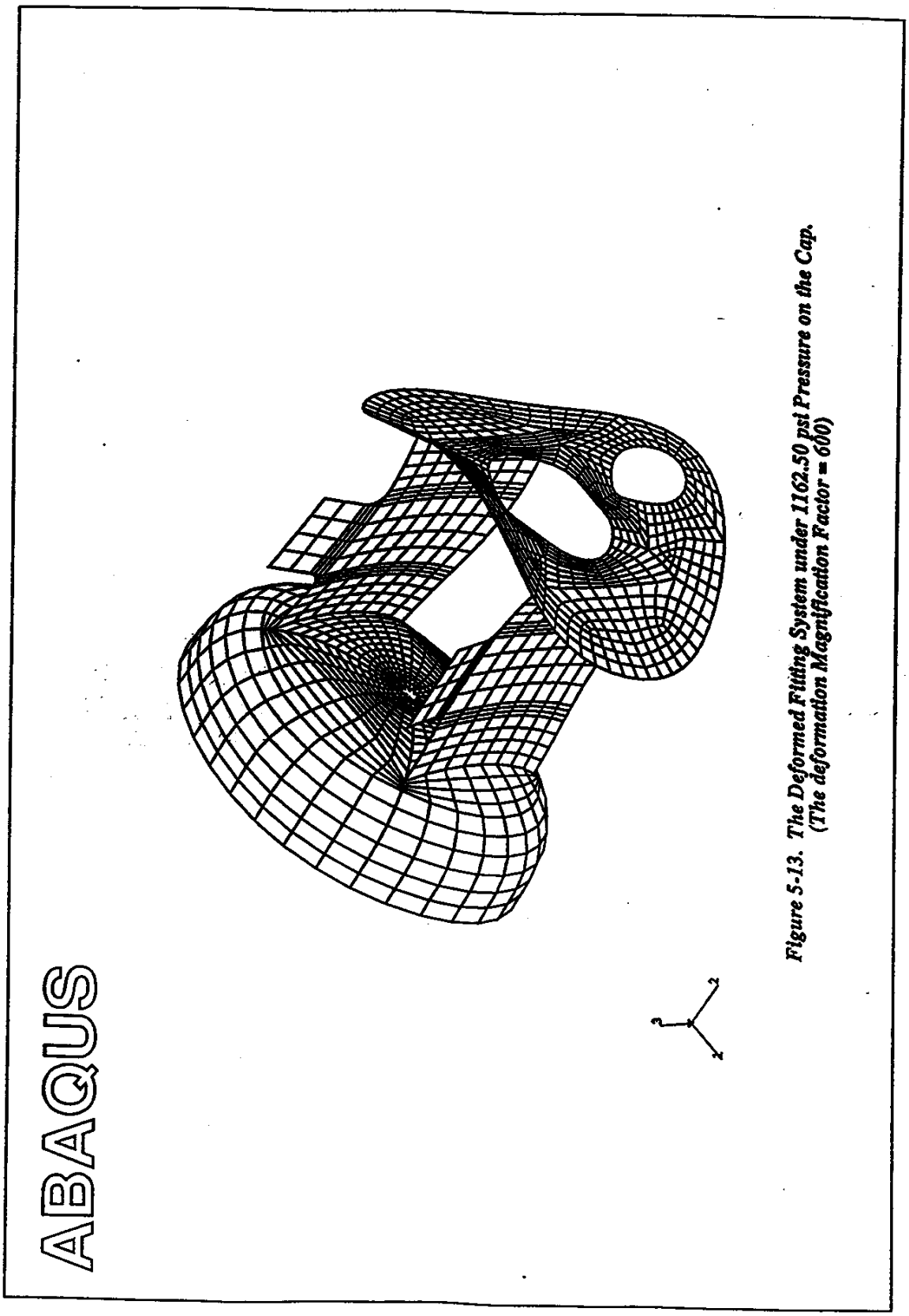

Figure 5-13. The Deformed Fitting System under 1162.50 psi Pressure on the Cap. (The deformation Magnification Factor = 600)

Figure 5-14. Maximum von Mises Stresses in the Flange, Cap and the Vertical Plates (INTER4 elements).

Figure 5-14. Maximum von Mises Stresses in the Flange, Cap and the Vertical Plates (INTER4 elements).

Figure 5-15. ***Maximum von Mises Stresses in the Flange, Cap and the Vertical Plates (Bézier surfaces).***

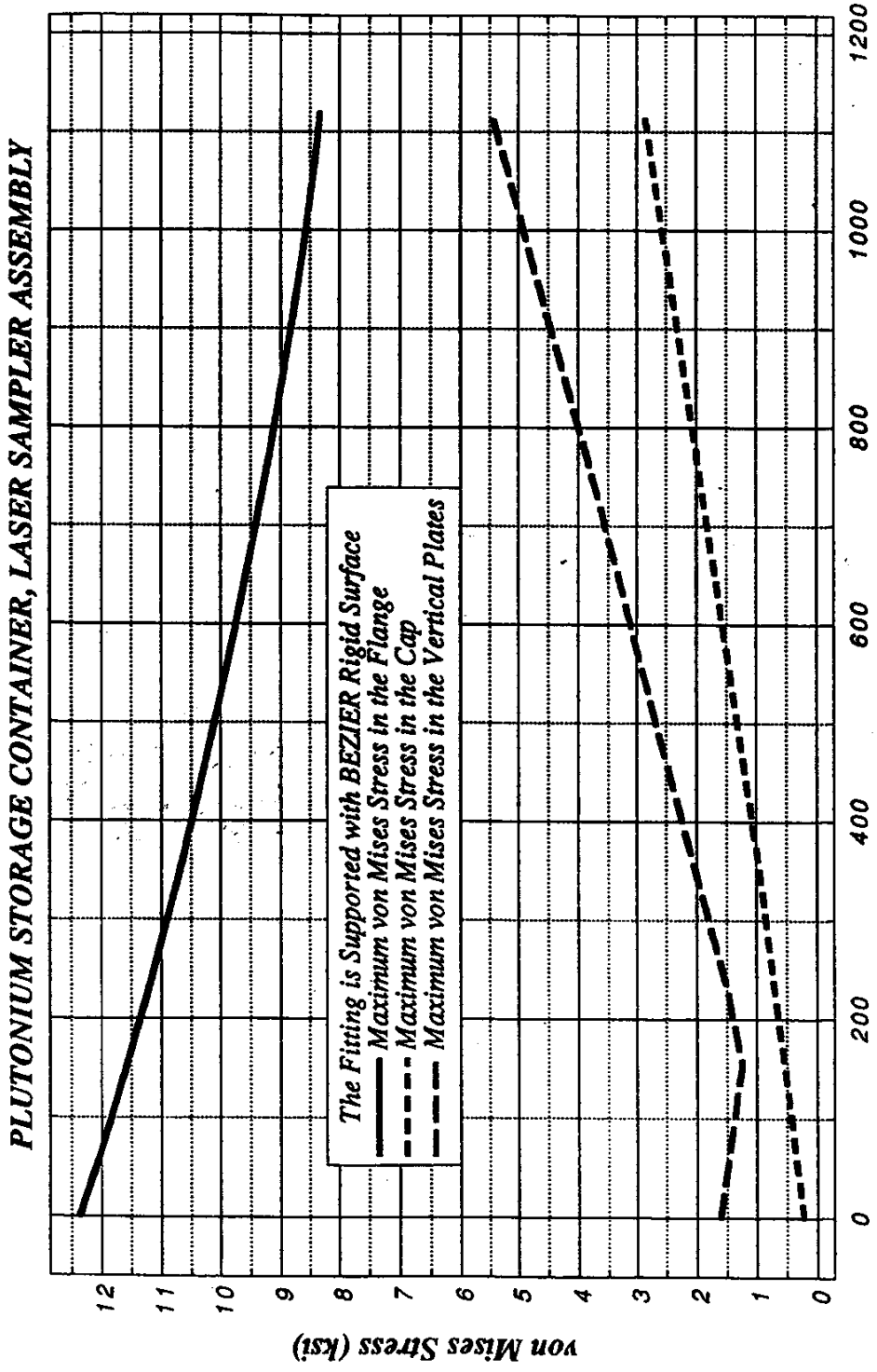

Figure 5-15. Maximum von Mises Stresses in the Flange, Cap and the Vertical plates.

Figure 5-16. ***Comparison of the Maximum von Mises Stresses in the Flange, Cap and the Vertical Plates (with two types of interfaces).***

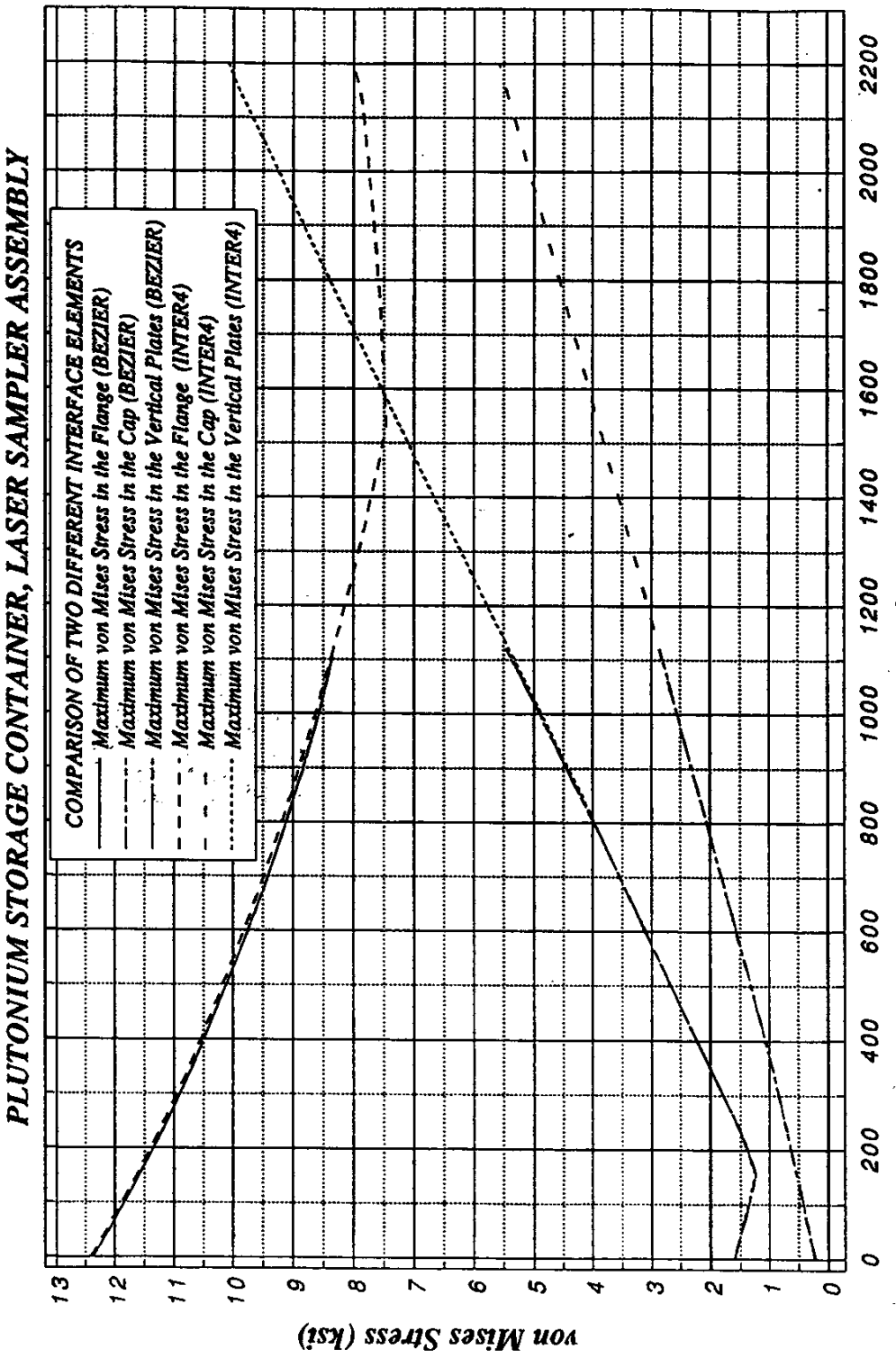

Figure 5-16. Maximum von Mises Stresses in the Flange, Cap and the Vertical Plates.

Figure 5-17. ***The Maximum von Mises Stresses in the Flange, Cap and the Vertical Plates (with relaxed interface constraints).***

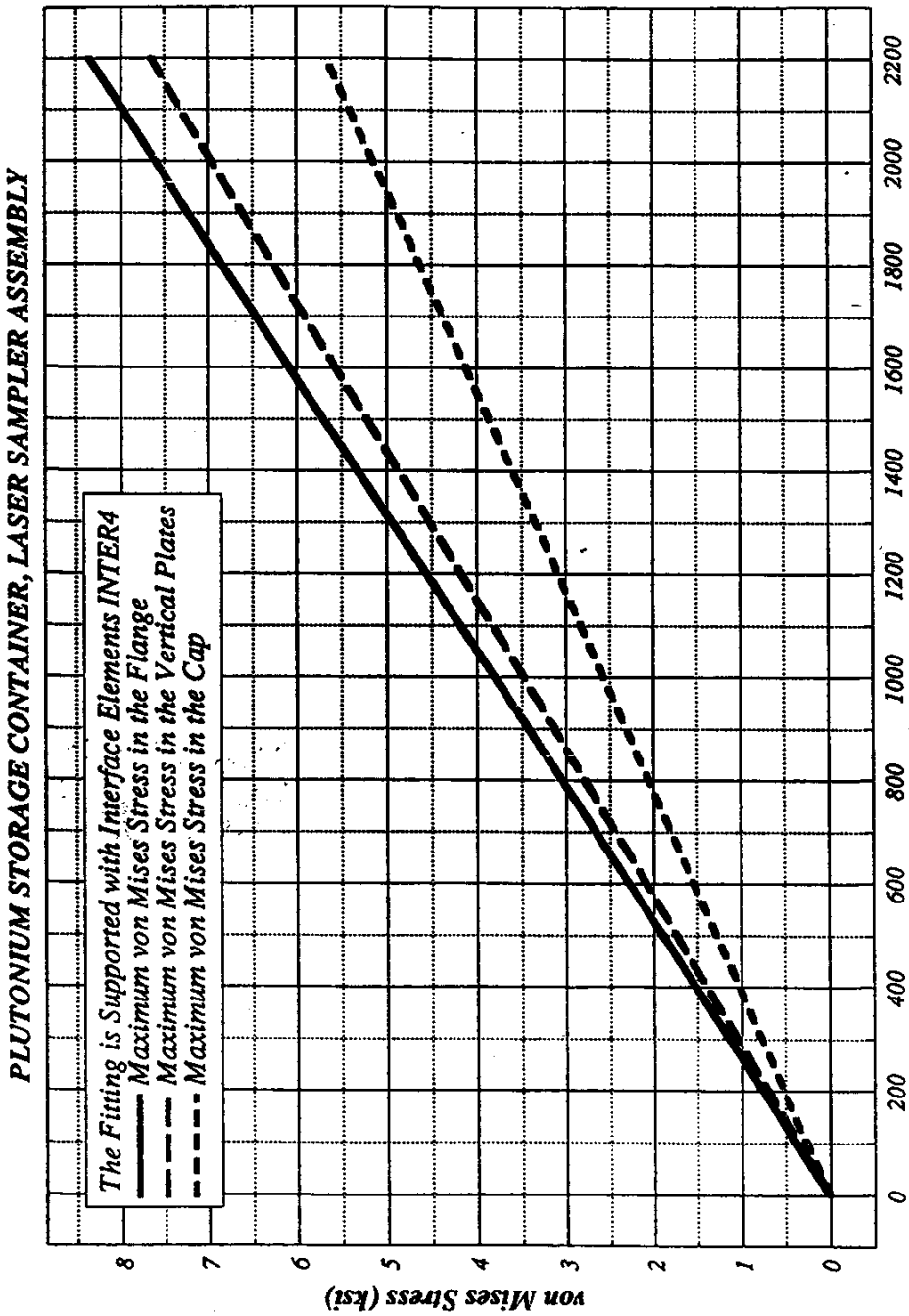

Figure 5-17. Maximum von Mises Stresses in the Flange, Cap and the Vertical Plates.

Figure 5-18. The Deformed Fitting System under 1162.50 psi Pressure on the Cap.(with relaxed interface constraints) (The deformation Magnification Factor = 600)

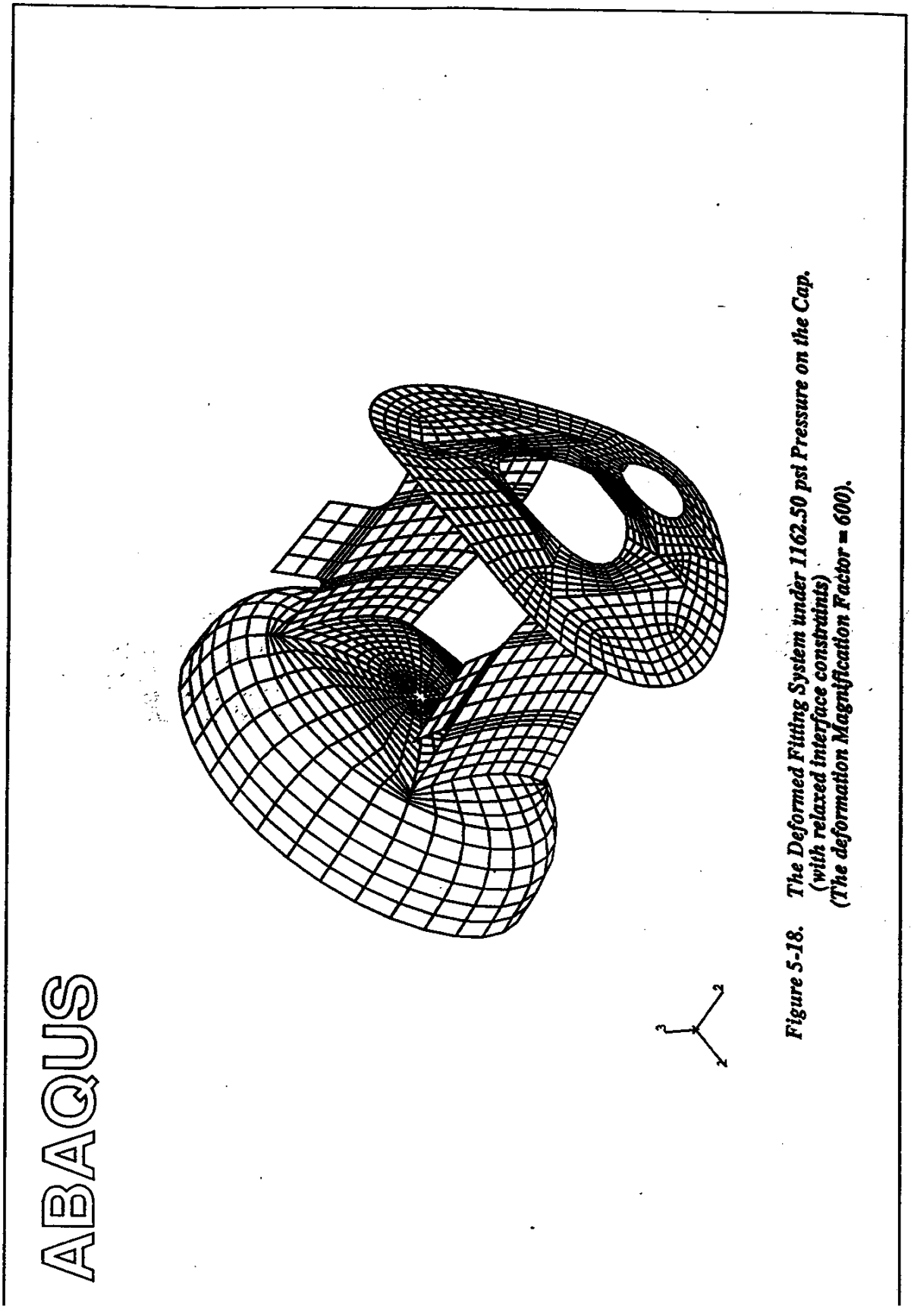

Figure 5-18. The Deformed Fitting System under 1162.50 psi Pressure on the Cap. (with relaxed interface constraints) (The deformation Magnification Factor = 600).

TABLES

Table 2-1. Digitized Stress Strain data for Type 304L Stainless Steel at 77°F (in True measurement)

True Stress (ksi)	*Natural Strain*	*True Stress (ksi)*	*Natural Strain*	*True Stress (ksi)*	*Natural Strain*
37.840	0.1337%	89.525	19.6837%	128.124	39.7037%
39.710	0.2737%	91.036	20.4037%	128.410	39.9237%
41.301	0.4237%	92.629	21.1137%	128.496	40.1437%
42.332	0.5937%	94.249	21.8137%	129.202	40.3637%
43.157	0.7537%	95.515	22.5137%	129.594	40.5837%
43.848	0.9237%	96.607	23.2137%	129.804	40.8037%
44.614	1.0837%	98.231	23.9037%	130.445	41.0237%
45.176	1.2437%	99.625	24.5937%	131.070	41.2437%
45.586	1.4037%	101.206	25.2737%	131.165	41.4637%
46.291	1.5637%	102.325	25.9537%	131.298	41.6837%
46.720	1.7537%	103.756	26.6337%	131.691	41.9037%
47.650	2.0537%	105.025	27.3037%	132.647	42.1337%
48.644	2.3537%	106.120	27.9737%	132.702	42.3437%
49.451	2.6637%	107.976	28.6537%	132.737	42.5637%
50.533	2.9737%	108.557	29.3137%	133.034	42.7837%
51.316	3.2637%	109.886	29.9737%	134.036	43.0137%
51.814	3.5637%	111.634	30.6437%	133.980	43.2337%
52.882	3.8637%	111.005	31.3037%	134.365	43.4637%
53.592	4.1737%	114.262	31.9637%	134.721	43.6837%
55.850	5.0337%	115.154	32.6137%	135.494	43.9037%
58.275	5.8637%	116.689	33.2737%	135.781	44.1237%
60.387	6.6737%	117.520	33.9237%	136.029	44.3537%
62.375	7.4837%	118.480	34.5837%	136.385	44.5837%
64.570	8.2937%	120.036	35.2337%	136.723	44.8037%
66.366	9.0837%	121.236	35.8837%	137.371	45.0337%
68.384	9.8737%	122.230	36.5337%	137.757	45.2637%
70.116	10.6637%	123.151	37.1037%	138.114	45.4937%
71.568	11.4437%	123.702	37.3237%	138.865	45.7237%
73.404	12.2137%	124.088	37.5437%	138.869	45.9537%
75.421	12.9837%	124.428	37.7637%	139.248	46.1837%
77.335	13.7537%	124.797	37.9637%	139.615	46.4137%
78.646	14.5137%	125.510	38.1937%	140.083	46.6537%
80.354	15.2637%	125.973	38.4137%	140.227	46.8837%
81.762	16.0037%	126.296	38.6237%	140.635	47.1137%
83.521	16.7537%	126.573	38.8437%	141.105	47.3437%
85.116	17.4937%	126.868	39.0637%	141.494	47.5837%
86.583	18.2337%	127.427	39.2737%	141.768	47.8137%
88.233	18.9537%	127.988	39.4937%	142.216	48.0637%

Table 2-2. Digitized Stress Strain data for Type 304L Stainless Steel at 77°F (in Engineering measurement)

Engineering Stress (ksi)	Engineering Strain	Engineering Stress (ksi)	Engineering Strain	Engineering Stress (ksi)	Engineering Strain
37.789	0.1338%	73.529	21.7546%	86.139	48.7411%
39.601	0.2741%	74.234	22.6344%	86.141	49.0687%
41.126	0.4246%	74.998	23.5082%	86.010	49.3970%
42.081	0.5955%	75.778	24.3758%	86.292	49.7260%
42.833	0.7566%	76.260	25.2494%	86.364	50.0558%
43.445	0.9280%	76.594	26.1293%	86.314	50.3863%
44.133	1.0896%	77.346	27.0026%	86.549	50.7175%
44.618	1.2515%	77.904	27.8819%	86.773	51.0495%
44.951	1.4136%	78.604	28.7545%	86.645	51.3821%
45.573	1.5760%	78.934	29.6330%	86.542	51.7155%
45.908	1.7692%	79.496	30.5175%	86.611	52.0497%
46.681	2.0749%	79.931	31.3949%	87.039	52.3998%
47.512	2.3816%	80.225	32.2782%	86.892	52.7202%
48.151	2.6995%	81.075	33.1808%	86.724	53.0565%
49.052	3.0184%	80.975	34.0627%	86.727	53.3936%
49.668	3.3176%	81.427	34.9504%	87.180	53.7468%
50.000	3.6280%	82.170	35.8576%	86.952	54.0854%
50.878	3.9393%	81.169	36.7572%	87.001	54.4402%
51.401	4.2620%	83.001	37.6628%	87.040	54.7804%
53.108	5.1626%	83.107	38.5605%	87.347	55.1213%
54.956	6.0390%	83.661	39.4781%	87.340	55.4629%
56.488	6.9014%	83.711	40.3876%	87.298	55.8209%
57.877	7.7709%	83.840	41.3172%	87.326	56.1797%
59.431	8.6473%	84.390	42.2388%	87.350	56.5237%
60.603	9.5091%	84.682	43.1664%	87.562	56.8841%
61.955	10.3776%	84.823	44.1000%	87.606	57.2453%
63.024	11.2530%	84.976	44.9237%	87.632	57.6074%
63.829	12.1242%	85.169	45.2429%	87.906	57.9703%
64.965	12.9909%	85.247	45.5628%	87.706	58.3341%
66.238	13.8643%	85.293	45.8833%	87.744	58.6987%
67.398	14.7444%	85.375	46.1754%	87.773	59.0641%
68.021	15.6198%	85.665	46.5120%	87.856	59.4463%
68.979	16.4902%	85.792	46.8347%	87.744	59.8135%
69.670	17.3554%	85.832	47.1434%	87.797	60.1815%
70.637	18.2389%	85.831	47.4674%	87.888	60.5503%
71.456	19.1171%	85.842	47.7922%	87.919	60.9361%
72.151	20.0019%	86.040	48.1029%	87.887	61.3067%
72.999	20.8690%	86.228	48.4291%	87.945	61.7104%

Table 2-3. Digitized Stress Strain data for Type 304L Stainless Steel at 257°F (in True measurement)

True Stress (ksi)	Natural Strain	True Stress (ksi)	Natural Strain	True Stress (ksi)	Natural Strain
24.580	0.0869%	34.020	1.3869%	75.840	19.1869%
26.530	0.1869%	38.830	2.8869%	78.180	20.6869%
27.930	0.2869%	43.470	4.4869%	80.300	22.0869%
29.100	0.3869%	47.620	6.0869%	82.400	23.5869%
29.920	0.4869%	51.510	7.5869%	84.420	25.0869%
30.690	0.5869%	55.210	9.0869%	86.380	26.5869%
31.200	0.6869%	58.740	10.5869%	88.320	28.1869%
31.750	0.7869%	61.940	11.9869%	90.260	29.7869%
32.310	0.8869%	65.040	13.4869%	91.810	31.3869%
32.730	0.9869%	67.870	14.8869%	93.720	33.0869%
33.130	1.0869%	70.720	16.2869%	95.440	34.8869%
33.660	1.2869%	73.350	17.7869%	147.120	148.5869%

Table 2-4. Digitized Stress Strain data for Type 304L Stainless Steel at 257°F (in Engineering measurement)

Engineering Stress (ksi)	Engineering Strain	Engineering Stress (ksi)	Engineering Strain	Engineering Stress (ksi)	Engineering Strain
24.559	0.0869%	33.551	1.3965%	62.600	21.1511%
26.480	0.1870%	37.725	2.9289%	63.570	22.9821%
27.850	0.2873%	41.563	4.5890%	64.386	24.7159%
28.988	0.3876%	44.808	6.2759%	65.086	26.6008%
29.775	0.4880%	47.747	7.8821%	65.689	28.5141%
30.510	0.5886%	50.414	9.5125%	66.214	30.4564%
30.986	0.6892%	52.839	11.1676%	66.626	32.5604%
31.501	0.7900%	54.943	12.7349%	67.009	34.6985%
32.025	0.8908%	56.834	14.4386%	67.078	36.8710%
32.409	0.9917%	58.482	16.0520%	67.319	39.2177%
32.772	1.0928%	60.091	17.6882%	67.332	41.7463%
33.230	1.2952%	61.398	19.4668%	33.294	341.8802%

Table 5-1 Maximum von Mises Equivalent Stress in the Primary Container and the Bagless Transfer Can

Time (Millisecond)	Maximum von Mises Stress in Bagless Can (ksi)	Maximum von Mises Stress in Primary Container (ksi)	Time (Millisecond)	Maximum von Mises Stress in Bagless Can (ksi)	Maximum von Mises Stress in Primary Container (ksi)
0.0003859	9.864	34.460	0.0997400	91.688	70.164
0.0013470	32.759	59.145	0.1030000	92.831	94.682
0.0031380	40.353	85.326	0.1058000	93.716	82.204
0.0054900	42.777	87.112	0.1083000	94.365	83.883
0.0082860	46.673	45.859	0.1113000	94.975	94.882
0.0104600	49.133	85.945	0.1142000	95.635	82.124
0.0120800	50.615	78.364	0.1165000	96.079	83.654
0.0143700	51.803	68.090	0.1190000	96.541	94.930
0.0168000	53.596	42.629	0.1218000	97.207	93.174
0.0192300	55.446	38.751	0.1247000	97.873	91.872
0.0215100	57.444	70.131	0.1279000	98.492	79.846
0.0239200	59.465	89.598	0.1310000	99.062	95.261
0.0263300	61.276	80.744	0.1336000	99.552	90.542
0.0286500	62.935	70.959	0.1365000	100.130	95.363
0.0312300	64.786	80.769	0.1397000	100.800	77.809
0.0339200	66.400	90.399	0.1431000	101.450	95.498
0.0364800	68.072	89.517	0.1461000	101.920	90.517
0.0386300	69.298	76.176	0.1490000	102.430	94.477
0.0411500	70.568	81.679	0.1521000	103.050	92.175
0.0437300	71.742	92.285	0.1552000	103.700	86.730
0.0463400	73.191	92.315	0.1585000	104.300	93.094
0.0491000	74.839	89.252	0.1616000	104.830	93.035
0.0516900	76.295	82.316	0.1648000	105.290	95.742
0.0539800	77.441	86.323	0.1683000	105.730	92.442
0.0564600	78.279	91.498	0.1717000	106.150	95.200
0.0592000	79.273	92.587	0.1750000	106.730	92.339
0.0619700	80.328	87.271	0.1787000	107.330	95.906
0.0648300	81.216	92.714	0.1825000	107.950	95.922
0.0676400	82.136	79.899	0.1865000	108.170	95.939
0.0703200	83.132	93.031	0.1901000	108.350	95.076
0.0726900	83.999	93.060	0.1936000	108.480	95.982
0.0753700	84.936	93.232	0.1974000	108.650	95.808
0.0779400	85.712	89.621	0.2016000	109.080	92.874
0.0806100	86.444	81.593	0.2049000	109.500	90.828
0.0834000	87.319	89.755	0.2088000	109.860	94.294
0.0855400	88.043	82.678	0.2127000	110.250	96.239
0.0881000	88.743	74.612	0.2175000	110.940	95.005
0.0909600	89.385	74.012	0.2221000	111.450	95.044
0.0940900	90.076	83.639	0.2269000	111.500	96.373
0.0969600	90.793	76.899	0.2317000	111.260	95.012

Table 5-1 Maximum von Mises Equivalent Stress in the Primary Container and the Bagless Transfer Can (Continued)

Time	Maximum von Mises Stress in Bagless Can	Maximum von Mises Stress in Primary Container	Time	Maximum von Mises Stress in Bagless Can	Maximum von Mises Stress in Primary Container
(Millisecond)	(ksi)	(ksi)	(Millisecond)	(ksi)	(ksi)
0.2371000	111.080	94.750	0.7116000	61.578	80.250
0.2426000	111.980	96.509	0.7309000	46.471	81.606
0.2484000	113.280	96.749	0.7468000	40.984	95.311
0.2541000	114.220	90.128	0.7640000	41.288	90.875
0.2611000	114.590	92.042	0.7853000	43.061	98.112
0.2680000	114.850	96.829	0.8135000	43.549	98.334
0.2771000	115.210	94.064	0.8432000	42.904	98.404
0.2872000	115.640	97.066	0.8627000	50.833	98.492
0.2991000	116.060	97.124	0.8838000	57.356	98.783
0.3134000	116.480	92.726	0.9061000	60.095	98.946
0.3232000	116.710	97.214	0.9307000	57.377	99.085
0.3297000	116.770	95.199	0.9654000	49.906	99.009
0.3394000	116.920	97.494	0.9918000	47.311	99.181
0.3500000	117.090	96.550	1.0010000	45.933	97.592
0.3553000	117.150	88.513	1.0200000	47.239	98.363
0.3622000	117.320	96.824	1.0460000	50.632	99.332
0.3710000	117.390	97.771	1.0640000	53.726	99.337
0.3815000	117.710	93.112	1.1050000	58.933	83.211
0.3926000	117.860	97.608	1.1610000	55.681	77.138
0.4064000	118.090	92.658	1.2230000	57.715	53.719
0.4200000	118.420	93.135	1.3170000	49.943	30.258
0.4386000	118.990	86.994	1.4250000	65.232	46.319
0.4563000	119.290	95.756	1.5930000	48.713	39.594
0.4648000	119.370	94.477	1.8660000	48.737	43.665
0.4775000	118.500	85.299	2.2790000	64.281	34.134
0.4901000	119.820	91.336	2.9250000	54.988	45.407
0.4991000	119.890	91.363	3.6180000	56.899	32.822
0.5145000	120.020	88.425	4.3980000	54.552	37.939
0.5268000	119.750	97.251	5.3260000	55.310	37.317
0.5408000	120.360	86.284	6.3220000	52.747	36.425
0.5528000	119.640	90.479	7.3250000	53.701	35.658
0.5625000	120.420	87.673	8.0560000	53.300	35.985
0.5714000	120.180	91.397	9.1960000	53.230	35.774
0.5840000	119.350	89.253	10.0200000	54.187	35.983
0.6013000	119.310	87.459	10.9600000	54.877	35.984
0.6179000	120.590	80.651	11.8200000	54.553	35.919
0.6344000	115.510	84.587	12.8800000	54.702	35.942
0.6519000	108.820	81.840	13.5400000	53.139	35.890
0.6737000	88.905	81.435	14.7500000	53.359	35.910
0.6938000	69.989	80.106	15.4800000	53.512	35.892

Table 5-2. Transfer of Kinetic Energy, Strain Energy and Plastic Dissipation in the Container System

Time	Time	Kinetic Energy	Recoverable Strain Energy	Plastic Dissipation
Increments	(Milliseconds)	Inch-pounds	Inch-pounds	Inch-pounds
1	0.0000	10540.0	0.02	0.00
10	0.0004	10560.0	3.35	0.43
20	0.0013	10630.0	13.90	19.20
25	0.0021	10640.0	22.70	48.40
30	0.0031	10600.0	30.20	90.20
40	0.0055	10530.0	35.50	143.00
50	0.0083	10500.0	40.90	170.00
60	0.0105	10490.0	43.70	185.00
70	0.0121	10480.0	42.90	194.00
80	0.0144	10470.0	43.70	203.00
90	0.0168	10450.0	46.10	212.00
100	0.0192	10440.0	51.90	220.00
150	0.0312	10340.0	84.40	283.00
200	0.0437	10210.0	122.00	363.00
250	0.0565	10070.0	151.00	463.00
300	0.0703	9900.0	185.00	593.00
350	0.0834	9727.0	210.00	731.00
400	0.0970	9551.0	228.00	879.00
450	0.1113	9353.0	232.00	1062.00
500	0.1247	9162.0	231.00	1248.00
550	0.1397	8944.0	231.00	1461.00
600	0.1552	8712.0	239.00	1677.00
650	0.1717	8457.0	263.00	1906.00
700	0.1901	8167.0	290.00	2173.00
750	0.2088	7871.0	309.00	2453.00
800	0.2317	7487.0	345.00	2795.00
850	0.2611	6993.0	368.00	3249.00
900	0.3134	6099.0	399.00	4080.00
1000	0.4064	4558.0	495.00	5516.00
1010	0.4200	4344.0	501.00	5725.00
1020	0.4386	4060.0	508.00	5990.00
1030	0.4563	3798.0	519.00	6235.00
1040	0.4648	3674.0	529.00	6344.00
1050	0.4775	3491.0	545.00	6511.00
1060	0.4901	3320.0	555.00	6673.00
1070	0.4991	3200.0	562.00	6788.00
1080	0.5145	3000.0	571.00	6978.00
1090	0.5268	2847.0	581.00	7116.00
1100	0.5408	2678.0	582.00	7285.00
1110	0.5528	2542.0	590.00	7413.00
1120	0.5625	2438.0	592.00	7510.00
1130	0.5714	2344.0	594.00	7598.00
1140	0.5840	2216.0	603.00	7716.00
1150	0.6013	2050.0	615.00	7871.00
1160	0.6179	1906.0	622.00	8013.00
1170	0.6344	1776.0	622.00	8141.00
1180	0.6519	1648.0	617.00	8281.00
1190	0.6737	1507.0	604.00	8447.00
1200	0.6938	1394.0	586.00	8588.00
1210	0.7116	1300.0	570.00	8711.00
1220	0.7309	1206.0	561.00	8837.00
1230	0.7468	1136.0	548.00	8934.00
1240	0.7640	1062.0	531.00	9047.00
1250	0.7853	971.0	525.00	9164.00
1260	0.8135	862.0	522.00	9285.00

Table 5-2. Transfer of Kinetic Energy, Strain Energy and Plastic Dissipation in the Container System (continued)

Time	*Time*	*Kinetic Energy*	*Recoverable Strain Energy*	*Plastic Dissipation*
Increments	*(Milliseconds)*	*Inch-pounds*	*Inch-pounds*	*Inch-pounds*
1270	0.8432	755.0	518.00	9418.00
1280	0.8627	690.0	515.00	9488.00
1290	0.8838	629.0	506.00	9568.00
1300	0.9061	570.0	497.00	9644.00
1310	0.9307	516.0	494.00	9704.00
1320	0.9654	455.0	491.00	9774.00
1330	0.9918	423.0	480.00	9808.00
1335	0.9962	418.0	478.00	9813.00
1340	1.0010	414.0	477.00	9817.00
1345	1.0080	409.0	475.00	9822.00
1350	1.0200	404.0	471.00	9833.00
1355	1.0350	398.0	472.00	9839.00
1360	1.0460	396.0	471.00	9844.00
1365	1.0530	397.0	472.00	9845.00
1370	1.0640	400.0	472.00	9846.00
1375	1.0820	407.0	467.00	9848.00
1380	1.1050	426.0	447.00	9850.00
1385	1.1320	457.0	410.00	9854.00
1390	1.1610	499.0	377.00	9858.00
1395	1.1880	545.0	342.00	9862.00
1397	1.2000	567.0	322.00	9864.00
1400	1.2230	606.0	283.00	9868.00
1403	1.2490	647.0	247.00	9871.00
1405	1.2670	671.0	228.00	9874.00
1407	1.2860	696.0	210.00	9875.00
1408	1.2950	707.0	201.00	9876.00
1409	1.3060	719.0	192.00	9876.00
1410	1.3170	728.0	186.00	9877.00
1411	1.3280	734.0	182.00	9878.00
1412	1.3390	740.0	179.00	9878.00
1413	1.3490	744.0	176.00	9878.00
1414	1.3600	748.0	174.00	9878.00
1415	1.3710	750.0	172.00	9878.00
1416	1.3820	751.0	172.00	9878.00
1417	1.3930	751.0	173.00	9878.00
1418	1.4030	750.0	173.00	9878.00
1420	1.4250	753.0	170.00	9879.00
1430	1.5930	773.0	148.00	9879.00
1440	1.8660	743.0	171.00	9883.00
1450	2.2790	749.0	161.00	9883.00
1460	2.9250	737.0	164.00	9887.00
1470	3.6180	747.0	148.00	9888.00
1480	4.3980	734.0	156.00	9889.00
1490	5.3260	740.0	145.00	9889.00
1500	6.3220	735.0	145.00	9889.00
1510	7.3250	727.0	149.00	9889.00
1520	8.0560	723.0	150.00	9889.00
1530	9.1960	713.0	155.00	9889.00
1540	10.0200	717.0	148.00	9889.00
1550	10.9600	704.0	157.00	9889.00
1560	11.8200	703.0	154.00	9889.00
1570	12.8800	699.0	153.00	9889.00
1580	13.5400	690.0	159.00	9889.00
1590	14.7500	690.0	154.00	9889.00
1600	15.4800	691.0	150.00	9889.00

Table 5-3 Spring Constants for the Springs on the Top of the Lid

Spring Element	*Node on the Lid*	*Node on the Primary Container*	*Radius*	*Spring Constant*
			inches	*pounds per inch*
630	*164*	*71*	*1.2135*	*20.9519*
631	*165*	*73*	*0.8090*	*13.9679*
632	*166*	*75*	*0.4045*	*6.9840*
633	*167*	*77*	*0.0*	*3.4963*

Table 5-4 Plutonium Oxide/Metal Storage Container Internal Pressure in the Bagless Can without Spring

Pressure	*Maximum Deflection*	*Maximum von Mises Stress*	*Maximum Plastic Strain*
psig	*inches*	*psi*	*inch/inch*
100.0	*0.023641*	*31,438.0*	*0.0000000*
200.0	*0.052053*	*40,207.0*	*0.0019054*
300.0	*0.103600*	*43,664.0*	*0.0076511*
400.0	*0.175500*	*46,299.0*	*0.0144810*
500.0	*0.231200*	*47,147.0*	*0.0175710*
600.0	*0.277200*	*47,556.0*	*0.0193310*
700.0	*0.321500*	*48,427.0*	*0.0219620*
800.0	*0.362100*	*49,585.0*	*0.0263280*
900.0	*0.401900*	*50,341.0*	*0.0299120*
1000.0	*0.438400*	*51,233.0*	*0.0327270*

Table 5-5 Plutonium Oxide/Metal Storage Container Internal Pressure in the Bagless Can with Springs on the Lid Top.

Pressure	*Maximum Deflection*	*Maximum von Mises Stress*	*Maximum Plastic Strain*
psig	*inches*	*psi*	*inch/inch*
100.0	*0.023616*	*31,399.0*	*0.0000000*
200.0	*0.051894*	*40,195.0*	*0.0018602*
300.0	*0.103000*	*43,629.0*	*0.0073735*
400.0	*0.175400*	*45,554.0*	*0.0144800*
500.0	*0.231000*	*46,550.0*	*0.0175750*
600.0	*0.278800*	*46,534.0*	*0.0200230*
700.0	*0.320800*	*48,472.0*	*0.0219120*
800.0	*0.361400*	*49,642.0*	*0.0263070*

Table 5-6 Plutonium Oxide/Metal Storage Container Internal Pressure in the Bagless Can with Pre-stress in Springs

Pressure	*Maximum Deflection*	*Maximum von Mises Stress*	*Maximum Plastic Strain*
psig	*inches*	*psi*	*inch/inch*
Spring Load	*-0.000923*	*1,209.0*	*0.0000000*
100.0	*0.022782*	*30,236.0*	*0.0000000*
200.0	*0.050505*	*40,037.0*	*0.0017110*
300.0	*0.101000*	*43,528.0*	*0.0071253*
400.0	*0.173000*	*45,555.0*	*0.0143270*
500.0	*0.229200*	*46,545.0*	*0.0175470*
600.0	*0.277300*	*46,330.0*	*0.0198640*
700.0	*0.319300*	*48,436.0*	*0.0217830*
800.0	*0.360000*	*49,619.0*	*0.0262080*

Table 5-7 Plutonium Oxide/Metal Storage Container Internal Pressure in the Primary Container without Internal Components.

Pressure	*Maximum Deflection*	*Maximum von Mises Stress*	*Maximum Plastic Strain*
psig	*inches*	*psi*	*inch/inch*
100.0	*0.000532*	*1,383.0*	*0.0000000*
200.0	*0.001087*	*2,765.0*	*0.0000000*
300.0	*0.001642*	*4,146.0*	*0.0000000*
400.0	*0.002196*	*5,526.0*	*0.0000000*
500.0	*0.002749*	*6,904.0*	*0.0000000*
600.0	*0.003301*	*8,280.0*	*0.0000000*
700.0	*0.003853*	*9,655.0*	*0.0000000*
800.0	*0.004404*	*11,029.0*	*0.0000000*
900.0	*0.004954*	*12,401.0*	*0.0000000*
1000.0	*0.005503*	*13,771.0*	*0.0000000*
1100.0	*0.006052*	*15,140.0*	*0.0000000*
1200.0	*0.006601*	*16,508.0*	*0.0000000*
1300.0	*0.007148*	*17,874.0*	*0.0000000*
1400.0	*0.007695*	*19,238.0*	*0.0000000*
1500.0	*0.008241*	*20,602.0*	*0.0000000*

Table 5-8 Plutonium Oxide/Metal Storage Container Internal Pressure in the Primary Container with Internal Components.

Pressure	*Maximum Deflection*	*Maximum von Mises Stress*	*Maximum Plastic Strain*
psig	*inches*	*psi*	*inch/inch*
100.0	*0.003744*	*34,394.0*	*0.014377*
200.0	*0.004343*	*34,574.0*	*0.014748*
300.0	*0.004889*	*34,671.0*	*0.015050*
400.0	*0.005440*	*34,800.0*	*0.015443*
500.0	*0.005991*	*34,939,0*	*0.015874*
600.0	*0.006544*	*35,086.0*	*0.016332*
700.0	*0.007098*	*35,242.0*	*0.016808*
800.0	*0.007652*	*35,398.0*	*0.017299*
900.0	*0.008206*	*35,558.0*	*0.017799*
1000.0	*0.008760*	*35,719.0*	*0.018308*
1100.0	*0.009314*	*35,881.0*	*0.018828*
1200.0	*0.009870*	*36,061.0*	*0.019367*
1300.0	*0.010435*	*36,265.0*	*0.020026*
1400.0	*0.011002*	*36,482.0*	*0.020701*
1500.0	*0.011579*	*36,727.0*	*0.021496*

Table 5-9 Plutonium Oxide/Metal Storage Container Laser Sampler Assembly Maximum von Mises Stresses in the Flange, Cap and the Vertical Plates- the Supporting Surfaces are modeled with 3-D Interface Elements

Applied Pressure	*Maximum von Mises stress in Flange*	*Maximum von Mises Stress in Cap*	*Maximum von Mises Stress in vertical plates*
(psi)	*(psi)*	*(psi)*	*(psi)*
0.60	12408.00	222.50	1604.00
1.20	12405.00	223.70	1603.00
2.10	12400.00	225.50	1601.00
3.45	12392.00	228.20	1597.00
5.48	12381.00	232.30	1592.00
8.51	12364.00	238.40	1585.00
13.07	12339.00	247.70	1574.00
19.90	12302.00	261.50	1558.00
30.16	12246.00	282.30	1533.00
45.53	12164.00	313.70	1496.00
68.40	12042.00	360.90	1441.00
103.20	11865.00	432.00	1360.00
154.80	11609.00	539.20	1241.00
232.80	11247.00	701.00	1493.00
349.80	10746.00	945.30	2006.00
525.00	10076.00	1378.00	2778.00
600.00	9814.00	1564.00	3107.00
600.30	9813.00	1565.00	3108.00
600.60	9812.00	1566.00	3110.00
601.05	9811.00	1567.00	3112.00
601.73	9809.00	1569.00	3115.00
602.74	9805.00	1571.00	3119.00
604.26	9800.00	1575.00	3126.00
606.53	9792.00	1581.00	3136.00
609.95	9781.00	1589.00	3151.00
615.08	9764.00	1602.00	3137.00
622.77	9738.00	1621.00	3207.00
634.20	9700.00	1650.00	3257.00
651.60	9643.00	1693.00	3333.00
677.40	9559.00	1757.00	3446.00
716.40	9436.00	1854.00	3615.00
774.90	9257.00	2000.00	3868.00
862.50	9002.00	2219.00	4248.00
900.00	8897.00	2312.00	4421.00
900.30	8896.00	2313.00	4422.00
900.60	8895.00	2314.00	4423.00
901.05	8894.00	2315.00	4425.00
901.73	8892.00	2317.00	4429.00
902.74	8889.00	2319.00	4433.00
904.26	8885.00	2323.00	4440.00
906.53	8879.00	2329.00	4451.00
909.95	8869.00	2337.00	4466.00
915.08	8855.00	2350.00	4490.00
922.77	8834.00	2369.00	4525.00
934.20	8803.00	2398.00	4578.00
951.60	8757.00	2441.00	4656.00
977.40	8688.00	2506.00	4775.00
1016.40	8587.00	2604.00	4951.00
1074.90	8440.00	2750.00	5216.00
1162.50	8230.00	2969.00	5609.00
1200.00	8143.00	3063.00	5777.00

Table 5-9 Plutonium Oxide/Metal Storage Container Laser Sampler Assembly Maximum von Mises Stresses in the Flange, Cap and the Vertical Plates- the Supporting Surfaces are modeled with 3-D Interface Elements (continued)

Applied Pressure	*Maximum von Mises stress in Flange*	*Maximum von Mises Stress in Cap*	*Maximum von Mises Stress in vertical plates*
(psi)	*(psi)*	*(psi)*	*(psi)*
1200.30	8143.00	3064.00	5779.00
1200.60	8142.00	3065.00	5780.00
1201.05	8141.00	3066.00	5782.00
1201.73	8139.00	3068.00	5785.00
1202.74	8137.00	3070.00	5790.00
1204.26	8134.00	3074.00	5796.00
1206.53	8128.00	3080.00	5807.00
1209.95	8121.00	3088.00	5822.00
1215.08	8109.00	3101.00	5845.00
1222.77	8092.00	3120.00	5879.00
1234.20	8066.00	3149.00	5930.00
1251.60	8027.00	3193.00	6008.00
1277.40	7970.00	3258.00	6123.00
1316.40	7887.00	3356.00	6295.00
1374.90	7765.00	3502.00	6553.00
1462.50	7590.00	3722.00	6938.00
1500.00	7518.00	3817.00	7102.00
1500.30	7517.00	3818.00	7104.00
1500.60	7517.00	3818.00	7105.00
1501.05	7516.00	3819.00	7107.00
1501.73	7514.00	3821.00	7110.00
1502.74	7513.00	3824.00	7114.00
1504.26	7510.00	3827.00	7121.00
1506.53	7505.00	3833.00	7131.00
1509.95	7499.00	3842.00	7146.00
1515.08	7489.00	3855.00	7168.00
1522.77	7475.00	3874.00	7202.00
1534.20	7461.00	3903.00	7252.00
1551.60	7468.00	3947.00	7327.00
1577.40	7478.00	4012.00	7440.00
1616.40	7495.00	4110.00	7609.00
1674.90	7523.00	4257.00	7861.00
1762.50	7573.00	4478.00	8238.00
1800.00	7597.00	4573.00	8399.00
1800.40	7597.00	4574.00	8400.00
1800.80	7598.00	4575.00	8402.00
1801.40	7598.00	4576.00	8405.00
1802.30	7599.00	4578.00	8409.00
1803.65	7600.00	4582.00	8414.00
1805.68	7601.00	4587.00	8423.00
1808.71	7603.00	4595.00	8436.00
1813.27	7606.00	4606.00	8455.00
1820.10	7611.00	4623.00	8485.00
1830.36	7618.00	4649.00	8528.00
1845.60	7628.00	4688.00	8594.00
1868.80	7644.00	4746.00	8692.00
1903.20	7670.00	4833.00	8840.00
1955.20	7710.00	4965.00	9060.00
2033.20	7774.00	5161.00	9389.00
2150.00	7894.00	5457.00	9897.00
2200.00	8015.00	5583.00	10089.00

Table 5-10 Plutonium Oxide/Metal Storage Container Laser Sampler Assembly Maximum von Mises Stresses in the Flange, Cap and the Vertical Plates- the Supporting Surfaces are modeled with BÉZIER Rigid Surface.

Applied Pressure	*Maximum von Mises stress in Flange*	*Maximum von Mises Stress in Cap*	*Maximum von Mises Stress in vertical plates*
(psi)	*(psi)*	*(psi)*	*(psi)*
0.60	12367.00	221.80	1602.00
1.20	12364.00	223.10	1600.00
2.10	12359.00	224.90	1598.00
3.45	12351.00	227.60	1595.00
5.48	12340.00	231.70	1590.00
8.51	12323.00	237.80	1582.00
13.07	12297.00	247.00	1571.00
19.90	12260.00	260.90	1555.00
30.16	12203.00	281.70	1530.00
45.53	12120.00	313.00	1493.00
68.40	11997.00	360.20	1438.00
103.20	11818.00	431.30	1357.00
154.80	11559.00	538.50	1237.00
232.80	11193.00	700.20	1497.00
349.80	10688.00	944.40	2010.00
525.00	10013.00	1377.00	2782.00
600.00	9747.00	1564.00	3112.00
600.30	9746.00	1565.00	3113.00
600.60	9745.00	1566.00	3114.00
601.05	9743.00	1567.00	3116.00
601.73	9741.00	1568.00	3119.00
602.74	9737.00	1571.00	3124.00
604.26	9732.00	1575.00	3130.00
606.53	9724.00	1580.00	3140.00
609.95	9713.00	1589.00	3155.00
615.08	9696.00	1602.00	3178.00
622.77	9670.00	1621.00	3211.00
634.20	9631.00	1649.00	3262.00
651.60	9574.00	1692.00	3337.00
677.40	9489.00	1757.00	3451.00
716.40	9365.00	1854.00	3620.00
774.90	9186.00	2000.00	3873.00
862.50	8933.00	2218.00	4278.00
900.00	8829.00	2312.00	4452.00
900.30	8829.00	2313.00	4453.00
900.60	8828.00	2313.00	4454.00
901.05	8827.00	2315.00	4456.00
901.73	8825.00	2316.00	4460.00
902.74	8822.00	2319.00	4464.00
904.26	8818.00	2323.00	4471.00
906.53	8812.00	2328.00	4482.00
909.95	8803.00	2337.00	4497.00
915.08	8789.00	2350.00	4521.00
922.77	8769.00	2369.00	4556.00
934.20	8738.00	2398.00	4609.00
951.60	8693.00	2441.00	4689.00
977.40	8627.00	2506.00	4808.00
1016.40	8532.00	2603.00	4986.00
1074.90	8404.00	2749.00	5253.00
1118.70	8331.00	2859.00	5455.00

APPENDIX I

A.1 Incremental plasticity theory

Incremental plasticity theory is based on a few fundamental postulates. A basic assumption of elastic-plastic models is that the deformation can be separated into an elastic part and a plastic part. In its most general form this statement is written as:

$$\mathbf{F} = \mathbf{F}^{el} \cdot \mathbf{F}^{pl}$$

where **F** is the total deformation gradient, $\mathbf{F}^{el}$ is the fully recoverable part of the deformation at the point under consideration, and $\mathbf{F}^{pl}$ is defined by $\mathbf{F}^{pl} = [\mathbf{F}^{el}]^{-1} \cdot \mathbf{F}$. The rigid body rotation at the point may be included in the definition of either $\mathbf{F}^{el}$ or $\mathbf{F}^{pl}$ or may be considered separately before or after either part of the decomposition. Conventionally an additive strain rate decomposition:

$$d\varepsilon = d\varepsilon^{el} + d\varepsilon^{pl}$$

has been used. Here $d\varepsilon$ is the total mechanical strain rate; $d\varepsilon^{el}$ is the elastic strain rate; and $d\varepsilon^{pl}$ is the plastic strain rate.

In ABAQUS, when the elastic strains are infinitesimal, the rate of deformation definition:

$$d\varepsilon = \text{symm}\,[\partial v / \partial x]\,dt$$

is applied to the total strain rate in the algorithms developed for all of the plasticity models. Practically the elastic strains in the clay cap soils and the FMLs are considerably small as compared with the inelastic deformations in the composite system. Thus, the use of the additive strain rate decomposition for the models in this analysis is an acceptable approximation.

The elastic part of the response is assumed to derivable from an elastic strain energy density potential, so that the stress is defined by:

$$\sigma = \partial U / \partial \varepsilon^{el}$$

where U is the strain energy density potential. For the elastic plastic model of von Mises which will be applied to the FMLs, the elasticity is linear. whereas for the soils and foam models the volumetric elastic strain is proportional to the logarithm of the equivalent pressure stress. The yield functions f_i define the limit to the region of pure elastic response, i.e.,

$$f_i\,(\sigma, \theta, H_\alpha) < 0$$

for pure elastic response. Here θ is the temperature, and H_α are a set of hardening parameters.

When the material is flowing inelastically the inelastic part of the deformation is defined by the flow rule, which can be written as

$$d\varepsilon^{pl} = \Sigma_i\, d\lambda_i (\partial g_i / \partial \sigma),$$

where $g_i\,(\sigma, \theta, H_\alpha)$ is the flow potential for the i th system, and $d\lambda_i$ is a scalar measuring the amount of the plastic flow rate on the i th system.

A.2 von Mises Equivalent Stress

The deformation of a solid body can be decomposed into two patterns, a dilatational mode (in which the solid changes volume), and an equivoluminal mode (in which the solid maintains constant volume, but distorts its shape). The corresponding stress fields are the hydrostatic and the deviatoric stresses.

For an isotropic material the criterion of yielding (i.e., in the state of plastic deformation), is a function of the stress state in the material element. In other words, the function is a constitutive law which must be independent of coordinate orientation. Then the yield criterion can be put in the form:

$$q = f(J_1, J_2, J_3)$$

where J_1, J_2, and J_3 are the first three invariants of stress tensor σ_{ij}.

Experimental work [Hill, 1950] has shown that for most metals (including steel) the hydrostatic stress has no influence on yielding. In 1913, von Mises suggested that yielding occurred when J'_2 (the second invariant of deviatoric stresses) reached a critical value, and that the yielding function may not involve J'_3, the third invariant of deviatoric stresses. J'_3 is not considered because its value changes from positive to negative for a triaxial state of stress that changes from tensile to compressive, and the isotropic material yielding does not depend on whether the stresses are tensile or compressive [Malvern, 1969]. In terms of deviatoric stresses, von Mises' yielding criterion can be written as:

$$q = f(J'_2),$$

$$J'_2 = \frac{1}{2} s_{ij} s_{ij},$$

where s_{ij} is the deviatoric stress tensor [Fung, 1965],

$$s_{ij} = \sigma_{ij} - \frac{1}{3} \sigma_{kk} \delta_{ij}.$$

Then in terms of Cauchy stresses, σ_{ij}

$$J'_2 = \frac{1}{2}\left(\sigma_{ij} \sigma_{ij} - \frac{1}{3} \sigma_{jj} \sigma_{kk} \right)$$

In terms of principal stresses,

$$J'_2 = \frac{1}{6} [(\sigma_1 - \sigma_2)^2 + (\sigma_2 - \sigma_3)^2 + (\sigma_3 - \sigma_1)^2]$$

If σ_y is the yield strength of the material, then the von Mises yielding criterion can be expressed as:

$$q = \sigma_y,$$

where q is the von Mises equivalent stress, in terms of principal stresses:

$$q = \sqrt{3 J'_2} = \left\{ \frac{1}{2} [(\sigma_1-\sigma_2)^2 + (\sigma_2-\sigma_3)^2 + (\sigma_3-\sigma_1)^2] \right\}^{\frac{1}{2}}$$

For materials exhibiting strain hardening properties, the equivalent stress or the true stress is a generalized yield criterion for any loading increase that causes additional plastic deformation according to the incremental theory of plasticity.

APPENDIX II

Initial Plutonium Storage Container Impact Analysis Results (U)

Robert F. Miller

1. Summary

Containers are being designed and developed for the long term storage of nuclear materials and components by the Equipment Engineering Section of the Savannah River Technology Center. One of many design requirements is that the containers must survive a fall from thirty feet onto a rigid floor and remain leak tight. Analysts from the Applied Technology Section used finite element analysis to assess the structural integrity of the damaged containers due to impact from this height. This document compares analytical and drop test results to establish the applicability of the analytical assumptions and techniques. This initial phase of the analysis shows that the containers are expected to remain leak tight when damaged from a fall from thirty feet onto a rigid surface.

2. Introduction

Containers are being designed for the long term storage of plutonium (Pu) powder[1] and components[2]. One of many design requirements is that the containers outer shell remain leak-tight after falling from thirty feet onto a rigid floor (the worst case impact scenario). This memorandum describes the initial analysis to predict the level of damage from such an impact and determine whether a breach of the container pressure boundary is possible. As the mechanical design is completed, further, more detailed analyses will—in tandem with drop testing—rigorously demonstrate the structural integrity of the containers.

Free fall impact from thirty feet was simulated with the ABAQUS[3] finite element code. Figure 1 shows the general dimensions and details that are modeled. Only the major components and features are simulated. The intention of this initial phase of the analysis is to evaluate the effectiveness of various analytical techniques and assumptions used in the simulation. This document is an attempt to quantify the effectiveness of those techniques and assumptions and is intended to provide a basis for future, more detailed analysis.

2.1. The Modeling Approach

There are a number of uncertainties involved in simulating the effect of impact on structures: material properties and quality; impact orientation; component interaction; etc. Depending on the purpose of the analysis and the limits of analytical software and hardware, different approaches, assumptions and simplifications are used. Optimally, physical test data is available to benchmark the analytical results. If the analysis can accurately predict the damage observed in the tests, then a higher degree of confidence in the analytical results for other orientations or impact scenarios may be warranted.

---

[1] Working drawing from M. A. Killian, "Metal/Oxide Reference Container"
[2] Working drawing from M. A. Killian, "Pit Reference Container"
[3] ABAQUS v.5.3.1, Hibbitt, Karlsson & Sorensen Inc., Pawtuckett, RI.

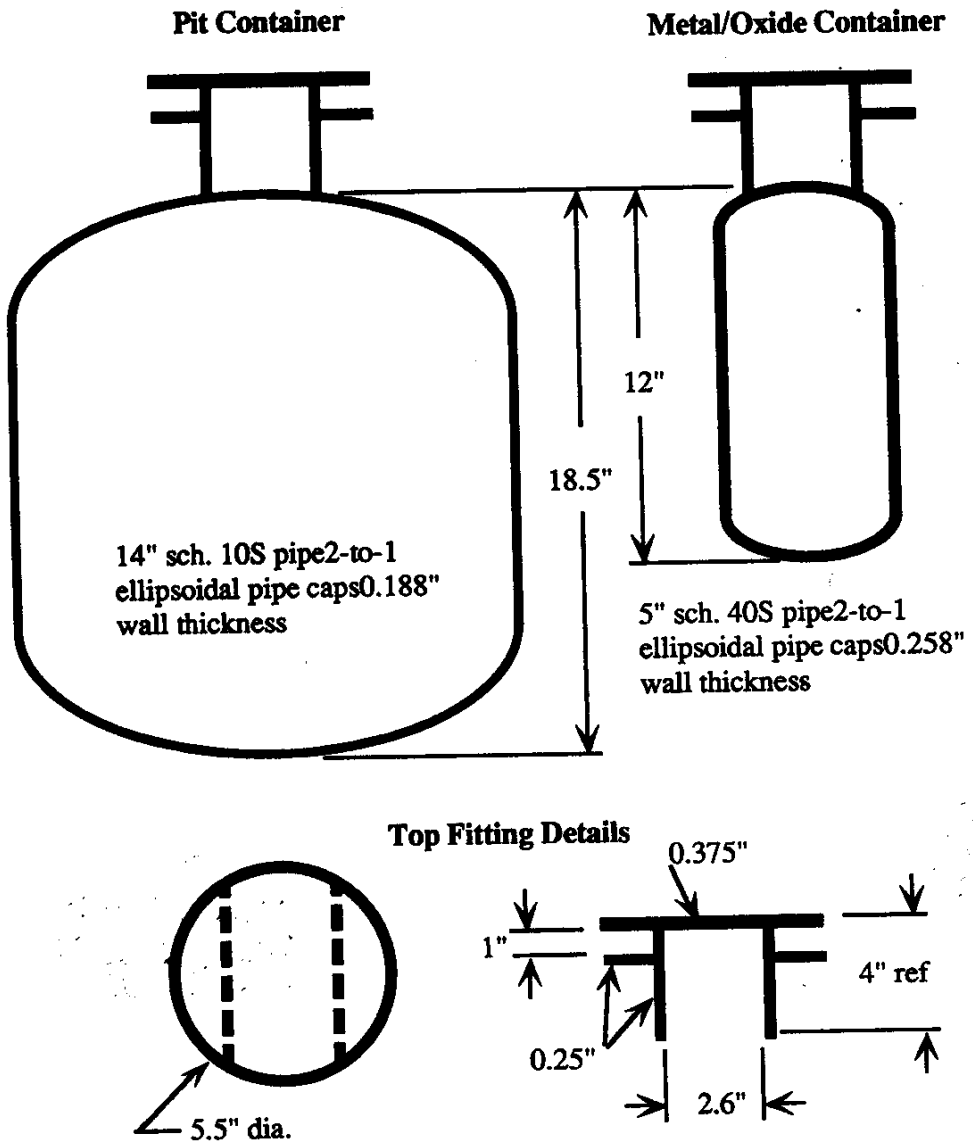

Figure 1 - Container Geometry Modeled with Finite Element Analysis

In this case, the Equipment Engineering Section performed several simple drop tests to investigate the impact capacity of the outer containers[4]. Empty pit containers and metal oxide containers filled with metal balls to simulate the contents were dropped in several orientations from thirty feet above a thick steel plate. The Applied Technology Section performed corresponding pre- and post-test best estimate analytical predictions.

3. Finite Element Models

Container impact was simulated with both two and three dimensional finite element models. Two dimensional models were used for impacts directly on the bottom cap (Figure 1) and three dimensional models were used elsewhere. The general purpose,

[4] Impact tests performed by S. E. Phillips et. al. 12/93.

commercially available finite element code ABAQUS was used in each case[5]. The analyses were performed on an IBM RISC 6000 workstation and pre- and post-processed on a SGI Indigo Elan.

3.1. Model Descriptions

This section describes the details of techniques used to simulate container impact with ABAQUS.

3.1.1. 2D Axisymmetric Models

For impact on the bottom cap of both the metal oxide and pit containers, the assumption of axial symmetry is reasonable. The top fitting is thus improperly modeled but this is acceptable as long as the mass is approximately equivalent because no top fitting deformation occurs in that orientation. First order, 2-node axisymmetric shell elements that allow transverse shear (SAX1) were used throughout the analysis. First order elements are recommended over higher order elements for large strain problems.

3.1.2. 3D Models

Off-axis impacts or direct impact on the top fittings of both containers necessitates the use of 3D models. Impact analysis with 3D models is far more computationally intensive than with 2D models. Indeed, 3D, true dynamic impact simulations of the containers were attempted without success in this analysis. An alternative method relying on quasi-static crushing of the containers was developed and employed instead. Details of this approach are described in the following sections of this document. First order, 4-node shell elements with reduced integration and transverse shear (S4R5) were used in all 3D models.

3.2. Modeling Techniques

Simulating container impact dynamically was found to be feasible only for 2D analyses. 3D models were too large to run given the large number of very small time increments (in the microsecond range) due to plastic deformation, geometric nonlinearities and the large number of contact points. A method of simulating impact using a quasi-static analysis for the large, 3D models was applied. The specific modeling techniques used in this analysis are described in the next two subsections.

3.2.1. Dynamic Analysis

For the 2D, axisymmetric models, it was possible to simulate the impact dynamically. The container nodes are given an initial velocity (527.5 in./sec for a free fall from thirty feet) and are tied to a rigid surface. The perfectly rigid surface does not allow penetration by any node of the container but does not directly effect any node not in contact with it. In other words, the container is allowed to "bounce" off the rigid surface unimpeded following impact. The kinetic energy of the container is dissipated by plastic deformation with a relatively small amount being stored as elastic energy. This elastic energy provides the energy for the container to rebound from the rigid surface.

Strain rate effects are important in impact events. ABAQUS provides a method for simulating the material hardening effect at high strain rates by equation (1).

$$\dot{\bar{\varepsilon}}^{pl} = D\left(\frac{\bar{\sigma}}{\sigma_o} - 1\right)^p \quad \text{for} \quad \bar{\sigma} \geq \sigma_o \qquad (1)$$

Where: $\dot{\bar{\varepsilon}}^{pl}$ = equivalent plastic strain (unitless)

[5] ABAQUS v.5.3.1, Hibbitt, Karlsson & Sorensen Inc., Pawtuckett, RI.

$\bar{\sigma}$ = equivalent plastic stress (psi)
σ_o = static yield stress (psi)
D = material parameter (40 for steels)[6]
p = material parameter (5 for steels)[5]

Careful consideration was given to develop the other material properties used in this analysis due to the critical nature of the application and the stringent requirement of being leak tight even after incurring considerable plastic deformation (refer to the material property section and Attachment I). The strain rate material parameters used in equation (1) were taken from ABAQUS documentation reporting the values for "steels" in general. One area of improvement in future analyses is to obtain more definitive inputs for our specific material based on literature or test data.

3.2.2. Quasi-Static Impact Analysis

The 3D models are too large to simulate dynamic impact with ABAQUS. The large number of time increments required due to the small time step make it unfeasible. An alternative approach is to crush the container statically. This less computationally intensive method was used in this analysis for all 3D simulations. The container is forced into a rigid surface either by acceleration or direct displacement and the plastic strain dissipation energy is monitored. When the plastic dissipation energy is equivalent to the initial kinetic energy of the container, the deformed shape approximates the deformed shape of the impacted container. This approach does not account for the inertia effects that occur during impact, like rotation, but should be useful for side impacts and other orientations that are not likely to impart a large rotation during the duration of plastic deformation. No direct strain rate hardening effect is possible with the quasi-static impact approach. By neglecting strain hardening effects, assuming all potential energy of the container is converted to plastic deformation in the container itself and neglecting any stiffening effects due to the inner structure, the degree of plastic deformation during impact is overestimated. If it can be shown, however, that even the conservative analysis results in acceptable plastic deformation to ensure that the container remains leak-tight, the results are useful.

3.2.3. Other Modeling Assumptions

Virgin material was assumed in all cases. The effects of manufacturing processes on the tensile properties and residual stresses was neglected. This is presumably a valid assumption because the large plastic stresses and strains associated with impact overwhelm the elastic residual stresses and the degree of cold work during manufacture. This is an area for further investigation in future, more detailed analysis. Another area of focus in the future is the behavior of weld material during impact. The models used for this analysis do not account for potential material property differences between base and weld metal. Geometric variations such as a weld bead were not simulated and a perfect joint was assumed. Regulations require 100% volumetric inspection of the body weld in the container so it is not necessary to attempt to simulate larger flaws such as lack of penetration etc.

---

[6] ABAQUS Examples Manual pg. 4.2.11, Hibbitt, Karllson & Sorenson Inc., Pawtuckett, RI.

3.3. Material Properties

The stringent requirement that the container remain, not only intact, but leak-tight after impact, necessitates a high degree of confidence in the material model used to simulate the 304L stainless steel container. Due to the large, plastic strains that occur during impact, an accurate true stress-true strain material model was required in this analysis. Attachment I describes in detail the tensile properties model used in the finite element models. Attachment I also provides the justification for a high level of confidence that the container will remain leak-tight even when damaged up to 40% local equivalent plastic strain.

Experimental data is available that supports the 40% plastic strain criteria[7]. A burst test of a 304L stainless steel sphere showed that 55% equivalent plastic strain occurred before rupture. This strain value was calculated by measuring the wall thickness of the burst sphere and comparing it to the original thickness. A sphere subjected to uniform, biaxial tensile stress such as in this case will fail at the weakest point in the material. The plastic strain present in a container following impact is a local phenomena and is not likely to occur at the weakest point in the material. This lends further credence to the 40% criteria because the plastic strain in the burst sphere exceeded it.

4. Results

4.1. Dynamic vs. Quasi-Static Analysis

Figure 2 shows the results of a comparison between the deformation due to dynamic impact and quasi-static crushing of the metal oxide container due to impact from thirty feet on the bottom cap. The container was simulated at the design temperature of 400°F and 0 psig internal pressure. This combination of parameters (compared to room temperature and design pressures of 100 psig for the pit container and 1000 psig for the metal oxide container) was shown to result in the highest plastic deformation as measured by equivalent plastic strain[8]. No strain rate effects were included in the dynamic analysis for this case in order isolate the differences between the two simulation methods. The centerline deformation for the dynamic case was 0.75 inch compared to 0.76 inch for the quasi-static crush case. The maximum equivalent plastic strain (PEEQ in ABAQUS) for the dynamic case and the quasi-static case was 20%. In both cases the maximum strain occurred at the center of the bottom cap on the inside surface as the cap is inverting upon impact. This comparison demonstrates that the quasi-static method reasonably approximates the actual dynamic simulation in this case. This is important in the 3D analyses where dynamic impact analysis is not feasible and the quasi-static approach was used exclusively.

4.2. Shell vs. Solid Elements

Shell elements are suitable for widespread deformation of plate or shell-like surfaces such as this case where bending stresses can dominate membrane stresses. A comparable model composed of first order solid elements requires many elements through the thickness in the regions of deformation. Figure 3 shows the result of a comparison between axisymmetric shell (SAX1) and axisymmetric solid (CAX4) elements using quasi-static crushing. There were eight elements through the thickness in the impacted zone of the bottom cap and sixteen along the cap radius. This compares to thirty shell elements in the bottom cap. There are 106 nodes and 107 elements in the entire shell

---

[7] Information and specimen provided by W. R. Kanne of SRTC/MTS.

[8] Subsequent to this analysis, the design pressure for the metal oxide container was reduced to 500 psi.

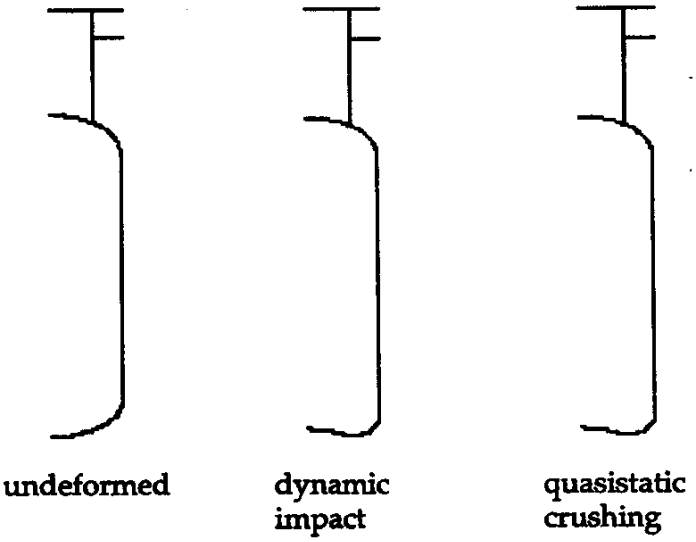

Figure 2 - Metal oxide Deformation—Dynamic vs. Quasi-static Analysis

model compared to 273 nodes and 224 elements in the solid model (that does not include the fitting). The results show that the solids do not pick up the snap-through behavior of the bottom cap as the shells do—even with eight elements through the wall thickness. This tendency toward snap-through behavior was observed in the test as will be described in Section 4.3.1. As a result, the model with solid elements under predicts the plastic deformation—16% equivalent plastic strain versus 20% for the shell model. Based on these results, shell elements were used throughout the remainder of the analysis.

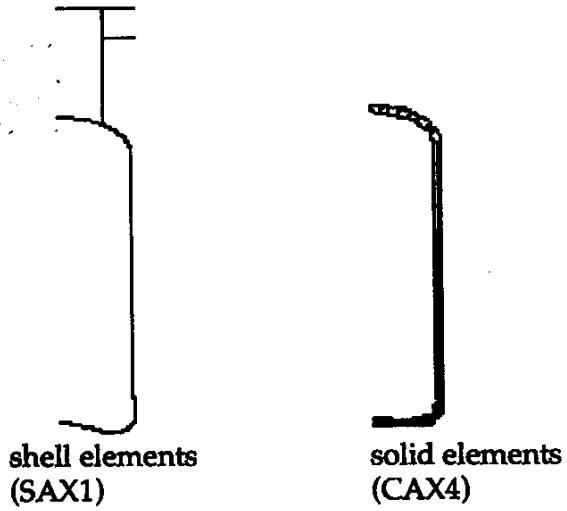

Figure 3 - Deformation Using Shell vs. Solid Elements

4.3. Best Estimate Test Predictions

Drop tests of both container designs were performed by the Equipment Engineering Section on December 6-7, 1993[9]. Pre-test analytical predictions of anticipated deformation were provided by the Applied Technology Section. Best estimate values of deformation and equivalent plastic strain were included. In addition, estimates of the rebound height of each container were provided for safety considerations during the tests.

4.3.1. The Metal Oxide Container

The two metal oxide containers each contained a bag of metal balls (BB's) to simulate the mass of the nuclear material in field use. No attempt was made in the analysis to properly account for the structural effects of the BB's within the container although the additional mass was simulated by simply enhancing the density of the 304L container forcing the total mass to be the same as the test containers. Room temperature material properties and no internal pressure was assumed. The force of gravity was included and an impact velocity of 527.5 in./sec was applied. In the manner previously described, the container was allowed to impact a rigid surface, deform and rebound.

Table 1 summarizes the test configurations for the metal oxide container and compares the predicted versus actual results.

Table 1 - Metal oxide Container Test Results vs. Predictions

	Container #4 - direct impact on the bottom cap		Container #3 - 18° rotation from container axis, bottom hit	
	Predicted (in.) (Note 1)	Measured (in.)	Predicted (in.) (Note 2)	Measured (in.)
Dent Depth (in.)	0.34	0.4375	-	0.15625
Plastic Strain (%)	17	-	-	-
Rebound Height (in.)	30	~0	-	~0

Note 1: Reported values are post-test analysis. The pre-test results contained a modeling error.
Note 2: Pre-test predictions of this orientation were not performed.

A comparison of the results for Container #4 is revealing. The predicted dent size is comparable to that measured. The test report indicates the difficulty in obtaining a definitive measurement of the deformation from the radiographs. Significantly, the observed dent is similar in shape to that predicted—the slight inverted or "snap-through" behavior. This feature was shown to have a significant effect on the degree of plastic straining in the bottom cap and it occurred even despite the opposing force of the BB's inside. The analytically predicted deformation for Container #4 is shown in Figure 4. The calculated value of 17% equivalent plastic strain is well below the proposed allowable equivalent plastic strain of 40%. Correspondingly, post-test leak testing of both containers showed that neither pressure boundary was breached during impact.

9 Phillips, S. E., "Plutonium Storage Container Drop Tests- Equipment Engineering Section," 12/93.

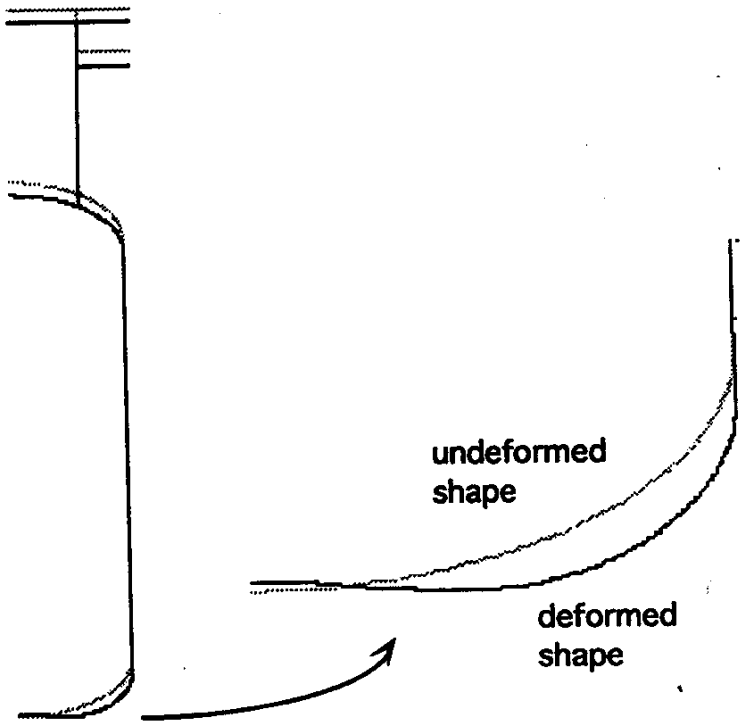

Figure 4 - The Predicted Structural Response of Container #4

Strain measurements were not taken during the test so no comparison to analysis is possible but a glaring disparity between predicted and observed rebound height occurred. Container rebound following impact occurs when the elastic energy stored in the container plate during impact is released after the bulk of the available energy is dissipated through plastic deformation. Recall that the weight of the BB's was evenly distributed around the container in the analysis. No attempt was made to simulate the structural effects of the BB's—only the added mass. It is speculated that the lack of predicted rebound occurred because of the downward momentum of the slower responding loose BB's. Regardless, the bounce height issue is secondary to plastic deformation of the container and it was only reported to provide safety information during the testing.

4.3.2. The Pit Container

The pit container was dropped empty because the top and bottom caps as fabricated were 0.375 inch thick, rather than the specified schedule 10S pipe nominal thickness of 0.188 inch. The mass of the test pit containers approximated the design mass of the design pit container in use in the field. The test results, because of the enhanced structural rigidity, are useful in understanding the impact response of the top fitting but are of limited value as far as the response of the container as designed are concerned. Still, they provide valid data with which to further benchmark the finite element results. Table 2 provides a summary of the test and analytical results.

Table 2 - Pit Container Test Results vs. Predictions

	Container #1 - direct impact on the bottom cap		Container #2 - top fitting hit at 45° from horizontal	
	Predicted (in.)	Measured (in.)	Predicted (in.) (Note 1)	Measured (in.)
Dent Depth (in.)	0.45	0.125	0	0.15625
Plastic Strain (%)	10	-	0	-
Rebound Height (in.)	38	21	-	~0

Note 1: This pre-test analysis was performed at 20° rather than 45°.

Figure 5 shows the predicted structural response of a direct bottom hit on the pit container similar to the drop test of Container #1. This model used the $^3/_8$ inch thick caps and a dynamic solution with strain hardening—a best estimate, pre-test prediction of the response. The dent depth was over predicted by the analysis although, as mentioned in the test report, it is difficult to obtain a definitive measurement for the dent depth using present techniques. The rebound height was over predicted by a factor of two as well. The strain rate effect was observed to have a large effect on the rebound height. When comparing the results between accounting for strain rate effects and neglecting them, a factor of two in the rebound height was calculated. An equivalent plastic strain of 10% is well below the proposed acceptance criteria of 40%. Post-test leak tests of Container #1 confirmed that the pressure boundary was intact after the test.

Figure 6 shows one view of the closest approximation to the Container #2 test. This analysis is 3D, and as described in the modeling section of this document, a quasi-static solution where the model is statically displaced into the rigid surface and the plastic energy dissipation is monitored. When all the available potential energy of the pit container suspended at thirty feet is dissipated, the analysis is halted. Only the portion of the container that could potentially see plastic strain was modeled in this case. The results showed that the top fitting was highly deformed, absorbing all of the energy of the fall leaving the container itself undamaged. This is not a realistic representation of the actual test. The test container was dropped at an angle of 45° and rotated upon impact. It contacted the top fitting and the container itself approximately simultaneously then spun and impacted the lower portion of the container, slightly denting this area. Clearly, this method of analysis lacks when the intent is a best estimate of the damage due to impact because important aspects of the physics involved are not taken into account. It is, it can be argued, a useful method where a conservative bounding estimate of the potential damage is required for qualifying the container design rather than a best estimate. Figure 7 shows the side view of the Container #1 analysis.

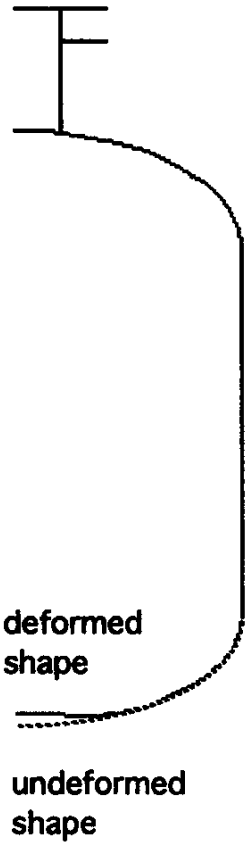

Figure 5 - The Predicted Structural Response of Pit Container #1

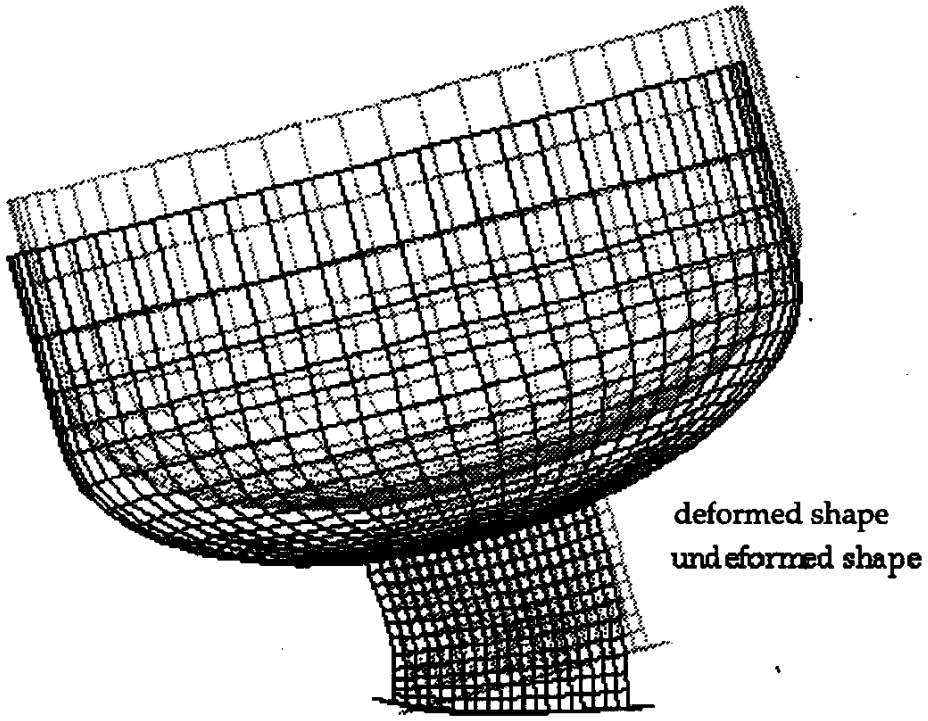

Figure 6 - Front View of the Predicted Structural Response of Pit Container #2

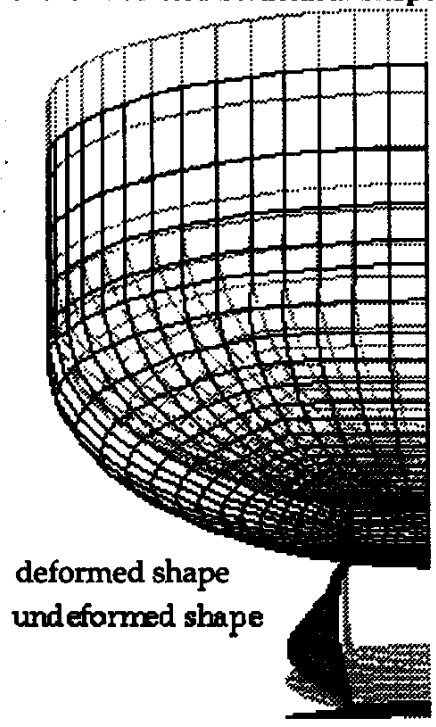

Figure 7 - Side View of the Predicted Structural Response of Pit Container #1

5. Conclusions

This document is intended to establish the applicability of using finite element analysis to predict container impact response. Among the many stringent design requirements for the nuclear material long term storage containers that are currently being designed; they must be able to remain leak-tight after a 30-foot fall onto a hard surface. In conjunction with drop tests, several pre- and post-test finite element simulations were performed and the results compared. In general, the simulations tended to compare favorably to the drop tests themselves lending support to using finite element analysis to augment drop test matrices in the future. The effectiveness of several simulation techniques including strain rate effects, temperature dependent material properties and quasi-static solutions were gauged and, in conjunction with the material constitutive relationship developed by R. L. Sindelar, a methodology was demonstrated that will provide a conservative estimation of material damage and the likelihood of breaching the pressure boundary.

The initial analysis indicates that the containers can survive a 30-foot fall in any orientation and remain leak-tight. Although significant plastic deformation will occur, the maximum strains are below the 40% value that 304 Stainless Steel can undergo without local failures leading to breach of the pressure boundary. Further, more detailed analyses should examine the effects of internal components and the likelihood of damage to the fill tube upon impact.

Attachment I - *Detailed Tensile Property Data for Container Materials*

WESTINGHOUSE SAVANNAH RIVER COMPANY

INTER OFFICE MEMORANDUM

November 10, 1993

SRT-MTS-93-3113

UNCLASSIFIED
DOES NOT CONTAIN
UNCLASSIFIED CONTROLLED
NUCLEAR INFORMATION

ADC & Reviewing Official: D.T. Rankin
Date: 11/23/93

TO: R. F. Miller, 773-41A

FROM: R. L. Sindelar, 773-41A

Technical Review: P. S. Lam, 773-41A

Responsible Mgr: N. C. Iyer, 773-41A
Mgr., Mat. Appl. & Corr. Tech.

Tensile Properties of Type 304/304L Stainless Steel for Impact Deformation Analysis of Nuclear Materials Containers (U)

Introduction and Summary

Impact (drop load) analysis of Plutonium Storage Facility containers includes finite element structural modeling [1]. The containers are constructed of Type 304L stainless steel with nominal thicknesses of 0.258 and 0.188" and the design temperature is 400°F. Material inputs to the analysis are the material stress-strain response and a limit to the deformation (plastic strain) to ensure the container would not be breached. This memorandum provides material stress-strain data and a strain limit for deformation analysis of structures of Types 304 or 304L stainless steel.

Data from literature sources of Type 304 and 304L stainless steel and previous site programs of Type 304 stainless steel were evaluated to provide the digitized true stress-strain data from tensile testing at 77°F and 257°F as shown on the curves in Figure 3. The digitized data are a best estimate approximation of the response of Type 304 or 304L stainless steel material in an initial solution-annealed condition (non-cold-worked). The data at 257°F can be applied as material input in the structural analyses for temperatures up to 400°F and for strain rates up to 10^2 s^{-1}.

A limit to the equivalent plastic strain of 40% is chosen based on considerations in plastic forming of metals and the results of the Type 304 and 304L stainless steel data.

Discussion

Impact structural analysis of a storage container for nuclear materials is being performed to evaluate the response to accident loading conditions [1]. User-input tensile properties (true

stress-strain data) for Type 304L stainless steel applicable to a design temperature (limit) of 400°F and the specification of a limit to strain deformation were requested [1] to support the impact analysis of the storage container with the ABAQUS finite element code [2].

Stress-strain data for rod and sheet stock of Type 304L stainless steels and for piping (plate) stock of Type 304 stainless steels are reported in references 3 and 4, respectively; these data were evaluated to produce the stress-strain data for input into the impact analysis. Evaluation of strain rate sensitivity, strain hardening, and yield behavior of Type 304L was performed in reference 3. Stress-strain data from tensile specimens of bar stock (initial diameter of 0.375" machined to a gage diameter of 0.091") and mill-annealed sheet stock (0.010" thick) tested at a strain rate of 10^{-3} s^{-1} and at room temperature are shown on Figure 1 (reproduced from Figure 1 of reference 3). Testing of the rod stock specimens in compression at strain rates between 2×10^{-4} and 1×10^{4} s^{-1} was also reported in reference 3. These results are reproduced (from Figure 6 of reference 3) in Figure 2 below. The results in Figure 2 show that the material responds with increased strength to an increase in strain rate and that the results for a strain rate of 10^{2} s^{-1} are within approximately 125% of the lower strain rate results for the entire stress-strain curve.

Extensive testing of archival Type 304 stainless steel piping (plate) materials included uniaxial tensile testing at temperatures of 77 °F and 257°F tested "statically" at approximate strain rates of 10^{-3} s^{-1} and "dynamically" whereby the time-to-maximum load was approximately 80 ms [4]. The specimens were machined from pipe nominally 0.5" thick to produce tensile specimens of gage diameter 0.2". The results from the base plate region materials tested statically at 257°F, which included up to twelve different heats of Type 304 stainless steel, are shown in Figure 5-1 of reference 4. This figure shows generally that the lower carbon (0.035 to 0.5 wt%) heats have slightly less strength than the higher carbon (0.05 to 0.079 wt%) heats. One of the low carbon materials, 5BA at 0.041% carbon, was tested at 77°F and 257°F and is chosen to provide the digitized stress-strain data for the impact analysis.

The digitized stress-strain results up to the maximum load (providing the true tensile or ultimate stress, σ_u, and the true uniform tensile strain, ε_u) of representative specimens 5BA31 at 77°F and 5BA42 at 257°F are plotted in Figure 3. Note that the total strain at specimen failure is not a valid failure strain for a structure potentially loaded under plane strain conditions as discussed below. The data at 77°F for the 5BA31 specimen are similar to the room temperature Type 304L data shown in Figure 1 (after conversion 1 ksi = 6.896 MPa). Also shown on Figure 3 is a power law estimate for the stress-strain curve for Type 304 stainless steel at 400°F provided in reference 5; the power law curve with a coefficient of 114.7 ksi and an exponent of 0.21 (as given in reference 5 from a fit to literature values of yield and tensile strengths) is above the 257°F curve results of specimen 5BA42.

The dynamic testing of the archival Type 304 stainless steel in tension was also reported in reference 4. The strain measurement system did not provide strain data up to the maximum load of the tests. Results comparing the true stress-strain curves for "static" and "dynamic" tests of base material 3BA are shown in Figure 4, reproduced from reference 4. It is seen that the total or failure strain of the material is not reduced as the failure strain of the specimen tested dynamically is 1.2 whereas the failure strain of the specimen tested statically is 0.9. It is not possible to accurately obtain the true ultimate strain of the specimen tested dynamically from the data, but it is assumed that the strain would be similar to the specimen tested statically (true ultimate strain of 40%). The strain rate for the dynamic test is therefore approximately 0.4/0.080 seconds = 5 s^{-1}.

As a best estimate approximation, the digitized uniaxial tensile stress-strain data from specimen 5BA42 at 257°F can be used as material input to the ABAQUS code to model the deformation in impact analysis for temperatures near 400°F. The data from specimen 5BA31 should be used at temperatures near room temperature. Note that since the strength results of 5BA31 are greater than 5BA42, the use of the 5BA42 data for all temperatures below 400°F would give conservative results (more deformation) than would actually occur at low temperatures. Also, the strengthening which occurs at higher loading rates is ignored which is conservative.

A limit to the amount of deformation (plastic strain) is necessary to preclude local necking in the material and possible failure of the canister. Forming Limit Diagrams provide combinations of major and minor (plastic) strains, ε_1 and ε_2, respectively, to which sheets of material can be deformed before local necking (thinning) or bands of thinning and fracture occur [6, 7]. For a strip of material undergoing deformation, diffuse necking develops, and, with continued deformation, a narrow, localized neck forms immediately prior to failure [6]. The limit to avoid local necking depends on the state of plastic strain which is usually denoted by the strain ratio, $\varepsilon_2/\varepsilon_1$ [6, 7]. The lowest level of strain before localized necking occurs at or near plane strain conditions (i.e., ε_2 is zero). Under plane strain conditions, the value of ε_1 prior to the onset of localized necking is the strain for necking (diffuse necking) in pure tension which is the true ultimate strain ε_u [reference 6, p.686]. From data in references 3, 4 and 5, and consistent with the results for specimens 5BA31 and 5BA42 shown in Figure 3, ε_u is approximately 40% for the materials at 77°F to 400°F. A limit to the major principal strain of 40% would preclude the occurrence of localized necking under all combinations of strain ratios for temperatures up to 400°F for solution-annealed Type 304 and 304L stainless steel. It is noted that for strain ratios other than plane strain, the higher strains would be generally accommodated without localized necking and therefore this strain limit is bounding. The limit of plastic strain to use in the finite element analysis with the ABAQUS code [2] is discussed next.

The equivalent plastic strain (or effective or significant plastic strain [6]) is invariant and is given by:

$$\bar{\varepsilon}_p = \frac{\sqrt{2}}{3}\left[(\varepsilon_1^p - \varepsilon_2^p)^2 + (\varepsilon_2^p - \varepsilon_3^p)^2 + (\varepsilon_3^p - \varepsilon_1^p)^2\right]^{\frac{1}{2}}$$

where ε_1^p, ε_2^p, and ε_3^p are the principal plastic strains.

The ABAQUS code [2] calculates the equivalent plastic strain (symbol PEEQ) by summing up the equivalent plastic strain increments in time or load which are denoted by $\dot{\bar{\varepsilon}}_p$. That is,

$$\text{PEEQ} = \int_0^t \dot{\bar{\varepsilon}}_p dt \text{ where } \dot{\bar{\varepsilon}}_p = \frac{\sqrt{2}}{3}\left[(\dot{\varepsilon}_1^p - \dot{\varepsilon}_2^p)^2 + (\dot{\varepsilon}_2^p - \dot{\varepsilon}_3^p)^2 + (\dot{\varepsilon}_3^p - \dot{\varepsilon}_1^p)^2\right]^{\frac{1}{2}} \text{ in terms of the plastic}$$

strain increments in the principal directions, $\dot{\varepsilon}_i^p$, where i = 1, 2, and 3. The value of PEEQ at each location in the container should be compared to the limit of 40% for PEEQ.

Examples of possible local stress conditions in the material are, for uniaxial tensile conditions, and assuming rigid plasticity (negligible elastic strains), ϵ_2 and $\epsilon_3 = -\frac{1}{2}\epsilon_1$ and thus $\bar{\epsilon}_p$ reduces to ϵ_1; under plain strain conditions, $\epsilon_2 = 0$ and $\epsilon_3 = -\epsilon_1$ and thus $\bar{\epsilon}_p$ reduces to $\frac{2\sqrt{3}}{3}\epsilon_1$ which is greater than ϵ_1.

Setting a limit to $\bar{\epsilon}_p$ of 40% in the deformation analysis would preclude the onset of local necking in the materials of the canister. No fracture or breach of the canister would therefore occur under impact conditions where $\bar{\epsilon}_p$ is less than 40% throughout the canister. A safety of margin of $0.40/\bar{\epsilon}_p$ is defined; a minimum safety margin of 1 is recommended to ensure container integrity.

References

1. Personal communication R. F. Miller to R. L. Sindelar, August 1993.

2. Hibbitt, Karlsson & Sorenson, Inc., Pawtucket, RI, version 5.2.

3. M. G. Stout and P. S. Follansbee, "Strain Rate Sensitivity, Strain Hardening, and Yield Behavior of 304L Stainless Steel," in Transaction of the ASME, Journal of Engineering Materials and Technology, Vol. 108, October 1986, pp. 344-353.

4. **WSRC-TR-91-10**, K. J. Stoner, R. L. Sindelar, and G. R. Caskey, Jr., Savannah River Laboratory, April 1991; and MEA-2221, "Sample Preparation, Irradiation, and Testing of 304 Stainless Steel Specimens," J. R. Hawthorne, et. al., Materials Engineering Associates, August 1987. (specimen full data set from the materials testing is in Reactor Materials Program task 89-023-1 files -- see report WSRC-RP-93-940 for records storage identification of the task files).

5. SRL-EDG-910065, Material Properties for 304 SS," W. L. Daugherty, March 14, 1991, (this memo is part of task 91-001-1 files -- see report WSRC-RP-93-940 for records storage identification of the task files).

6. Chapters 3 and 20 in Mechanical Metallurgy, 2nd edition, George E. Dieter, McGraw-Hill, Inc., 1976.

7 Metals Handbook Ninth Edition, Volume 8, Mechanical Testing, "Formability Testing, "American Society for Metals, April 1989.

Figure 1. Stress-strain data for Type 304L stainless steel from rod and sheet stock tested in tension at room temperature at a strain rate of 10^{-3} s^{-1} [3].

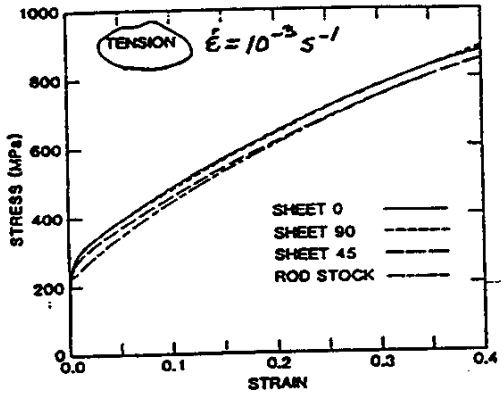

Figure 2. Strain rate effects to the stress-strain behavior of Type 304L stainless steel rod stock tested in compression [3].

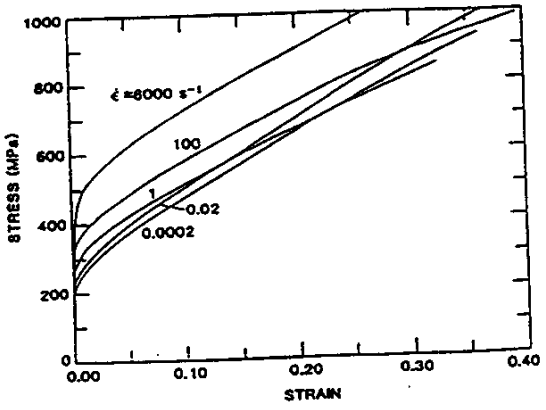

Figure 3. Stress-strain for Type 304 stainless steel [4, 5].

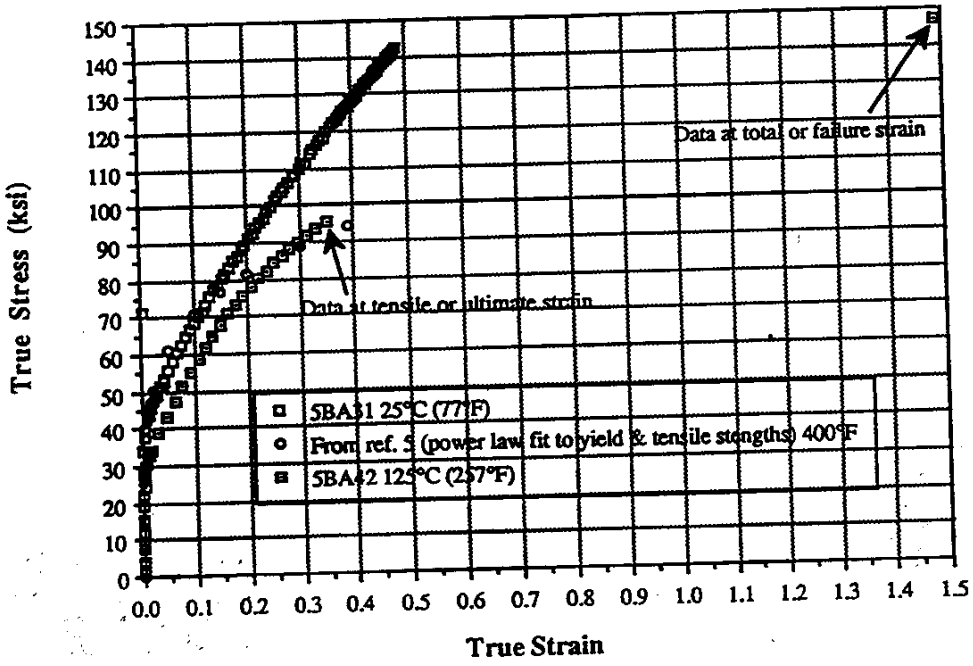

November 10, 1993
Page 7 of 7

SRT-MTS-93-3113

Figure 4. Strain rate effects to the stress-strain behavior of Type 304 stainless steel tested in tension [reproduced from Figure 5.23 of MEA-2221, reference 4]. The fracture points (denoted by "x") are from post-test measurements. If the strain extensometer used for the dynamic tests had provided data up to maximum load, then the entire dynamic curve would have plotted above the static curve.